Lignin-based hydrogels

A thesis presented to

The Faculty of Graduate Studies

Lakehead University

by

Alyssa Zerpa

In partial fulfillment of the requirements for the degree of

Master of Science in Environmental Engineering

September 2017

AKNOWLEDGEMENTS

First and foremost, I want to thank my supervisors, Drs. Pedram Fatehi and Leila Pakzad for their guidance, advice, and support throughout the composition of this thesis. It is with their time and dedication to this project, that I was able complete my research and analysis of lignin-based hydrogels. I would also like to extend my gratitude to my other committee member, Dr. Amir Azimi for his interest and participation in my research, as well as my external examiner, Dr. Biaoqing Liao, for taking the time to review my work. Furthermore, I would like to thank my Graduate Coordinator, Dr. Siamak Elyasi, for his help and encouragement.

I would also like to give a special thank you to my laboratory supervisor, Dr. Weijue Gao, and all of the group members from the Biorefinery Research Laboratory, without which, I would not have received the necessary laboratory training and experimental knowledge. In addition, I would like to mention and thank Dr. Carlos Zerpa for his help on the statistical analysis of my experimental work. Finally, special thanks to FPInnovations, NSERC, Canada Research Chair, Canada Fund for Innovation, Ontario Research Fund programs as well as Northern Ontario Heritage Fund Corporation for their supply of lignocellulosic materials and research funding for the advancement of lignin-based hydrogels.

ABSTRACT

Currently, limited information is available on lignin-based hydrogels, but its potential in commercial applications presents a promising avenue for the utilization of lignocellulosic materials. Recent studies have employed an array of techniques for crosslinking various types and species of lignin, combined with both synthetic and natural polymers.

This MSc thesis elaborated on effects of incorporating kraft lignin supplied in hydrogel production The hydrogels were synthesized through the radical polymerization of kraft lignin and N-isopropylacrylamide (NIPAAm) with N,N'-methylenebisacrylamide (MBAAm) as the crosslinker, and azobisisobutyroitrile (AIBN) as the initiator. The MANOVA and Tukey Post Hoc analyses determined that the reaction temperature, time, NIPAAm content, and pH exhibited significant effects on the responses for both the control and lignin-based hydrogel Taguchi L9 models. The hydrogel samples were optimized using the SN ratio to maximize yield and swelling ratio; these were determined to be samples 3C and 6C, as well as 2L and 9L, for the control and lignin-based hydrogel models, respectively. The structural analysis of the hydrogels was analyzed using ^{1}H NMR, FTIR, and CHNS, and indicated a high content of NIPAAm within the gels. TGA and DSC indicated an increased thermal stability due to the incorporation of N,N'-methylenebisacrylamide and lignin. The glass transition temperature (T_g) of the hydrogels was also found to be present between 141.45^{o}C to 148.60^{o}C.

In addition, the swelling behavior of the lignin-based hydrogels in water was found to obey pseudo-Fickian diffusion and second order kinetics. This was also found to correlate with the surface properties of the hydrogels determined by surface area analyzer (via BET method); an increase in surface area, as well as pore volume and size, leading to higher swelling rates and

capacities, respectively. Moreover, the equilibrium absorption of the hydrogels in methylene blue dye was found to better follow the Freundlich isotherm model, indicating a heterogeneous surface.

Furthermore, the oscillatory rheological measurements conducted to determine the viscoeleastic properties of swollen hydrogels. The hydrogels were found to be predominately elastic, for which the amount of energy dissipated was greater for the control samples than for the lignin-based samples. The structure recovery of the control hydrogels indicated a well-developed polymer network, recovering 87.2% to 96.7% of their elastic moduli following 100% deformation. The lignin-based samples, however, were found to withstand a higher amount of applied stress, indicating that lignin improved the flow point of the hydrogels. In addition, the elastic properties of the hydrogels were found to decrease with increasing temperature, exhibiting a lower critical solution temperature (LCST) between 34^{o}C to 37^{o}C.

TABLE OF CONTENTS

Aknowledgements i

Abstract ii

List of tables viii

List of figures ix

1 Introduction 1

1.1 Overview 1

1.2 Objectives 3

1.3 Novelty 3

1.4 References 3

2 Literature review 5

2.1 Lignocellulosic biomass 5

2.1.1 Lignin 6

2.2 Biorefinery 7

2.3 Lignin recovery 7

2.3.1 LignoBoost 8

2.3.2 LignoForce 9

2.4 Current lignin applications 10

2.4.1 Resins/adhesives 10

2.4.2 Adsorbants 11

2.4.3 Dispersants/plasticizers 12

2.5 Hydrogels 13

2.5.1 Background and synthesis of hydrogels 13

2.5.2 Current and potential commercial applications of hydrogels 17

2.5.3 Wound dressings 23

2.6 Recent advances in lignin-based hydrogels 29

2.6.1 Crosslinked with N-isopropylacrylamide 29

2.6.2 Crosslinked with acrylic acid 30

2.6.3 Crosslinked with acrylamide and poly(vinyl alcohol) 32

2.6.4 Crosslinked with polyethylene glycol diglycidyl ether 32

2.6.5 Crosslinked with ethyleneglycol dimethacrylate 33

2.6.6 Crosslinked with polyurethane 34

2.6.7 Crosslinked with glutaraldehyde 35

2.6.8 Effect of crosslinker 35

2.6.9 Incorporation of alginate 36

2.6.10 Incorporation of xanthan gum 36

2.6.11 Incorporation of cellulose 36

2.6.12 Incorporation of hemicellulose 39

2.7 Conclusion 41

2.8 References 42

3 Experimental methodology 57
3.1 Materials 57
3.2 Crosslinking reaction 57
3.3 Elemental analysis 58
3.4 ^{1}H nuclear magnetic resonance spectroscopy 58
3.5 Experimental design and statistical analysis 59
3.6 Yield 60
3.7 Swelling ratio 61
3.8 Brunauer–Emmett–Teller (BET) analysis 61
3.9 Fourier transform infrared spectroscopy 62
3.10 Absorption equilibrium 62
3.11 Focused beam reflectance measurement 63
3.12 Thermogravimetric analysis 63
3.13 Differential scanning calorimetry 64
3.14 Rheology 64
3.14.1 Frequency sweep 65
3.14.2 Amplitude sweep 65
3.14.3 Temperature ramp 65
3.14.4 Structure recovery 65
4 Results and discussion 66

4.1 Free radical polymerization 66
4.2 Nitrogen content 68
4.3 ^{1}H nuclear magnetic resonance spectroscopy 68
4.4 Effect of reaction conditions 69
4.5 Fourier transform infrared spectroscopy 86
4.6 Surface properties and swelling behavior 89
4.7 Absorption isotherm studies 94
4.8 Focused beam reflectance measurement 96
4.9 Thermogravimetric analysis 99
4.10 Differential scanning calorimetry 108
4.11 Rheology 110
4.11.1 Frequency sweep 111
4.11.2 Amplitude sweep 117
4.11.3 Temperature ramp 128
4.11.4 Structure recovery 133
4.12 References 136
5 Conclusions and recommendations 144
5.1 Conclusions 144
5.2 Future work 146

LIST OF TABLES

Table 2.1: Lignocellulosic biomass compositions 5

Table 2.2. Commercially available cellulose-based hydrogel-containing wound dressings 25

Table 3.1. Reaction parameters 58

Table 3.2. Taguchi L9 orthogonal design parameters 60

Table 4.1. Multivariate analysis of the Taguchi L9 orthogonal model for the control and lignin-based hydrogels 74

Table 4.2. Descriptive statistics 83

Table 4.3. Reliability analysis 84

Table 4.4. Signal-to-noise ratio for the responses of the control and lignin-based hydrogels 85

Table 4.5. Surface properties of control and lignin-based hydrogels 89

Table 4.6. Diffusion parameters of lignin-based hydrogels 92

Table 4.7. Pseudo-first order and pseudo-second order kinetic parameters of lignin-based hydrogels 93

Table 4.8. The isotherm parameters for the control hydrogels 95

Table 4.9. The isotherm parameters for the lignin-based hydrogels 95

Table 4.10. Glass transition and heat capacity of the control hydrogels, lignin-based hydrogels, and kraft lignin 110

Table 4.11. Flow point and yield flow point for control and lignin-based hydrogels 123

LIST OF FIGURES

Figure 2.1. LignoBoost process scheme 9

Figure 2.2. LignoForce process scheme 10

Figure 2.3. Preparation of chemical and physical crosslinked hydrogels 16

Figure 2.4. Synthesis of poly(2-hydroxyethylmethacrylate) (PHEMA) hydrogel contact lenses 18

Figure 2.5. Contact lenses production methods 19

Figure 2.6. Synthesis of SAPs and SPHs 21

Figure 2.7. Post-synthesis treatment for SAPs and SPHs 23

Figure 2.8. Diffusion-controlled drug release 26

Figure 2.9. Swelling-controlled drug release 27

Figure 4.1. Radical polymerization reaction of the lignin-based hydrogels: (a) Decomposition of AIBN initiator, (b) Crosslinking reaction mechanism 67

Figure 4.2. Nitrogen content of the control and lignin-based hydrogels 68

Figure 4.3. ^{1}H NMR spectrum for lignin-based hydrogels 69

Figure 4.4. The effect of responses on control hydrogel samples with respect to (a) temperature, (b) time, (c) N-isopropylacrylamide content, and (d) pH 78

Figure 4.5. The effect of responses on lignin-based hydrogel samples with respect to (a) temperature, (b) time, (c) N-isopropylacrylamide content, and (d) pH 82

Figure 4.6. FTIR analysis of the AIBN initiator, kraft lignin (LGN), N-isopropylacrylamide (NIPAAm), and N,N'-methylebisacrylamide (MBAAm) 86

Figure 4.7. FTIR analysis for the control and lignin-based hydrogels 88

Figure 4.8. Swelling ratio of lignin-based hydrogels 90

Figure 4.9. FBRM of control and lignin-based hydrogels: (a) 2C and 2L, (b) 3C and 3L, (c) 6C and 6L, and (d) 9C and 9L 98
Figure 4.10. TGA of the initiator and reactants: (a) AIBN (b) kraft lignin (c) N,N'-methylebisacrylamide (d) N-isopropylacrylamide 102
Figure 4.11. TGA of control hydrogels: (a) 2C, (b) 3C, (c) 6C, and (d) 9C 105
Figure 4.12. TGA of lignin-based hydrogels: (a) 2L, (b) 3L, (c) 6L, (d) 9L 107
Figure 4.13. DSC of the control hydrogels, lignin-based hydrogels, and kraft lignin 108
Figure 4.14. Frequency sweep of the control and lignin-based hydrogels: (a) Moduli of 2C and 2L (b) Dynamic viscosity of 2C and 2L, (c) Moduli of 3C and 3L, (d) Dynamic viscosity of 3C and 3L, (e) Moduli of 6C and 6L, (f) Dynamic viscosity of 6C and 6L, (g) Moduli of 9C and 9L, (h) Dynamic viscosity of 9C and 9L 116
Figure 4.15. Strain amplitude sweep of the control and lignin-based hydrogels: (a) Strain of 2C, (b) 2L, (c) 3C, (d) 3L, (e) 6C, (f) 6L, (g) 9C, (h) 9L 122
Figure 4.16. Stress amplitude sweep of the control and lignin-based hydrogels: (a) Strain of 2C, (b) 2L, (c) 3C, (d) 3L, (e) 6C, (f) 6L, (g) 9C, (h) 9L 127
Figure 4.17. Temperature ramp of the control and lignin-based hydrogels: (a) 2C, (b) 2L, (c) 3C, (d) 3L, (e) 6C, (f) 6L, (g) 9C, (h) 9L 132
Figure 4.18. Structure recovery of the control hydrogels: (a) 2C, (b) 3C, (c) 6C, (d) 9C 135

1 INTRODUCTION

1.1 Overview

Hydrogels are polymer matrices that have great affinity to absorb and maintain water. Themoresponsive hydrogels, particularly those that are responsive to the human body temperature, have received much attention in drug delivery systems (Uraki et al., 2004). Poly (N-isopropyl acrylamide) has been widely studied for the formation of hydrogels due to its phase transition between 32ºC and 34ºC, which is close to the body's core temperature (Deen, 2012; Erbil et al., 2004; Ling & Lu, 2009). Poly (N-isopropyl acrylamide)-based hydrogels have been developed as an injectable polymer scaffold for tissue engineering applications (Stile et al., 1999).

Recently, lignocellulosic materials have also been incorporated in the production of hydrogels since they present the advantages of being biocompatible, biodegradable, and low toxic (Fernandes et al., 2013). In addition to their availability as a renewable resource, lignocellulosic biomass are inexpensive (Thakur & Thakur, 2015; Ciolacu et al., 2013). Physically or chemically stabilized hydrogels, which are highly hydrated and porous, may be developed using aqueous solutions of cellulosic biomass (Fernandes et al., 2013; Ciolacu et al., 2013). In this MSc study, the synthesis of hybrid lignin-based hydrogels is introduced as an alternative to synthetic ones. Moreover, the experimental design, characterization, and performance of the hydrogels are compressively assessed for various applications. This current chapter, Chapter 1, provides a summary of the subsequent chapters in this thesis. Furthermore, the objectives and novelty of this work are also presented in this chapter.

Chapter 2 elaborates on the general background of hydrogels. Their unique properties as well as their methods of synthesis are elaborated. Their current commercial and potential applications are discussed, with an emphasis on the incorporation of lignocellulosic materials. In addition, a detailed review on the lignin incorporation within synthetic hydrogels is included. Their synthesis and effect performance is discussed, as well as their potential for current medical and agricultural applications.

Chapter 3 discusses the methodology to produce hydrogels. Also, various procedures followed for characterizing the produced hydrogels were discussed in detail. Also, the experimental design of the production of hydrogels were explained. The independent variables considered were reaction temperature, time, N-isopropylacrylamide content, and pH. The dependent variables were yield and maximum swelling ratio.

Chapter 4 discusses the radical polymerization of kraft lignin with N-isopropylacrylamide (NIPAAm) and N,N'-methyelenbisacrylamide (MBAAm) with azobisisobutyronitrile (AIBN) as the initiator. Control samples were produced without lignin and the performance of these samples were compared with lignin based ones.

The diffusion and kinetic of swelling of the lignin-based hydrogels were investigated in deionized water. The equilibrium absorption of the control and lignin-based hydrogels in methylene blue were analyzed via fitting the data into Langmuir and Freundlich isotherms. Finally, the rheological properties of the crosslinked hydrogels were investigated by applying frequency sweep, amplitude sweep, temperature ramp, and structure recovery tests.

Chapter 5 states the overall conclusions of the work presented in the thesis are stated. In addition, based on the obtained results, future work is suggested for the improvement of on the research lignin-based hydrogels.

1.2 Objectives

The objectives of this thesis were to:

1. synthesize hybrid crosslinked hydrogels based using kraft lignin;
2. optimize reaction conditions using experimental design methods;
3. characterize the structural and rheological properties of the hydrogels; and
4. analyze the swelling and absorption performance of the hydrogels in water and dye solutions.

1.3 Novelty

The novelties of thesis study were:

1. the incorporation of kraft lignin for hydrogel production;
2. the use of experimental design for the production of hydrogels; and
3. the detailed investigation on rheological behavior of lignin-based hydrogels.

1.4 References

Ciolacu, D., Oprea, A.M., Anghel, N., Cazacu, G., Cazacu, M. (2012). New cellulose-lignin hydrogels and their application in controlled release of polyphenols. Material Science and Engineering C, 32, 462-463

Deen, G. R. (2012). Solution Properties of Water-Soluble “Smart” Poly (N-acryloyl-N′-ethyl piperazine-co-methyl methacrylate). Polymers, 4(1), 32-45

Erbil, C., Kazancıoğlu, E., Uyanık, N. (2004). Synthesis, characterization and thermoreversible behaviours of poly (dimethyl siloxane)/poly (N-isopropyl acrylamide) semi-interpenetrating networks. European polymer journal, 40(6), 1145-1154

Fernandes, E.M., Pires, R.A., Mano, J.F., Reis, R.L. (2013). Bionanocomposites from lignocellulosic ressources: Properties, applications and future trends for their use in the biomedical field. Progress in Polymer Science, 38, 1415-1441

Ling, Y., Lu, M. (2009). Thermo and pH dual responsive Poly (N-isopropylacrylamide-co-itaconic acid) hydrogels prepared in aqueous NaCl solutions and their characterization. Journal of Polymer Research, 16(1), 29-37

Stile, R. A., Burghardt, W. R., Healy, K. E. (1999). Synthesis and characterization of injectable poly (N-isopropylacrylamide)-based hydrogels that support tissue formation in vitro. Macromolecules, 32(22), 7370-7379

Thakur V.K., Thakur M.K. (2015). Recent advances in green hydrogels from lignin: a review. International Journal of Biological Macromolecules, 72, 834-847

Uraki, T., Imura, T., Kishimoto, T., Ubukta, M. (2004) Body temperature-responsive gels derived from hydroxypropylcellulose bearing. Carbohydrate Polymers, 123-130

2 LITERATURE REVIEW

2.1 Lignocellulosic biomass

Renewable resources such as lignocellulosic biomass presents a large potential in replacing current synthetic polymers. Lignocellulosic materials are the products of plant-based materials, and their compositions vary based on species and type. For instance, wood contains four main components; cellulose, hemicellulose, lignin, and extractives. Hardwoods usually contain 43-47% cellulose, 25-35% hemicellulose, 26-24% lignin and 2-8% extractives (Smook, 2002). Softwoods, on the other hand, have larger lignin content, but lesser quantity of hemicelluloses (Thakur, 2014; Smook, 2002). Table 2.1 demonstrates the varying lignocellulosic compositions for different types and species of wood.

Table 2.1: Lignocellulosic biomass compositions (Yu et al. 2008)

Type	Species	Cellulose (wt.%, dry mass)	Hemicellulose (wt.%, dry mass)	Lignin (wt.%, dry mass)
Hardwood	White poplar	49	25.6	23.1
	European birch	48.5	25.1	19.4
	White willow	49.6	26.7	22.7
Softwood	White spruce	44.8	30.9	27.1
	Monterey pine	41.7	20.5	25.9
	Douglas fir	42	23.5	27.8

2.1.1 Lignin

In natural biomass, lignin is the glue that holds all the plant fibers together, providing strength to the cell wall. It obtains its rigid properties from the presence of aromatic groups as well as the hydrogen bonding between the alcohol, aldehyde, and ether functional groups. Its complex structure is composed of three major phenylpropanoid alcohols; coniferyl, coumaryl and sinapyl (Carraher, 2013; Smook, 2002). The large polymer also contains approximately 50 to 60% of β-O-4 linkages between phenyl propane units. The most reactive sites in lignin are the phenolic and alcoholic hydroxyl groups, which are targeted during its separation from plants (Carraher, 2013; Kumar et al., 2009; Chakar & Ragauskas, 2004). At a relatively low cost, lignin presents the greatest available aromatic renewable resource worldwide, as well as the major supplier of soil organic matter (Thakur, 2015; Calvo-Flores & Dobado, 2010). It accounts for approximately 10% to 25% of lignocellulosic biomass, and is the most abundant natural polymer after cellulose (Watkins et al., 2015; Rastogi & Dwivedi, 2008).

Lignin has been proposed to be used as emulsifiers, fuels, dispersants, adhesives, and synthetic floorings and in polymer blends and fiber composites (Kumar et al., 2009; Wang et al., 2009; Mankar et al., 2012). In addition, lignin has received much attention in hydrogel production due to its biocompatible, antimicrobial, and degradable properties (Thakur & Thakur, 2015). With increasing developments in organic chemistry, the generation of smart materials has improved substantially in recent years. Thermo- and pH-sensitive hydrogels are among the most widely researched environmentally responsive materials. In these systems, the gelling behavior is governed by the variations in pH and temperature (Buwalda et al., 2015). This review will expand on the background of biorefinery and hydrogels with a focus on the production and applications of lignin-based hydrogels.

2.2 Biorefinery

The developments in biorefinery to utilize biomass resources has become a more increasingly global effort due to environmental issues with the use of synthetic fossil-based materials and energy demands (Arthur et al., 2014). Biorefinery is the exploitation of biomass feedstocks, such as lignocellulosic materials, crops, and algae for the production of value-added products (Vishtal & Kraslawski, 2011; Cherubini, 2010; Demibras, 2009). The utilization of lignin is a critical component to the advancement of biorefining processes, representing an economically viable and a commercially sustainable resource management. In the past, research has been conducted to depict how plant-based materials can be altered to produce valorized materials (Arthur et al., 2014; Saeed et al., 2011; Stewart, 2008).

2.3 Lignin recovery

In pulp mills, cellulose fibers are required to produce paper products but cellulose must essentially be removed from wood chips in pulping processes. The most common form of chemical pulping is the kraft process, for which the main goal is the removal of lignin (Hamaguchi et al., 2012).

Kraft pulping produces about 85% of the world's lignin, which accounts for 630, 000 tons annually (Tejado et al., 2007; Mohan, 2006). Currently, approximately 98% of lignin from pulp mills is burned for energy recovery, resulting in less than 100, 000 tons annually of commercially exploited kraft lignin for value-added products (Lora & Glasser, 2002; Thielemans et al., 2002; Gosselink et al., 2004).

In modern kraft pulp mills, the lignin-containing waste stream, i.e. black liquor, is ultimately burnt for energy production. Black liquor consists of spent inorganic cooking

chemicals, as well as the organic residues from pulping. This stream contains high lignin content (Sixta, 2006). Since lignin is present in large concentrations within black liquor, it is ultimately burned for its energy recovery (Sixta, 2006).

Recently, alternative methods for extracting lignin from black liquor have been developed. The commercialization of value added products produced from the currently underutilized lignin would allow for additional revenues for pulp mills. In addition, the removal of lignin would reduce the capacity required for both the reboiler and chemical recovery process of the pulp mills (Tomani, 2010).

2.3.1 LignoBoost

In the LignoBoost process, shown in Figure 2.1, acidification is used for the separation of lignin from black liquor. Black liquor is acidified with carbon dioxide in order to reduce its pH to 10, at which point the precipitation of lignin occurs. The lignin filter cake is then re-dispersed and acidified once again before undergoing washing. This re-dispersing allows for a lower volume of acidic washing water, as well as a smaller filter area, which in turn may be attributed to lower investment costs. Another advantage of the LignoBoost process is the diminution of sulfuric acid required in the kraft process, which reduces operational costs (Tomani, 2010; Hamaguchi et al., 2012).

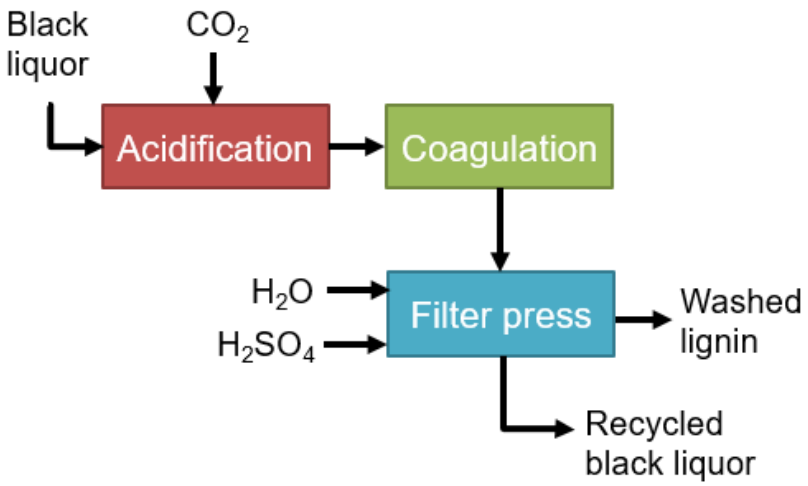

Figure 2.1. LignoBoost process scheme (Tomani, 2010)

2.3.2 LignoForce

A more recent alternative to the LignoBoost is the LignoForce process, which was developed by FPInnovations and NORAM (shown in Figure 2.2). This method is similar to LignoBoost, but it has an additional oxidation step at the start of the process, which was employed to improve the filtration properties of produced lignin. In this process, the black liquor stream first undergoes oxidation under controlled conditions before its acidification with carbon dioxide. Once acidified, the black liquor stream, now containing precipitated lignin, is coagulated before being sent to a filter press. The resulting product of this process is a high purity kraft lignin. This process has the advantages of a reduction in carbon dioxide consumption and hydrogen sulfide emissions compared with other alternatives (Kousini et al., 2012).

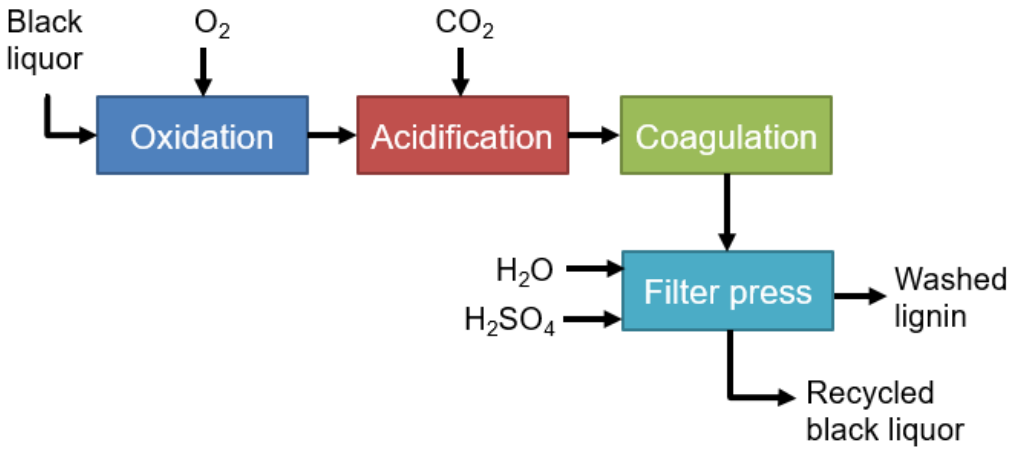

Figure 2.2. LignoForce process scheme (Kousini et al., 2012)

2.4 Current lignin applications

2.4.1 Resins/adhesives

Available in large quantities, lignosulfonate presents an ideal candidate to produce phenol-formaldehyde resins. Similar to phenol formaldehyde (PF) resins, lignosulfonate contains large molecules which allow for quick gelation. Its main limitation, however, is its lack of reactive sites which greatly affect its incorporation for resin synthesis (Tejado et al., 2007). Tejado et al. (2007) studied the synthesis of phenol-formaldehyde from various types of lignin. Phenolation is largely used to provide it with additional phenolic hydroxyl groups. Çetin & Ozmen (2002) reported that organosolv lignin can be used to replace 20 to 30% of phenol in PF resins for particleboard production. The properties of the resins with this substitution were found to be comparable with those of commercial PF resins. (Çetin & Ozmen, 2002).

Lin et al. (2010) also determined that methylated and unmethylated lignin generated similar results in PF resins when the concentrations of lignin was below 30% in the resin. At 50% substitution, however, methylated lignin samples produced stronger and more thermally

stable PF resin. On the other hand, methylated lignin PF resins were limited by their low storage stability, as well as their increased content of residual formaldehyde (Lin et al., 2010).

Alonso et al. (2001) studied the methylation of softwood ammonium lignosulfonate for PF resin manufacturing. Ammonium lignosulfonate demonstrated better reactivity with formaldehyde than other lignosulfonate samples due to having an increased number of aromatic protons, as well as a relatively high content of phenolic hydroxyl groups. Its optimum conditions were found to be a reaction temperature of 45^{o}C as well as a 1:1 and 0.83:1 ratio of formaldehyde to lignin and sodium hydroxide to lignin, respectively (Alonso et al., 2001). Alonso et al. (2003) further studies the synthesis of ammonium lignosulfonate PF resins in order to determine the optimum operating conditions for utilization in plywood manufacturing. The synthesized lignosulfonate based resins were found to exhibit similar properties to commercial PF resins at a molar ratio of 0.6 and 2.5 for sodium hydroxide to phenol modified lignosulfonate and formaldehyde to phenol modified lignosulfonate, respectively (Alonso et al., 2003).

2.4.2 Adsorbants

Lignin may also prove useful in the adsorption of organic dyes, this being a low-cost alternative for isolating pollutants from aqueous solutions. Da Silva et al. (2011) produced a chemically modified lignin capable of adsorbing Brilliant Red 2BE dye from wastewater. Acid hydrolysis sugarcane bagasse obtained from bioethanol production was carboxymethylated and complexed with iron (III) to form a water-soluble macromolecule (Da Silva et al., 2011). Adebayo et al. (2014) also investigated the adsorption of Procion Blue MX-R textile dye from the same species of lignin. In this particular case, the acid hydrolysis lignin was carboxymethylated and complexed with aluminum and manganese. The aluminum complexed carboxymethylated lignin sample was found to have a higher absorbance capacity than the

sample complexed with manganese; 73.52 mg/g and 55.15 mg/g at 25ºC, respectively. In addition, the aluminum complexed sample was also capable of removing up to 93.97% of the dye in a saline medium, while the manganese complexed sample only removed 75.91%. Both samples, however, exhibited efficient regenerations of up to 98.33% and 98.03% after four cycles for aluminum and manganese complexed samples, respectively (Adebayo et al., 2014).

Furthermore, aminated lignin derivatives have also been utilized in the recovery of gold, palladium and platinum as a replacement for conventional metallurgical processing which utilize toxic chemicals. Parajuli et al. (2006) produced two types of lignin-based absorptive gels containing primary amine and ethylenediamine functional groups, respectively. Lignophenol was prepared and cross-linked with the previously mentioned aminating reagents (Parajuli et al., 2006). The adsorption tests revealed both gels to be effective in absorbing gold, palladium and platinum according to the Langmuir model, but ineffective in absorbing copper, iron and zinc. The process of adsorption was presumed to have occurred due to the protonation of gels and the formation of metal-chloro anions (Parajuli et al., 2006).

2.4.3 Dispersants/plasticizers

Softwood kraft lignin has undergone carboxymethylation in alkaline conditions with sodium chloroacetate to produce lignin-based dispersants. Its low molecular weight and moderately high charge density proved to be a viable application for clay suspension (Konduri et al., 2015). Kamoun et al. (2003) also developed a water-reducing dispersant from esparto grass lignin for cement admixture. Lignin was extracted from the black liquor of a soda esparto grass pulping process, and then sulfomethylated with sodium sulfite and formaldehyde.

Similarly, Yu et al. (2013) produced a concrete superplasticizer by a combined oxidation and sulfomethylation of sodium lignosulfontate. An increase of 20% polyacetic acid for 0.3 wt.% lignosulfonate resulted in 7.6% improvement of cement paste fluidity (Yu et al., 2013).

Sulfomethylated alkali lignin dispersants were developed from corn stalk at a 1:1 ratio of lignin to sodium sulfite. The maximum content of sulfonate groups was achieved at 1.29 mmol/g, and was found to improve solubility, as well as reduce the pH required for precipitation. The increased sulfonate groups also lead to improved surface activity and surface tension (Wu et al., 2012).

Qin et al. (2015) also prepared sulfonated alkali lignin for the application of dispersants in coal-water slurry. The adsorption trend of these dispersants was shown to follow the Langmuir isotherm model with an optimum adsorption capacity of 1.58 mg/g. At high molecular weights, a decrease in adsorption capacity was exhibited due to its hydrophobic effect with coal particles. In addition, the sulfonate alkali lignin dispersants were determined to be more efficient at reducing viscosity of coal-water slurry than commercial naphthalene sulfonate dispersants (Qin et al., 2015).

2.5 Hydrogels

2.5.1 Background and synthesis of hydrogels

Hydrogels are often described as three-dimensional polymer networks formed from crosslinked hydrophilic homopolymers, copolymers, or macromers (Preppas Khare, 1993; Buwalda et al., 2014). Hydrogel is an insoluble polymer matrix capable of retaining a large amount of water in its swollen state; in some cases, up to a thousand times their dry weight. It is also capable of swelling in various solvents. Their swelling capabilities allow them to obtain

their form and adopt the shape of their surroundings when confined (Fernandes et al., 2013; Buwalda et al., 2014; Thakur & Thakur, 2015).

Depending on the source of the polymers, hydrogels may be synthetic, natural or hybrid (Buwalda et al., 2014). Thus, hydrogels may be degradable in aqueous environments, making them biocompatible in most cases and a good transportation mechanism for nutrients to cells and their metabolic products. They have been deemed to be efficient in the protection of cells and fragile drugs such as peptides and proteins. In addition, the properties of hydrogels may be easily modified; for instance, through the cell adhesion of ligands (Allan, 2002; Fernades et al., 2013). Some have even exhibited stimuli-induced swelling and deswelling capabilities without disintegration (Li & Pan, 2010; Malafaya et al., 2007; Peppas et al., 2006). The added advantage of tunable properties has given them much attention for biomedical and environmental applications (Zhu Ryberg et al., 2011; Sewalt et al., 1996).

Hydrogel applications in regenerative medicine is currently an emerging topic in the medical research field (Fernades et al., 2013; Thakur & Thakur, 2015). According to Thakur & Thakur (2015), hydrogels have demonstrated an ability to simulate natural tissues due to their large water content, excellent biocompatibility, and good surface properties. Their fundamental structure and composition is similar to that of the extracellular matrix which enables cell multiplication and survival. Furthermore, their soft and rubber-like properties have added benefits of minimizing inflammation of the surrounding cells (Fernandes et al., 2013; Buwalda et al., 2014). Although this topic remains in the research stage, various hydrogel applications have already been commercialized as medical and hygiene products (Fernandes et al., 2013).

The molecular interactions, which affect water sorption of the special polymer, include capillary, osmotic and hydration forces. The swollen equilibrium state of the polymer is dependent on the forces exerted from the crosslinked chains, which act as counterbalance, resisting expansion and preventing dissolution (Buwalda et al., 2014). To some extent, the magnitude of the effects, as well as the nature and morphology of the polymer, directly affects certain properties such as internal transport, diffusion characteristics, and mechanical strength (Buwalda et al., 2014). One of the most common methods for tuning the properties of hydrogels is to alter the chemical structure of the polymer by including functional groups which are susceptible to cleavage (Guarino et al., 2012).

Among all aspects of hydrogel preparation, the binding of polymer chains is the most important when considering water retention capabilities, specifically the monomers used in the synthesis and the backbone density of the network structure (Thakur & Thakur, 2015). Some of the most common methods of hydrogel formation include free radical polymerization, irradiation crosslinking, as well as physical and chemical crosslinking. However, more attention is dedicated to the physical and chemical crosslinking of polymers due to their inherent properties (Thakur & Thakur, 2015; Caló Khutoryanskiy, 2015). A proposed synthesis for these methods is illustrated in Figure 3, where hydrogels are formed from hydrophobic polymers. A hydrophobic polymer may first undergo chemical modification, such as oxidation, to create polar groups across the polymer network. The newly polarized polymer will then have the option to undergo two different pathways to produce either chemical or physical hydrogels via crosslinking (Hoffman, 2012).

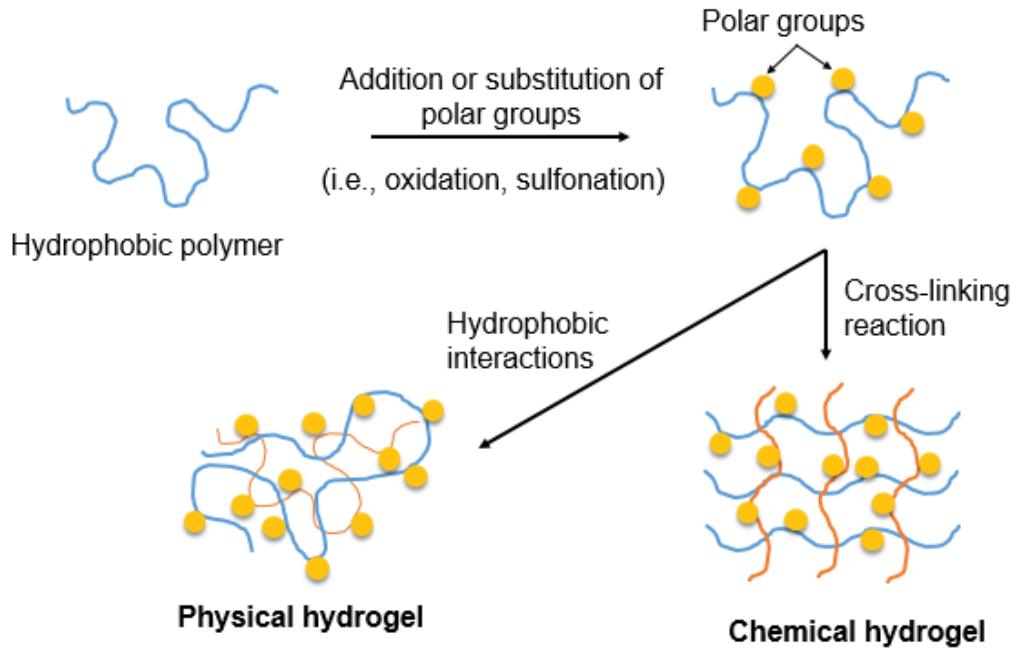

Figure 2.3. Preparation of chemical and physical crosslinked hydrogels (Hoffman, 2012)

Physical hydrogels, also referred to as reversible hydrogels, consist of chemicals with hydrogen bonding, electrolyte complexation, hydrophobic association, molecular entanglement, and/or secondary forces. The weak nature of this force often causes the hydrogels to dissolve in water and disintegrate by varying environmental conditions such as pH, temperature, and ionic strength of the solution (Hoffman, 2012; Shewan & Stokes, 2013; Thakur & Thakur, 2015). Chemical hydrogels, however, are non-reversible and referred to as permanent hydrogels. These gel networks are joined by covalent bonding and have the potential of being charged or non-charged depending on the functional groups present in their structure. Charged hydrogels may exhibit changes in swelling properties by modifying pH, as well as undergoing changes in shape through electrical exposure (White et al., 2013; Rosiak & Yoshii, 1999).

Chemical hydrogels can be classified by two methods of preparation: three-dimensional polymerization and direct crosslinking of water-soluble polymers. Polymerization normally

occurs by initiation of a free-radical or through exposure of radiation (ultraviolet, gamma or electron beam) (Kumari et al., 2011; Pal et al., 2013; Rani et al., 2010; Uliniuc et al., 2012; Caló & Khutoryanskiy, 2015). In the case of three-dimensional polymerization, however, where the hydrophilic monomer is polymerized via a polyfunctional crosslinking agent, the resulting material is usually found to contain residual monomers. This in turn affects hydrogel purification as unreacted monomers may be toxic and may potentially leach out of from the polymer matrix. Typically, the monomer-containing hydrogels undergo a purification process by allowing them to soak in excess water. This form of extraction, although efficient at removing residual monomers, is a lengthy procedure, taking up to several weeks (Caló & Khutoryanskiy, 2015; Mathur et al., 1996). Other alternative treatments include the selection of non-toxic monomers (i.e., water-soluble monomers) for the initial polymerization step, as well as subsequent post-polymerization curing via thermal treatment or irradiation (Park & Nho, 2003; Rosiak et al., 1995; Lin-Gibson et al., 2004).

2.5.2 Current and potential commercial applications of hydrogels

2.5.2.1 Contact lenses

The first patented hydrogel technology dates to 1960 when hydrogels based on poly(2-hydroxyethylmethacrylate) (PHEMA) were used in the development of contact lenses (Caló & Khutoryanskiy, 2015; Buwalda et al., 2014). These were prepared by the radical polymerization of 2-hydroxyethylmethacrylate) (HEMA) with ethylene glycol dimethacrylate, as shown in Figure 2.4 (Buwalda et al., 2014; Kopecek, 2009). These new ‘soft’ contact lenses were preferred over the existing ‘hard’ hydrophobic-based contact lenses since hydrogels resulted in better oxygen transmission to the cornea, increasing comfort for the user. Oxygen transmission through the hydrogel was found to be directly related to its affinity for water and gel thickness

(Caló & Khutoryanskiy, 2015; Buwalda et al., 2014; Cornway, 2017). The basic PHEMA contact lenses consisted of 38% water and a 0.035mm to 0.060mm thickness (Cornway, 2017; Scholtz & Auffarth, 2012).

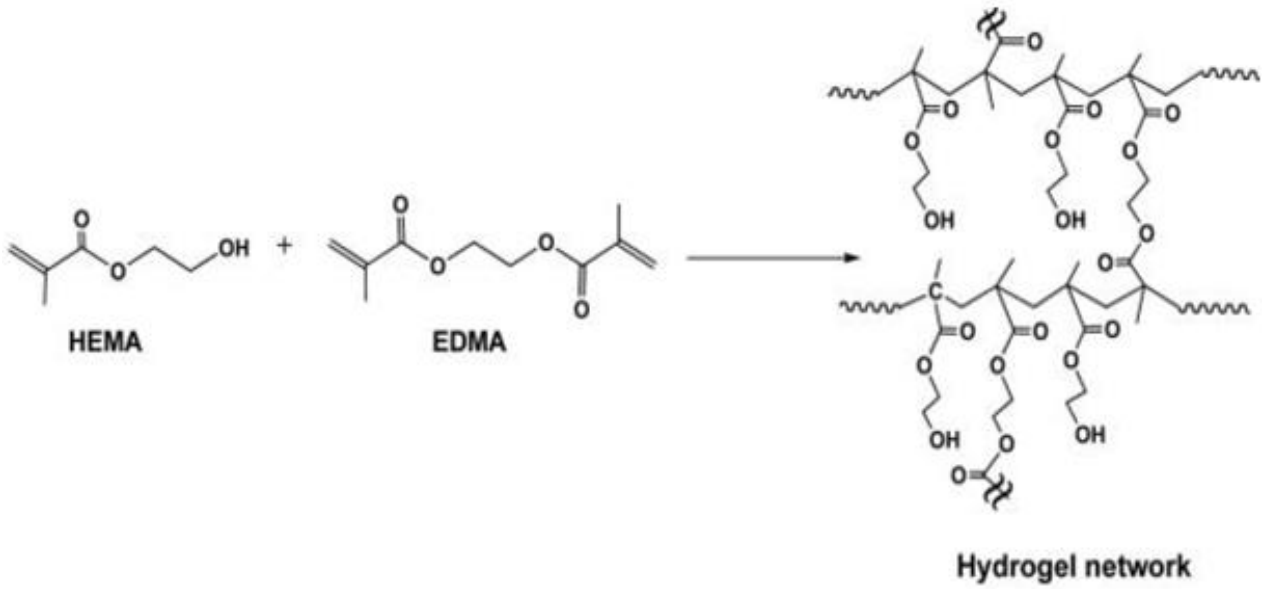

Figure 2.4. Synthesis of poly(2-hydroxyethylmethacrylate) (PHEMA) hydrogel contact lenses (Kopecek, 2009)

The production methods for soft contact lenses include spin-casting and mold-casting, which employ a similar process, as illustrated in Figure 2.5. Essentially, a liquid monomer mixture is placed into a small concave optical mold which gives shape to the contact lens (i.e., diacetone acrylamide, ethoxyethyl methacrylate, 2-hydroxyethyl methacrylate, methacrylic acid, methyl methacrylate, N-vinylpyrrolidone, polyvinyl(alcohol), etc.) (Hamilton & Macfarlane, 2006; Bahmra & Tighe, 2007). In spin-casting (left), the mold rotates to disperse the liquid uniformly across the concave shape and coat it evenly in the form of the lens. Mold-casting (right) on the other hand, uses an additional convex mold to press down upon the concave mold containing the liquid monomer; this forms the back surface of the lens. The polymerization step

is then carried out at elevated temperatures for both processes, and the residual monomer is removed (Hamilton & Macfarlane, 2006).

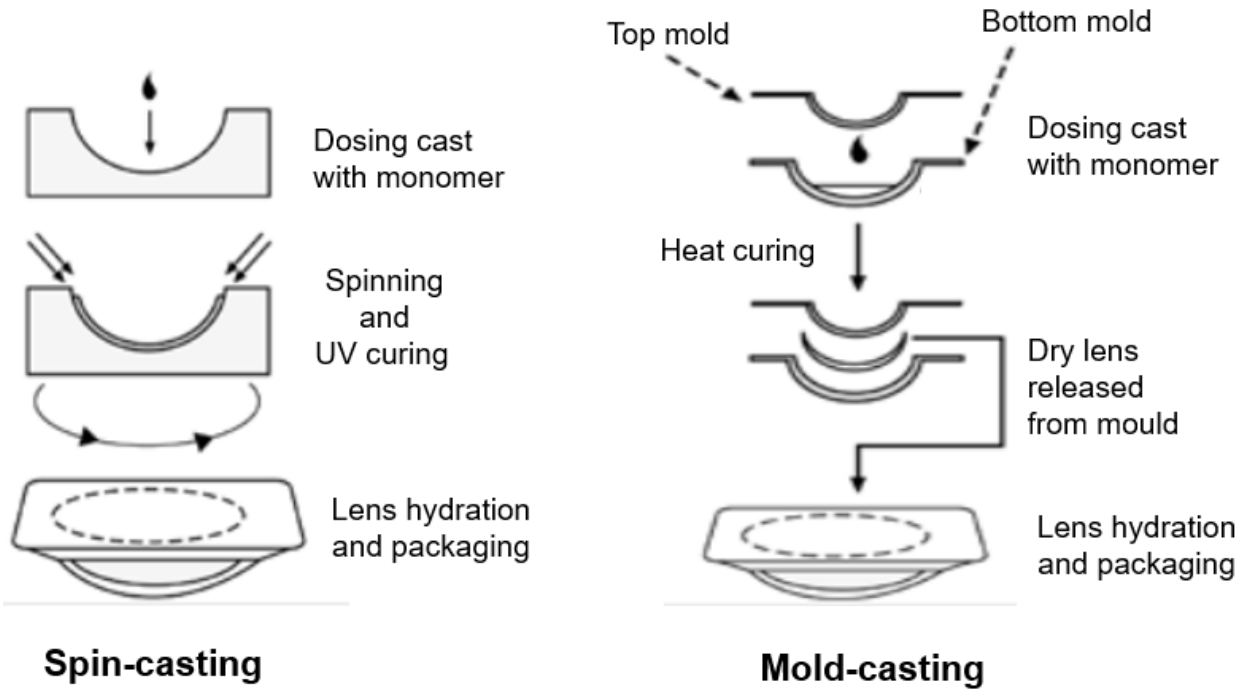

Figure 2.5. Contact lenses production methods (Hamilton & Macfarlane, 2006)

An alternative technique employed in industry is lathe-cutting. First, a liquid monomer mixture normally undergoes bulk polymerization via free-radical initiation in low-temperature water tanks (Maldano-Codina & Efron, 2003). This takes place over a long period of time and allows for the formation of long polymer chains of high molecular weight (i.e., creating chain entanglements) in the shape of the cylindrical tank. The dehydrated material is then cut into button shapes before undergoing the lathing process where they are shaped into precision contact lenses. The lathing process also serves as the removal of surface layers that may have been subjected to degradation during the bulk polymerization (Maldano-Codina & Efron, 2003).

2.5.2.2 Hygiene products

In 1978, superabsorbent polymers (SAPs) were first commercialized for the use of feminine napkins using crosslinked starch-g-polyacrylate (Caló & Khutoryanskiy, 2015; Masuda et al., 1994). Their exceptional water retention properties and ability to prevent germ colonization allowed them to gain increasing popularity in the commercial markets, growing to include applications in agriculture and the diaper industry in the years that followed (Sannino et al., 2009; Caló & Khutoryanskiy, 2015). A disadvantage of SAPs, however, is that they are limited by their dependence to size and only exhibit fast swelling in small sample sizes (Omidan et al., 2005).

Superporous hydrogels (SPHs) were later presented an alternative to SAPs as they shared similar properties, apart from being size-independent. The swelling SPHs occurs directly upon contact in the dried state, and exhibit fast swelling kinetics regardless of the final product size. (Omidian, 2005; Caló & Khutoryanskiy, 2015). This is due to their interconnected cellular matrix, their open porous structure allowing for fast absorption on water by capillary force. Recent SPHs have also exhibited certain desirable properties such as mechanical strength and elasticity, even in their swollen state (Omidian, 2005). Newer generations of hybrid SPHs are also being produced by employing natural "hybrid agents"; water-soluble or dispersible polymers capable of physical or chemical crosslinking (Omidian, 2005).

SPHs have been largely used in the development of various hygiene products and even help to promote skin health by keeping moisture away from the skin. Their high absorbency is efficient at preventing issues such as diaper rash, and allow for comfortable usage (Sannino et al., 2009; Caló & Khutoryanskiy, 2015). According to Sannino et al. (2009), the standard weight of a diaper was reduced by 50% with the incorporation of SPH, with leakage values below 2%,

and reduced manufacturing cost. Thus, an increasing market for degradable SPHs has become available due to the high demand of diapers.

The ecological impact of disposable diapers is of great concern; for example, one child accounts for approximately 1092 cubic meters of litter per year (Sannino et al., 2009). Innovative solutions such as cellulose-based hydrogels are currently being explored; Some options include hydroxyethyl cellulose (HEC) and sodium carboxymethylcellulose (NaCMC) crosslinked with divynyl sulfone (DVC). These hydrogels are said to exhibit the similar swelling capacities of SAPs, as well as high water retention, even when applying centrifugal force (Sannino et al., 2009). Furthermore, Pampers and Huggies, disposable diaper companies, account for 57% of the global market share, making lignocellulosic-based hydrogels an attractive area for research (Zohuriaan-Mehr & Kabiri, 2008).

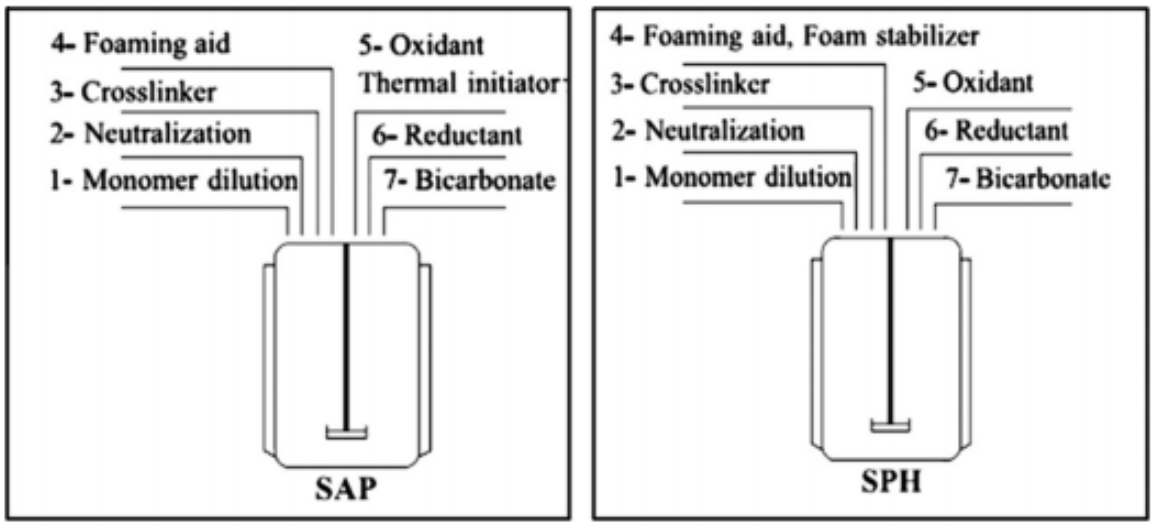

Figure 2.6. Synthesis of SAPs and SPHs (Omidan et al., 2005)

The synthesis for SPHs is similar to that of SAPs, as demonstrated by both processes illustrated in Figure 2.6. The general procedure to produce SAPs requires the use of various process stages. 50 wt.% acrylamide (500 µL) and acrylic acid (50 µL) are first diluted with

deionized water (750 μL) at room temperature under gentle mixing. This is to prevent violent exothermic reactions during bulk polymerization associated with the high heat of polymerization of hydrophilic monomers (Omidian, 2009). The solution is then neutralized to approximately 75 mol%, for which the heat released is absorbed by the internal or external cooling jackets or coils of the double-surfaced reactor. The crosslinker, 1 wt.% bisacrylamide crosslinker, is added to the monomer solution, followed by a foaming aid, such as acetic acid (30 μL) (Omidian, 2009). This is to promote the generation of gas bubbles during polymerization, which helps with the formation of pores within the superabsorbent polymer, a necessary property for efficient water absorption. For the production of homogeneous SPHs, this is often coupled with the addition of a foaming stabilizer, such as 10 wt.% Pluronic F127 (50 μL), a poly(ethylene oxide) and poly(propylene oxide) triblock polymer (PEO-PPO-PEO) (Omidian et al., 2005).

To promote polymerization, SPHs use redox couples, whereas SAPs use both thermal and redox systems. The oxidant, 20 wt.% ammonium persulfate (40 μL), and reductant, 20 v/v% tetramethylenediamine (50 μL) are added to the solution under gentle mixing. For the SAPs, the reaction temperature is increased from 25ºC to 65ºC within 66 seconds at a rate of 1ºC/s, whereas the SPHs is increased from 25ºC to 55ºC within 78 seconds at a rate of 0.7ºC /s (Omidian, 2005).

In order to control the foaming and gelation of the hydrogels, an acid-dependent foaming agent, sodium bicarbonate (35 mg) is added to the mixture. The dispersion and dissolution of bicarbonate increases the pH of the solution, and thus allows for faster decomposition of the initiator. This is because, as more radicals are formed, the polymerization reaction occurs more rapidly, resulting in an increase in viscosity of the mixture. Thus, sodium bicarbonate reacts with

the acidic components, forming carbon dioxide gas which essential to the blowing process (Omidian, 2005).

The post-synthesis treatment for SAPs and SPHs may be compared by the process steps demonstrated in Figure 2.7. SPHs normally undergo dehydration before the drying process by soaking in a non-solvent, such as ethanol. This allows for stabilization of the foamed product and prevents shrinking. Following dehydration, the resulting product becomes a solid and brittle porous structure, which may then be processed as ground particle (such as SAPs), or absorbent sheet (Omidian et al., 2005).

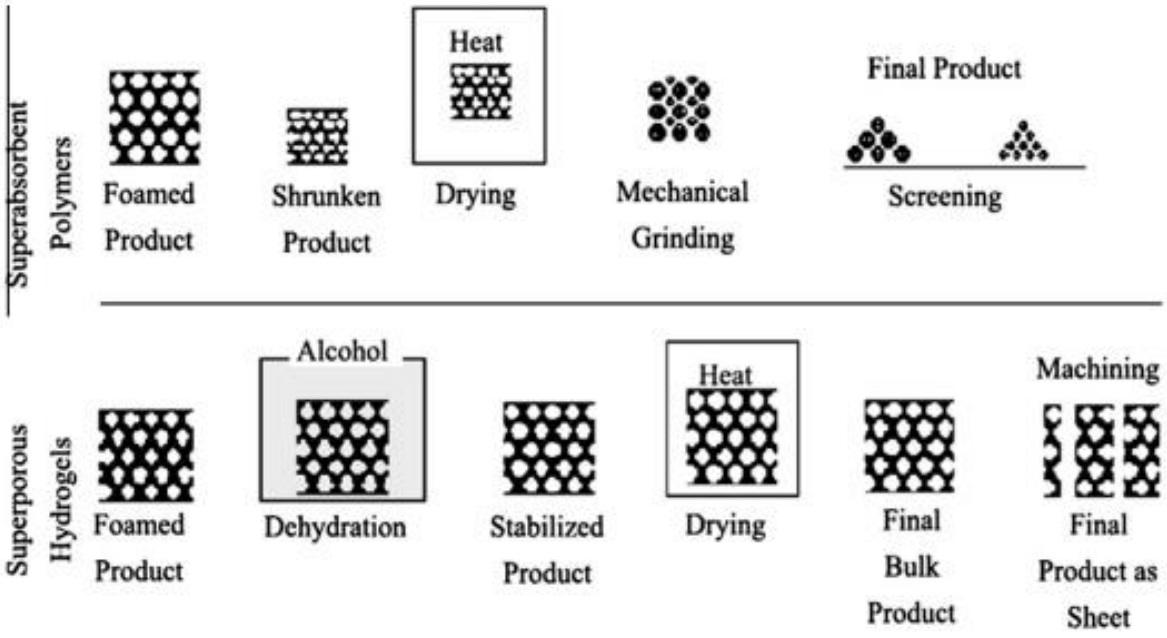

Figure 2.7. Post-synthesis treatment for SAPs and SPHs (Omidan et al., 2005)

2.5.3 Wound dressings

Hydrogels are largely used as wound care in the form of debriding agents, moist dressings and paste components (Murphy & Evans, 2012). They are considered as optimal candidates for wound dressings due to their capabilities to maintain an appropriate moisture

content, relieve pain, restrain from adhering to the wound surface, as well as adapt to the body's shape (Sussman & Bates-Jensen, 2007; Fernandes et al., 2015). They are efficient in retaining and isolating contaminated exudate within their gel mass through absorption, eliminating contact with bacteria, detritus and odour molecules. Their large water content allows for the transmission of oxygen and vapour to the wounds, in addition to presenting a hydrating and cooling effect, which is particularly beneficial for emergency burns. Hydrogel dressings may also play an important role for treatment of pressure sores, ulcers, surgical and necrotic wounds, lacerations, as well granulating cavity wounds (Osti & Osti, 2004; Caló & Khutoryanskiy, 2015).

Currently, natural and synthetic based hydrogel dressings feature non-adherent properties and antimicrobial-containing agents with water content varying between 70% to 90% (Fernandes et al., 2015). Xylos Corporation has received FDA approval for commercialization of their skin substitute, XCell, based on bacterial cellulose (BC) (Fernades et al., 2015; Hutchens et al., 2006). This material is described to accelerate healing and epithelization while maintaining an appropriate moisture balance. Other forms of bacterial cellulose based dressing are also available in the market, whose sought-after purity and water retention properties are efficient alternatives for wound treatment. These are listed in Table 2.2, along with other cellulose derivative based hydrogel dressings (Fernandes et al., 2015; Hutchens et al., 2006)

Table 2.2. Commercially available cellulose-based hydrogel-containing wound dressings (Fernandes et al., 2015)

Producer	Product Name	Composition
Xylos Corporation	XCell	Water, bacterial cellulose, polyhexamethylenebiguanide
Smith and Nephew	IntraSite Gel	Water, propylene Glycol, sodium carboxymethyl cellulose
ConvaTec	Aquecel Ag	Sodium carboxymethyl cellulose, silver ions (1.2%)
Johnson Johnson	Silvercel	Calcium alginate, carboxymethyl cellulose, silver ions (8%)
ConvaTec	GranuGel	Water, sodium carboxymethyl cellulose, propylene glycol, pectin
BMS/ConvaTec	DuoDERM Gel	Water (81.5%), sodium carboxymethyl cellulose, pectin, propylene glycol
Smith Nephew Healthcare Limited	IntraSite Gel	Water (78%), modified carboxymethyl cellulose (2.3%), propylene glycol (20%)
Coloplast	Purilon Gel	Water (90%), carboxymethyl cellulose, calcium alginate
BioFill, Produtos Biotechnologicos	Biofill	Microbial cellulose
BioFill, Produtos Biotechnologicos	Bioprocess	Microbial cellulose

2.5.3.1 Drug delivery systems

Although various patents and research papers have been produced about hydrogel-based drug delivery systems (DDS), very few have resulted in commercial products. The considerable interest in this topic is due to the capability of hydrogels to exhibit controlled release of material. Drugs may be loaded into the porous polymer mesh and, depending on their characterization, allow for the release of the drug at a specified or varying dosage over time. This may occur via diffusion-controlled, swelling-controlled, chemically-controlled or by environmental-responsive mechanisms (Hoare & Kohane, 2008; Caló & Khutoryanskiy, 2015).

Diffusion-controlled release systems essentially involve a constant de-swelling over time. In other words, the drug may be loaded into the core of the gel in the form of a capsule for instance, and slowly diffuse from the pores of the polymer matrix at a constant rate. The concentration of the drug is the greatest in the center of the capsule in order to allow an even release, as illustrated in Figure 2.8 (Caló & Khutoryanskiy, 2015).

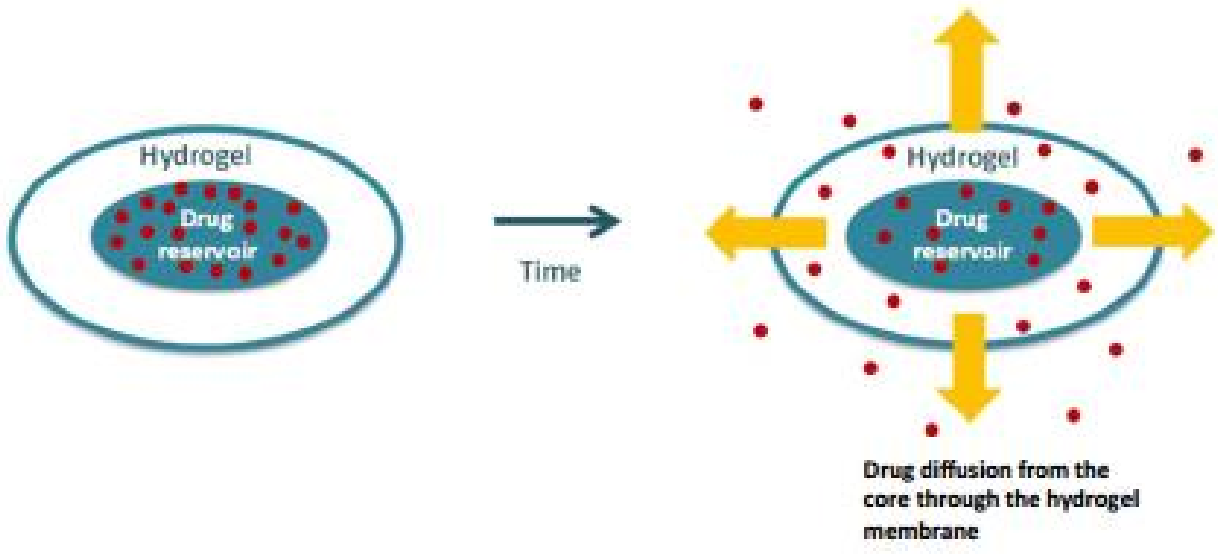

Figure 2.8. Diffusion-controlled drug release (Caló & Khutoryanskiy, 2015)

Swelling-controlled release, on the other hand, employs a slightly different technique which delivers varying drug dosages over a period of time. The drug can be dispersed or dissolved uniformly within the three-dimensional network structure of the hydrogel, as shown in Figure 2.9 (Caló & Khutoryanskiy, 2015). When the gel encounters the bio-fluid, it begins to expand beyond its boundaries, relaxing the polymer chains and allowing for the diffusion of the drug across the macromolecular matrix. In this case, the initial release rate is proportional to the square root of time, making it time-independent unlike the previous diffusion-controlled system (Caló & Khutoryanskiy, 2015).

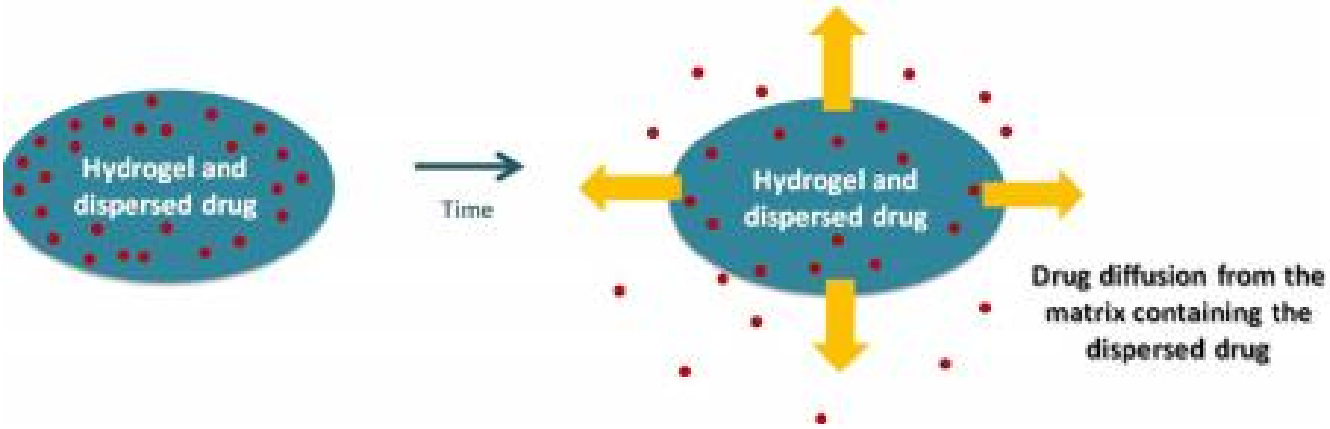

Figure 2.9. Swelling-controlled drug release (Caló & Khutoryanskiy, 2015)

2.5.3.2 Regenerative tissue engineering

Tissue engineering (TE) is a more recent application of hydrogels that has received much attention due to their biocompatibility and potential ability to promote cell development. Damaged tissue may be repaired via space filling agents, which act as scaffolds used for bulking to prevent adhesion as a type of biological glue (Drury & Mooney, 2003; Caló & Khutoryanskiy, 2015). Existing materials used to substitute bone and cartilage normally possess a higher stiffness than those of the surrounding tissues, which impose additional stresses and may result

in mechanical failure (Fernades et al., 2015). Hydrogels, on the other hand, may have contact with human organs without causing undesirable responses or damaging the surrounding tissues (Fernades et al., 2015; Chen et al., 2000). In addition, porosity is a mandatory property for tissue regeneration as it allows for cell attachment to the bulk, as well as the exchange of oxygen and nutrients necessary to cell survival (Fernades et al., 2015). This approach is used to promote tissue formation while the filling agent undergoes slow degradation (Fernades et al., 2015; Caló & Khutoryanskiy, 2015). Recent studies have determined that hydrogels may be injected as liquids and form gels at body temperature and pH, as well as be easily modified using cell adhesion ligands. Certain disadvantages, however, may include poor handling, low mechanical strength, and difficult cell and drug loading within the polymer network structure (Hoffman, 2012).

The ideal system would be to produce an injectable hydrogel, potentially carrying necessary cells required for regeneration within its network structure, and capable of in situ gel formation (Place et al., 2009; Robb et al., 2007). An injectable polymer would provide a less invasive method of applying the filling agent with minimal damage to the surrounding tissue. This would be beneficial if the gel was characterized, under normal body conditions, to fill and mold itself into the irregularly-shaped area (Place et al., 2009). Covalently-bonded chemical gels are produced via UV radiation or by using reactive groups with or without initiators, whereas physical gels may undergo various forms of intermolecular bonding (Hiemstra et al., 2007; Lee et al., 2006; Place et al., 2009). The production of physical hydrogels, however, may be extended to include biological agents such as peptides. In addition, hydrogels can be potentially applied, in some forms, to tissue engineering scaffolds with fibrous, custom, and porous structures (Place et al., 2009).

2.6 Recent advances in lignin-based hydrogels

2.6.1 Crosslinked with N-isopropylacrylamide

Although research on lignin-based hydrogels remains limited, several studies have been conducted on the effect of lignin composition and backbone structure on gel properties and characteristics. For instance, the copolymerization of N-isopropylacrylamide and hardwood kraft lignin via atom transfer radical polymerization (ATRP) was achieved with the use of lignin-macroinitiators prepared by the bromoisobutyryl esterification of the kraft lignin's phenolic hydroxyl groups. The degree of polymerization of poly-N-isopropylacrylamide was found to depend on the dimethylformamide (DMF)/water solvent system for which DP>40 was achieved at 1:4 DMF to water ratio (v/v) (Kim & Kadla, 2010).

Feng et al. (2011) developed hydrogels from acetic acid lignin (AAL) and N-isopropylacrylamide (NIPAAm) with N,N'-methylenebisacrylamide (MBAAm) as a crosslinker and peroxide as the initiator. The conversion efficiency of the hydrogels was reduced from 87.9% to 81.3% with 0.05 g to 0.15 g of AAL, respectively. In addition, the hydrogels containing lower contents of AAL exhibited faster swelling rates (reaching of 42% its total swelling capacity) in 2 hours of experimentation. This reduction in water uptake was attributed to the hydrophobicity of AAL. The deswelling kinetics indicated that the hydrogels with the highest content of lignin retained water 7.2% more than hydrogel without lignin over 10 minutes. The unexpected trend for deswelling might be attributed to the presence of lignin resulted in a decreased density of the gel surface due to the highly porous matrix (Feng et al., 2011). In this analysis, the swelling ratio decreased with increasing temperature for all samples, although lignin was determined to improve the swelling properties of the hydrogels and this behavior was related

to the fact that the hydrogels exhibited a phase change, also known as the lower critical solution temperature (LCST).

2.6.2 Crosslinked with acrylic acid

Ma et al. (2016) studied the controlled release of pesticides from composite porous hydrogels. Commercial alkali lignin from wheat straw was crosslinked with acrylic acid and N, N'-methylenebisacrylamide via free radical polymerization using ammonium persulfate as an initiator. The effect of salt concentration was investigated using potassium chloride; this salt was selected in order to prevent the interference of sodium ions, which may affect the swelling behavior of the composite hydrogels that were neutralized with sodium hydroxide during their preparation (Ma et al., 2016). The swelling capacity of the hydrogels were shown to decrease with increasing the salt concentration, which is attributed to the reduction of osmotic pressure difference between the polymer matrix and the surrounding solution. The polyacrylamide hydrogels (0 wt.% lignin) also achieved a water absorbency of 194.75 g/g at 0.09 mM of potassium chloride, whereas the lignosulfonate-grafted-poly(acrylamide) hydrogels (40 wt. % lignin) absorbed 340.54 g/g (Ma et al., 2016).

Furthermore, the composite hydrogels were loaded with three different pesticides; paraquat, cyfluthrin, and cyhalofopbutyl. The loading capacity and cumulative release was found to be greater for hydrogels containing 40 wt.% lignin compared to those containing 0 wt.% lignin (Sun et al., 2016b). The presence of grafted lignin was also shown to increase the swelling capacity of hydrogels from 180 g/g to 465 g/g for 0 wt.% and 40 wt.% lignin, respectively. Cyfluthrin exhibited the most effective loading capacity of all the studied pesticides, as well as the fasted cumulative release of 53.7% and 84.3% for 3 and 10 days, respectively. The polyacrylamide hydrogels (0 wt.% lignin) were only capable of releasing approximately 50% of

the pesticides, resulting in not only an inefficient delivery, but also potential pesticide pollution due to poor degradability (Sun et al., 2016b).

Sun et al. (2016a) also developed a polyacrylic acid hydrogel containing acid hydrolysis lignin. The addition of lignin was found to greatly improve the surface morphology, the swelling ratio, and the absorption capacity of the hydrogel. The maximum swelling ratio in distilled water was determined to be 392 g/g, whereas the optimum absorbance capacity for Pb(III) was found to be 244.12 mg/g. Further analysis of the absorption kinetics characterized the Langmuir isotherm as a suitable model (Sun et al., 2016a).

Yu et al. (2016) developed lignosulfonate-g-acrylic acid hydrogels by grafting acrylic acid onto lignosulfonate with N,N'-methylenebisacrylamide as a crosslinker and lacase/tert-butyl hydroperoxide (t-BHP) as the initiator. The hydrogels achieved an equilibrium absorbance capacity of 2013 mg/g of methylene blue (MB) for which the Freundlich isotherm model (R^2=0.99) was deemed the best correlation. In other words, the lignosulfonate-g-acrylic acid hydrogels are most likely composed of a heterogenous sorbent surface due to the heterogeneously distributed carboxylic acid groups within lignin's three-dimensional aromatic structure. The kinetic absorption model was also studied, and shown to follow a pseudo second-order trend (R^2=0.999) with a rate constant of 3.53×10^{-5} min^{-1} (Yu et al., 2016).

In addition, the hydrogels exhibited higher absorption capacities with increasing pH. It was determined that at high pH values, the electrostatic repulsion forces are more predominant within the polymer network due to the increased levels of ionized groups, which in turn, results in the electro-osmotic expansion of the hydrogel's three-dimensional network structure (Yu et al., 2016).

2.6.3 Crosslinked with acrylamide and poly(vinyl alcohol)

El-Zawawy (2004) reported a new method of producing green hydrogels with high swelling ratios. Alkaline lignin (AL) and kraft lignin (KL) were crosslinked with acrylamide (AM) and poly(vinyl alcohol) (PVA). The swelling ratio was found to increase with increasing temperature and its optimal rate was ranged between 25 and 35^{o}C. At higher temperatures, the swelling ratio was found to slightly decrease, indicating the breaking of hydrogen bonds due to dominant hydrophobic interactions between polymer chains. In addition, AL hydrogels were found to have a much higher swelling ratio compared to KL, and this behavior was due to the ionized particles and bulk matrix of AL. (El-Zawawy, 2004).

In another study, black liquor from alkaline pulping of rice straw was crosslinked with poly(vinyl alcohol) (PVA) and polyacrylamide (PAAm) to produce hydrogels via following two techniques of crosslinking by radical polymerization and addition reaction. The hydrogels prepared via radical polymerization exhibited higher swelling capacities compared to those prepared by addition reaction (El-Zawawy & Ibrahim, 2011).

2.6.4 Crosslinked with polyethylene glycol diglycidyl ether

Acetic acid lignin based hydrogels crosslinked with polyethylene glycol diglycidyl ether (PEDGE) were also found to swell in both alkaline and aqueous ethanol solutions. When comparing hydrogels containing only the crosslinker, it was determined that lignin offered unique swelling properties in ethanol, which was otherwise unavailable (Nishida et al., 2003).

Passauer et al. (2011) produced both kraft and organosolv based lignin hydrogels by crosslinking them with PEDGE, which were found to be mechanically stable and highly absorbent. The lignin samples were pre-activated with either peroxide treatment under alkaline conditions or by oxidation with peroxide and ferrous ions under weak acidic conditions. This

was found to form gels with much higher swelling capacities than those obtained from unmodified lignin due to the additional hydroxyl ion content. The rheological studies were also conducted and revealed viscoelastic properties and mechanical sturdiness for oxidized lignin hydrogels (Passauer et al., 2011).

The radical co-polymerization of polyethylene glycol (PEG) methyl ether and methacrylamide cathechol with lignin was developed, and studied for drug delivery. The lignin-based hydrogels achieved a good swelling degree of 2400%, and a storage modulus of up to 390 Pa in its swollen state (Marcelo, et al., 2016). The incorporation of magnetic magnetite nanoparticles and cytodextrin macrorings (CD) were found to increase the mechanical properties of the hydrogels, resulting in a storage modulus of approximately 1900 Pa in its swollen state. In addition, the hydrogels demonstrated a high loading capacity of doxorubicin, 0.6 mg/g, and exhibited a controlled temporal release of the drug (Marcelo, et al., 2016).

2.6.5 Crosslinked with ethyleneglycol dimethacrylate

The graft copolymerization of acetic acid lignin (AAL) and acrylamide was also performed with hydrogen peroxide as the initiator and ethyleneglycol dimethacrylate (EGDMA) as the crosslinker. The thermal stability and pore size of the hydrogels were shown to be independent of the AAL, whereas the swelling ratio decreased with increasing AAL to acrylamide ratio (Feng et al., 2014). In addition, the absorption of methylene blue (MB) was demonstrated to favor high AAL content with a maximum absorption capacity of 29.65 mg/g of MB (based on the weight of the hydrogel sample). The absorption equilibrium data was also demonstrated a strong correlation of the Langmuir isotherm model (R^2=0.99), suggesting a monolayer coverage of MB onto the hydrogel. Furthermore, at 75 mg/L MB, the absorption

kinetics of the AAL-based hydrogels followed a pseudo-second order model (R^2=0.99) with a rate constant of 0.0002 min^{-1} (Feng et al., 2014).

2.6.6 Crosslinked with polyurethane

Acetic acid lignin (AAL) based hydrogels crosslinked with polyurethane ionomers (IPUI) was also studied as a coating for ammonium sulfate fertilizer. It was determined that sodium sulfate produced strong bonding characteristics with the AAL based hydrogels (Peng & Chen, 2015). The gel content was found to decrease with AAL composition due to its lower crosslinking density which resulted in lower molecular weight polymers and unreacted lignin. The effect of temperature and pH were also evaluated, demonstrating lignin improved the thermostability of the gels, but less swelling occurred with low pH values.

The hydrogels were also found to have increased swelling with increasing AAL content but up until a maximum composition of 35% (Peng & Chen, 2015). The release ratio of the gels was studied by showering the sample with distilled water every 15 minutes. It was determined that an increase ammonium sulfate also resulted in an increased release ratio; this is because the resistance of the fertilizer permeating through the gel layer was decreased when the amount fertilizer contained within the gel was greater. The AAL content was determined to decrease the release ratio, which demonstrated similar characteristics to their swelling properties (Peng & Chen, 2015). In addition, a US patent was also developed for similar applications. DelliColli et al. (1981) patented their technology on alkali lignin based hydrogels for the controlled release of pesticides.

2.6.7 Crosslinked with glutaraldehyde

Yamoto et al. (2000) developed lignin-based hydrogels from a methanol-diluted lignin-phenol-resorcinol (LPR) resin with glutaraldehyde (GA) as a crosslinker. The lignin-based resin was prepared via condensation of unmodified kraft lignin with phenols, and subsequently with resorcinol in an alkaline medium. The hydrogels were found to exhibit reversible contraction-expansion behavior when submerged in ethanol and in water. The higher ethanol concentrations were demonstrated to cause the hydrogels to contract, whereas those containing a larger amount of water resulted in their expansion. (Yamoto et al., 2000).

2.6.8 Effect of crosslinker

Shen et al. (2016) prepared and compared bulk membrane hydrogels based on kraft and ionic-liquid-isolated lignin for the potential applications of drug delivery, wound dressings, and food packaging. The two types of lignin were crosslinked with epichlorohydrin (ECH), polyethylene glycol (PEG)/ECH, and epoxide-terminated PEG (ETPEG), for which the ETPEG crosslinker produced the most absorbingly efficient hydrogels. The water vapor transmission (WVT), an important factor for controlled humidity of the target, of the membranes was studied for both dry and wet hydrogel membranes (Shen et al., 2016). The dry membranes exhibited low WVT between 2.4 to 3.6 mg /cm^2 ·h, making them a good potential material for food packaging due to their capacity to lock in moisture. The dry membrane also falls within the WVT range of commercial occlusive film dressings, 1.82 to 3.59 mg/cm^2·h, an evaporative rate similar to that of skin and suitable for minor wounds. The WVT of the wet hydrogels, on the other hand, was much higher, ranging from 24 to 27 mg/cm^2·h (Shen et al., 2016).

2.6.9 Incorporation of alginate

The enzymatically synthesized lignin model compound dehydrogenate polymer (DHP) from coniferyl alcohol in sodium alginate hydrogel (Alg) was studied as a potential antimicrobial agent in wound treatment. The hydrogel was active against both gram-positive and gram-negative bacterial strains, exhibiting higher activity against the bacterial biofilms than the antibiotics streptomycin and ampicillin. This suggests a potential application as a wound healing agent, which may be administered in suspension or as a gel (Spasojevic et al., 2016)

2.6.10 Incorporation of xanthan gum

Raschip et al. (2013) produced various xanthan-lignin hydrogels containing different species of lignin with epichlorohydrin as the crosslinking agent. It was determined that the thermo-oxidative stability of xanthan gum was increased when lignin was incorporated in the hydrogel (Raschip et al., 2013). Their application in drug delivery was also studied to determine their effectiveness as vanillin carriers; lignin obtained from fiber crops was incorporated with xanthan gum to produce hydrogel films. The resulting gels demonstrated a high swelling capacity in aqueous solvents, although this was reduced with increasing lignin content. In addition, the hydrogels exhibited better retention properties due to lignin. In other words, the percentage and the rate of vanillin released was shown to decrease with increasing lignin content. Furthermore, the antioxidant properties of lignin also allowed for improved biocompatibility for drug delivery (Raschip et al. 2011).

2.6.11 Incorporation of cellulose

In addition to lignin, other lignocellulosic materials have also been incorporated in the formation of hydrogels. The integration of cellulose and hemicellulose in synthetic hydrogels is a

topic that has been more frequently investigated than that of lignin. Recently, however, there has been more studies on the combination of cellulose and/or hemicellulose with traces of lignin. For instance, the release of polyphenols using cellulose-lignin hydrogels was studied with the purpose of applying them for cosmetic and pharmaceutical uses, combining the non-toxic and biocompatible properties of cellulose with the antioxidant and free radical scavenger properties of lignin (Ciolacu et al., 2012). Microcrystalline cellulose was dissolved in a sodium hydroxide solution before being mixed with steam explosion aspen lignin. The mixture was then crosslinked with epichlorohydrin in order to form cellulose-lignin hydrogels. The resulting gels were immersed in a 5% polyphenol solution, extracted from grape seeds, containing 19:1 water to ethanol ratio. These hydrogels produced high swelling capacities and increased with an increase in lignin content. Additionally, the release of polyphenols was also shown to be lignin dependent, showing a similar trend to that of swelling. In other words, the release of polyphenols increased with increasing lignin compositions (Ciolacu et al., 2012).

Uraki et al. (2004) also developed cellulose and lignin-based hydrogels for drug delivery applications. Both urethane and epoxy hydrogels were prepared for hydroxypropylcellulose bearing lignin (HPC-L) and hydroxypropylcellulose (HPC) by crosslinking them with hexamethylene diisocyanate (HDI) and polyethylene glycol diglycidyl ether (PEDGE), respectively. HPC-L gels demonstrated a much larger swelling compared to that of HPC in organic solvents (i.e., ethanol). Since lignin is a hydrophobic polymer, the hydrogels' sensitivity to hydrophobic environments was assumed to be affected by the incorporation of residual lignin. When comparing the different crosslinkers, urethane gels were shown to exhibit a high degree of swelling in the ethanol solution, whereas the epoxy gels resisted swelling even for HPC-L (Uraki et al., 2004). Therefore, the epoxy based hydrogels were considered as the most promising for

DDS and were further analyzed for absorption and release behavior. Cationic methylene blue (MB) and anionic methyl orange (MO) dyes were used for measuring swelling behaviors of epoxy hydrogel formed by HPC and HPC-L crosslinked with PEDGE (Uraki et al., 2006). In general, MB was better absorbed by the gels than MO, although HPC-L based hydrogels were found to have a greater absorption compared to HPC. In other words, the gels were found to favor the absorption of cationic organic materials, its performance also being affected by residual lignin. Therefore, epoxy HPC based hydrogels were found to be more suitable over HPC-L for DDS applications, although the gels must be subject to additional modifications in order to become practical (Uraki et al., 2006).

Cellulose and alkali lignin were co-dissolved with 1-ethyl-3-methulimidazolium acetate [Emim][Ac] and reconstructed with distilled water for the formation of hydrogel beads. Lipase was then immobilized on the beads with varying cellulose and lignin compositions (Park et al., 2015). The loaded content, activity and stability of immobilized lipase were shown to improve greatly at low pH values with increasing lignin compositions. Thus, the cellulose/lignin hydrogel beads were proven to be good support materials for enzyme immobilization through optimization of surface hydrophobicity in order to induce interfacial activation of enzymes and increase their interactions with the hydrogel beads (Park et al., 2015).

Nakosone & Kobayashi (2016) purified sugarcane bagasse to cellulose before dissolving it in a lithium chloride and N,N-dimethylacetamide (DMAc) solution. The hydrogel films were obtained by coagulating the mixture and allowing phase inversion to occur from liquid to solid. In the subsequent purification process, the films underwent a sodium hydroxide treatment varying from 1 to 12 hours, resulting in decreasing residual concentrations of lignin from 1.68% to 0.68%, respectively (Nakosone & Kobayashi, 2016). The effect of lignin residuals on the

hydrogel films' performance was studied, and determined that high lignin content improved the fibroblast cytocompatibility of the cell cultures. Lignin was also found to enhance the mechanical properties of the hydrogels, increasing the tensile strength and elongation from 0.43 N/mm^2 to 0.80 N/mm^2 and 26.5% to 45.2%, respectively. Consequently, the swelling capacity in water was significantly reduced with increasing lignin content, the swelling ratio decreasing from 1525% to 1153% (Nakosone & Kobayashi, 2016).

Composite hydrogels containing a semi-interpermeating network were produced via the in situ polymerization and crosslinking of lignosulfonate-graft-poly(acrylic acid) and hydroxyethyl cellulose (Zhao et al., 2017). The incorporation of lignosulfonate was determined to increase the hydrogels' elastic modulus from 0.15 MPa to 1.55 MPa with acrylic acid to lignosulfonate ratios of 1:0 and 1:1.5, respectively. The fracture stress, on the other hand, increased from 110 kPa to 400 kPa with a critical compression ranging from 63.7% to 84.2%. The mechanical properties, however, were not further increased with ratios less than 1:1.5 of acrylic acid to lignosulfonate, respectively (Zhao et al., 2017).

2.6.12 Incorporation of hemicellulose

Furthermore, absorption studies were investigated to determine the hydrogels' capabilities for removing Congo Red dye. The presence of lignosulfonate was found to improve the absorption capacity of composite hydrogels by increasing the number of homogeneous pores within the crosslinked network structure (Zhao et al., 2017). In addition, it was observed that the increasing content of lignosulfonate resulted in an increased equilibrium swelling ratio in water. The effect of pH was also studied, the overall swelling ratio increasing with pH values ranging from 2.0 to 6.7, but slightly decreasing with pH 6.7 to 8.5 (Zhao et al., 2017). This behavior is due to the free volume of the polymer matrix and the increase of free ions within the carboxyl

groups of the hydrogel, which increase the osmotic pressure on the hydrogen ions. This, in turn, allows for more molecules to be driven into the polymer matrix, and thus explains the increase in swelling with increasing pH. The decrease in swelling ratio, however, is due to the deprotonation of the carboxyl groups at pH 6.7, which would result in the opposite effect (Zhao et al., 2017).

Recently, Farhat et al. (2017) published a study comparing starch, lignin and hemicellulose polymers for the reactive extrusion process of drug delivery hydrogels formulated with citric acid. The degree of hydration for all samples were shown to significantly increase with increasing pH values. At pH 9, the equilibrium hydration degree was 1380% for starch, 590% for lignin, and 446% for hemicellulose. This was due to the electrostatic repulsion caused by the ionized citric acid functional groups within the polymer structure (Farhat et al., 2017). Furthermore, the effect on mechanical properties was also investigated through the correlation the compression modulus with the hydrogels' immersion time in a sodium chloride solution. The compression modulus was shown to decrease with increasing immersion time due to a combination of hydrogel swelling and degradation. In other words, the stiffness of the hydrogels was largely reduced with an increased swollen state and the breakdown of its network structure (Farhat et al., 2017).

In addition, an acetylated hemicellulose-based acrylic acid hydrogel containing sodium lignosulfonate was prepared. Sodium lignosulfonate was demonstrated to have a good physical interaction with acrylic acid, resulting in a high swelling ratio and absorption capacity. The maximum swelling ratio was increased from 210 g/g to 2503 g/g when the mass ratio of sodium lignosulfonate to acrylic acid was increased from 0 to 0.17 (Song et al., 2016). However, when the mass ratio was increased to 0.5, the swelling ratio decreased to 148 g/g due to the potential decrease in surface tension of the absorbed water related to the surface activity of sodium

lignosulfonate. Similarly, the absorption of methylene blue increased from 328 mg/L to 362 mg/L with an increase in the mass ratio from 0 to 0.33, but decreased to 297 mg/L at 0.5. Another potential reasoning may be attributed to the rigid phenyl propane units present in the sodium lignosulfonate polymer (Song et al., 2016). Furthermore, the absorption capacity of the lignin-containing hemicellulose-based hydrogels was found to best follow the Langmuir isotherm model. The reusability of the hydrogels for methylene blue absorption was also investigated, and were found to achieve an 80% recycle efficiency after four recycles (Song et al., 2016).

2.7 Conclusion

Currently, limited information is available on lignin-based hydrogels, but its potential in commercial applications presents a promising avenue for utilization of lignocellulosic materials. Recent studies have employed an array of techniques for crosslinking various types and species of lignin, combined with both synthetic and natural polymers. For instance, lignin has been incorporated with other lignocellulosic materials, such as cellulose and hemicellulose, in the production of smart hydrogels. The integration of lignocellulosic materials in currently developed synthetic gels exhibited additional functionalities such as biocompatibility and degradability. This presents a potential for various commercial applications in the field of both medicine and agriculture. In fact, cellulose-based materials are currently commercially available as wound dressings due to its added antimicrobial properties.

The intrinsic properties of lignin have also exhibited added benefits when incorporated with crosslinked polymers. In some cases, the swelling ratio and absorbance capacity were demonstrated to increase with lignin-containing hydrogels. The incorporation of this natural

polymer also included the added capability for biodegradation, as well as increased activity in the presence of bacterial cultures. Although lignin presents many added benefits, its complex structure and unpredictable behavior remains the major difficulty with its integration in market products. Nonetheless, recent advances in lignin-based hydrogels have proved them to be a potential application for wound dressings, drug delivery, and fertilizers.

2.8 References

Abu-Dalo, M.A., Al-Rawashdeh, N.A.F., Ababneh, A. (2013). Evaluating the performance of sulfonated Kraft lignin agent as corrosion inhibitor for iron-based materials in water distribution systems. Desalination, 313, 105-114

Adebayo, M.A., Prola, L.D.T., Lima, E.C., Puchano-Rossero, M.J., Cataluna, R., Saucier, C., Umpierres, C.S., Vaghetti, S.C.P., da Silva, L.G., Ruggiero, R. (2014). Adsorption of Procion Blue MX-R dye from aqueous solutions from lignin chemically modified with aluminium and manganese. Journal of Hazardous Materials, 268, 43-50.

Alonso, M.V., Oliet, M., Rodriguez, L., Echeverria, J.M. (2004). Use of a Methylolated Softwood Ammonium Lignosulfonate as Partial Substitute in Phenol Resol Resins Manufacture. Journal of Applied Polymer Science, 94, 643-650.

Alonso, M.V., Oliet, M., Rodriguez, L., Garcia, J., Gilarranz, M.A., Rodriguez, R. (2001). Characterization of and Structural Modification of Ammonic Lignosulfonate by Methylolation. Journal of Applied Polymer Science, 82, 2661-2668.

Alonso, M.V., Oliet, M., Rodriguez, L., Garcia, J., Gilarranz, M.A., Rodriguez, R. (2005). Modification of ammonium lignosulfonate by phenolation for use in phenolic resins. Bioressource Technology, 96, 1013–1018.

Buwalda, S.J., Boere, K.W.N., Dijkstra, P.J., Feijen, J., Vermonden, T., Hennik, W.E. (2014). Hydrogels in a historical perspective: From simple networks to smart materials. Journal of Controlled Release, 190, 254-273

Caló, E., Khutoryanskiy, V.V. (2015). Biomedical application of hydrogels: A review of patents and commercial products. European Polymer Journal, 65, 252-267

Calvo-Flores, F. G., Dobado, J. A. (2010). Lignin as renewable raw material. ChemSusChem, 3(11), 1227-1235.

Carraher, C. E. Jr. (2013). Introduction to Polymer Chemistry, 3rd ed., CRC Press Taylor Francis Group: London

Çetin, N.S., Ozmen, N. (2002). Use of Organosolv lignin in phenol-formaldehyde resins for particleboard production-I. Organosolv lignin modified resins. International Journal of Adhension Adhensives, 22, 477-480

Çetin, N.S., Ozmen, N. (2002). Use of Organosolv lignin in phenol-formaldehyde resins for particleboard production-II. Particleboard Production. International Journal of Adhension Adhensives, 22, 481-486

Chakar, F. S., Ragauskas, A. J. (2004). Review of current and future softwood kraft lignin process chemistry. Industrial Crops and Products, 20(2), 131-141.

Chen, J., Blevins, W. E., Park, H., Park, K. (2000). Gastric retention properties of superporous hydrogel composites. Journal of Controlled Release, 64(1), 39-51.

Cherubini, F. (2010). The biorefinery concept: using biomass instead of oil for producing energy and chemicals. Energy conversion and management, 51(7), 1412-1421.

Ciolacu, D., Oprea, A.M., Anghel, N., Cazacu, G., Cazacu, M. (2012). New cellulose-lignin hydrogels and their application in controlled release of polyphenols. Material Science and Engineering C, 32, 462-463

Cornway, M. (2017). Understanding contact lens materials. Optometry Today, 57(8), 81.

Da Silva, L.G., Ruggiero, R., Gontijo, P.M., Pinto, R.B., Royer, Lima, E.C., Fernandez, T.H.M., Calvete, T. (2011). Adsorption of Brilliant Red 2RB dye from water solutions by chemically modified sugarcane bagasse lignin. Engineering Journal, 168, 620-628

Dellicolli, H. T., Dilling, P., Falkehag, S. I. (1981). U.S. Patent No. 4,244,728. Washington, DC: U.S. Patent and Trademark Office

Demirbas, M. F. (2009). Biorefineries for biofuel upgrading: a critical review. Applied Energy, 86, S151-S161.

Drury, J. L., Mooney, D. J. (2003). Hydrogels for tissue engineering: scaffold design variables and applications. Biomaterials, 24(24), 4337-4351.

Du, X., Li, J., Lindstrom, M.E. (2014). Modification of industrial softwood Kraft lignin using Mannich reaction with and without phenolation pretreatment. Industrial Crops and Products, 52, 729-735

El-Zawawy, W. (2015). Preparation of hydrogel from green polymer. Polymers for Advanced Technologies, 16, 48-54

El-Zawawy, W.K., Ibrahim, M.M. (2012). Preparation and Characterization of Novel Polymer Hydrogel from Industrial Waste and Copolymerization of Poly(vinyl alcohol) and Polyacrylamide. Journal of Applied Polymer Science, 124, 4362-4370

Farhat, W., Venditti, R., Mignard, N., Taha, M., Becquart, F., Ayoub, A. (2017). Polysaccharides and lignin based hydrogels with potential pharmaceuticals use as drug delivery system produced by a reactive extrusion process. International Journal of Biological Macromolecules, 104, 564-575

Feng, Q., Chen, F., Wu, H. (2011). Preparation and characterization of a temperature-sensitive lignin-based hydrogel. BioResources, 6(4), 4942-4952

Feng, Q., Li, J., Cheng, H., Chen, F., Xie, Y. (2014). Synthesis and Characterization of Porous Hydrogel Based on Lignin and Polyacrylamide. BioResources, 9(3), 4369-4381

Fernandes, E.M., Pires, R.A., Mano, J.F., Reis, R.L. (2013). Bionanocomposites from lignocellulosic ressources: Properties, applications and future trends for their use in the biomedical field. Progress in Polymer Science, 38, 1415-1441

Gaurino, V., Gloria, A., Raucci, M.G., Ambrosio, L. (2012). Hydrogel-based platforms for the regeneration of osteochondral tissue and intervertebral disc. Polymers, 4(3), 1590-1612

Gosselink, R. J. A., De Jong, E., Guran, B., Abächerli, A. (2004). Co-ordination network for lignin—standardisation, production and applications adapted to market requirements (EUROLIGNIN). Industrial Crops and Products, 20(2), 121-129.

Grishechko, L.I., Amaral-Labat, G., Szczurek, A., Fierro, V., Kuznetsov, B.N., Pizzi, A., Celzard, A. (2013). New tannin-lignin aerogels. Industrial Crops and Products, 41, 347-355

Hamaguchi, M., Cardoso, M. and Vakkilainen, E., 2012. Alternative technologies for biofuels production in kraft pulp mills—Potential and prospects. Energies, 5(7), 2288-2309.

Hayashi, J.; Shoij, T.; Watada, Y.; Muroyama, K. (1997). Preparation of Lignin-Silica Xerogel. 13, 4185−4186.

Hiemstra, C., Zhou, W., Zhong, Z., Wouters, M., Feijen, J. (2007). Rapidly in situ forming biodegradable robust hydrogels by combining stereocomplexation and photopolymerization. Journal of the American Chemical Society, 129(32), 9918-9926.

Hoare, T.R. (2008). Hydrogels in drug delivery: Progress and challenges. Polymer, 49(8), 1993-2007

Hoffman, A.S. (2002). Hydrogels for biomedical applications. Advanced Drug Delivery Reviews, 64, 18-23

Hu, L., Pan, H., Zhou, Y., Zhang, M. (2011). Methods to improve lignin's reactivity as a phenol substitute and as replacement for other phenolic compounds: A brief review. BioResources, 6(3), 3515-3525.

Hutchens, S. A., Benson, R. S., Evans, B. R., O'Neill, H. M., Rawn, C. J. (2006). Biomimetic synthesis of calcium-deficient hydroxyapatite in a natural hydrogel. Biomaterials, 27(26), 4661-4670.

Kamoun, A., Jelidi, A., Chaabouni, M. (2003). Evaluation of the performance of sulfonated esparto grass lignin as a plasticizer-water reducer for cement. Cement and Concrete Research, 33, 995-1003

Kamoun, A., Jelidi, A., Chaabouni, M. (2003). Evaluation of the performance of sulfonated esparto grass lignin as a plasticizer-water reducer for cement. Cement and Concrete Research, 33, 995-1003.

Kim, Y.S., Kadla, J.F. (2010). Preparation of a Thermoresponsive Lignin-Based Biomaterial through Atom Transfer Radical Polymerization. Biomacromolecules, 11, 981-988

Klein, D. (2012). Organic Chemistry, Wiley & Sons: Danvers

Konduri, M., Kong, F., Fatehi, P. (2015). Production of carboxymethylated lignin and its application as a dispersant. European Polymer Journal, 70, 371-383

Konduri, M., Kong, F., Fatehi, P. (2015). Production of carboxymethylated lignin and its application as a dispersant. European Polymer Journal, 70, 371-383.

Kopecek, J. (2009). Hydrogels: From soft contact lenses and implants to self-assembled nanomaterials. Journal of Polymer Science Part A: Polymer Chemistry, 47(22), 5929-5946.

Kouisni, L., Holt-Hindle, P., Maki, K., Paleologou, M. (2012). The Lignoforce system: A new process for the production of high quality lignin from black liquor. Journal of Science & Technology for Forest Products and Processes, 2(4), 6-10

Kumar, S.M.N., Mohanty, A.K., Erickson, L., Misra, M. (2009). Lignin and Its Applications with Polymers. Journal of Biobased Materials and Bioenergy, 3, 1-24

Lee, J., Bae, Y. H., Sohn, Y. S., Jeong, B. (2006). Thermogelling aqueous solutions of alternating multiblock copolymers of poly (L-lactic acid) and poly (ethylene glycol). Biomacromolecules, 7(6), 1729-1734.

Li, X., Pan, X. (2010). Hydrogels based on hemicellulose and lignin from lignocellulose biorefinery: a mini-review. Journal of Biobased Materials and Bioenergy, 4(4), 289-297.

Lin, Z.X., Ouyang, X.P., Yang, D.J., Deng, Y.H., Qiu, X.Q. (2010). Effect of hydroxymethylation of lignin on the properties of lignin-phenol-formaldehyde resins. World Sci-Tech RD, 32(3), 348-351

Lin, Z.X., Ouyang, X.P., Yang, D.J., Deng, Y.H., Qiu, X.Q. (2010). Effect of hydroxymethylation of lignin on the properties of lignin-phenol-formaldehyde resins. World Sci-Tech RD, 32(3), 348-351.

Lin-Gibson, S., Bencherif, S., Cooper, J. A., Wetzel, S. J., Antonucci, J. M., Vogel, B. M., ... Washburn, N. R. (2004). Synthesis and characterization of PEG dimethacrylates and their hydrogels. Biomacromolecules, 5(4), 1280-1287.

Lora, J. H., Glasser, W. G. (2002). Recent industrial applications of lignin: a sustainable alternative to nonrenewable materials. Journal of Polymers and the Environment, 10(1), 39-48.

Ma, Y., Sun, Y., Fu, Y., Fang, G., Yan, X., Guo, Z. (2016). Swelling behaviors of porous lignin based poly(acrylic acid). Chemosphere, 163, 610-619

Malafaya, P. B., Silva, G. A., Reis, R. L. (2007). Natural–origin polymers as carriers and scaffolds for biomolecules and cell delivery in tissue engineering applications. Advanced drug delivery reviews, 59(4), 207-233.

Maldano-Codina, C., Efron, N. (2003)., Hyrogel Lenses – Materials and Manufacture: A Review. Optometry In Practice, 4, (2003); 101-115

Maldonado-Codina, C., Efron, N. (2003). Hydrogel lenses-materials and manufacture: A review. Optometry in Practice, 4, 101-113

Mankar, S. S., Chaudhari, A. R., Soni, I. (2012). Lignin in phenol-formaldehyde adhesives. International Journal of Knowledge Engineering, ISSN, 0976-5816.

Marcelo, G., Lopez-Gonzalez, M., Trabado, I., Rodrigo M.M., Valiente, M., Mendicuti, F. (2016). Lignin inspired PEG hydrogels for drug delivery. Materials Today Communications, 7, 73-80

Masuda, F. (1994). Trends in the development of superabsorbent polymers for diapers. Superabsorbant Polymers, 7, 88-98.

Mathur, A. M., Moorjani, S. K., Scranton, A. B. (1996). Methods for synthesis of hydrogel networks: A review. Journal of Macromolecular Science, Part C: Polymer Reviews, 36(2), 405-430.

McFarlane, I. D., Hamilton, M. A., Carnaby, G. A. (1993). U.S. Patent No. 5,252,215. Washington, DC: U.S. Patent and Trademark Office

Murphy, P. S., Evans, G. R. (2012). Advances in wound healing: a review of current wound healing products. Plastic surgery international, 2012.

Nakasone, K., Kobayashi, T. (2016). Cytocompatible hydrogels containing trace lignin. Material Science and Engineering C, 64, 269-277

Nishida, M., Uraki, Y., Sano, Y. (2003). Lignin gel with unique swelling property. Bioresource Technology, 88, 81-83

Omidian, H., Rocca, J.G., Park, K. (2005). Advances in superporous hydrogels. Journal of Controlled Release, 102, 3-12

Osti, E., Osti, F. (2004). Treatment of cutaneous burns with burnshield (Hydrogel) and a semi-permeable adhesive film. Annals of Burns and Fire Disasters, 17, 137-141.

Pal, K., Singh, V. K., Anis, A., Thakur, G., Bhattacharya, M. K. (2013). Hydrogel-based controlled release formulations: designing considerations, characterization techniques and applications. Polymer-Plastics Technology and Engineering, 52(14), 1391-1422.

Parajuli, D., Kawakita, H., Inoue, K., Funaoka, M. (2006). Recovery of Gold(III), Palladium (II), and Platinum (IV) by Animated Lignin Derivatives. Industrial & Engineering Chemistry Research, 45(19), 6045-6412

Park, K. R., Nho, Y. C. (2003). Synthesis of PVA/PVP hydrogels having two-layer by radiation and their physical properties. Radiation Physics and Chemistry, 67(3), 361-365.

Park, S., Kim, H.E., Kim, J.H., Yu, H., Kim, H.J., Yang, Y.-H., Kim, Y.H., Ha, S.H., Lee, S.H. (2015). Application of cellulose/lignin hydrogel beads as novel supports for immobilizing lipase. Journal of Molecular Catalyst B: Enzymatic, 119, 33-39

Passauer, L., Fischer, K., Liebner, F. (2011). Preparation and physical characterization of strongly swellable oligo(oxyethylene) lignin hydrogels. Holzforschung, 65, 309-317

Passauer, L., Struch, M., Schuldt, S., Appelt, J., Schneider, Y., Jaros, D., Rohm, H. (2012). Dynamic Moisture Sorption Characteristics of Xerogels from Water-Swellable Oligo(oxyethylene) Lignin Derivatives. ACS Applied Material & Interfaces, 4, 5852-5862

Peng, Z., Chen, F. (2011). Synthesis and Properties of Lignin-Based Polyurethane Hydrogels. International Journal of Polymeric Materials, 60, 674-683

Peppas, N. A., Hilt, J. Z., Khademhosseini, A., Langer, R. (2006). Hydrogels in biology and medicine: from molecular principles to bionanotechnology. Advanced materials, 18(11), 1345-1360.

Peppas, N. A., Khare, A. R. (1993). Preparation, structure and diffusional behavior of hydrogels in controlled release. Advanced drug delivery reviews, 11(1-2), 1-35.

Place, E.S., George, J.H., Williams, C.K., Stevens, M.M. (2009). Synthetic polymer scaffolds for tissue engineering. Chemical Society Review, 38, 1139-1151

Qin, Y., Yang, D., Guo, W., Qiu, W. (2015). Investigation of grafter alkali sulfonated lignin polymer as a dispersant in coal-water slurry. Journal of Industrial and Engineering Chemistry, 27, 292-200.

Ragauskas, A. J., Beckham, G. T., Biddy, M. J., Chandra, R., Chen, F., Davis, M. F., Davidson, B.H., Dixon, R.A., Gilna, P., Keller, M., Langan, P, Naksar, A.K., Saddler, J.N., Tschaplinski, T.J., Tuskan, G.A., Wyman, C.E. (2014). Lignin valorization: improving lignin processing in the biorefinery. Science, 344(6185), 1246843

Rani, M., Agarwal, A., Negi, Y. S. (2010). Chitosan based hydrogel polymeric beads–As drug delivery system. BioResources, 5(4), 2765-2807.

Raschip, I.E., Hitruc, G.E., Oprea, A.M., Popescu, M.-C, Vasile, C. (2011). In-vitro evaluation of the mixed xanthan/lignin hydrogels as vanillin carriers. Journal of Molecular Structure, 1003, 67-74

Raschip, I.E., Hitruc, G.E., Vasile, C., Popescu, M.-C. (2013). Effect of the lignin type on the morphology and thermal properties of the xanthan/lignin hydrogels. International Journal of Biological Macromolecules, 54, 230-237

Rastogi, S., Dwivedi, U. N. (2008). Manipulation of lignin in plants with special reference to O-methyltransferase. Plant Science, 174(3), 264-277.

Robb, S. A., Lee, B. H., McLemore, R., Vernon, B. L. (2007). Simultaneously physically and chemically gelling polymer system utilizing a poly (NIPAAm-co-cysteamine)-based copolymer. Biomacromolecules, 8(7), 2294-2300.

Rosiak, J. M., Ulański, P., Pajewski, L. A., Yoshii, F., Makuuchi, K. (1995). Radiation formation of hydrogels for biomedical purposes. Some remarks and comments. Radiation Physics and Chemistry, 46(2), 161-168.

Rosiak, J. M.,Yoshii, F. (1999). Hydrogels and their medical applications. Nuclear Instruments and Methods in Physics Research Section B: Beam Interactions with Materials and Atoms, 151(1), 56-64

Saeed, A., Fatehi, P., Ni, Y. (2011). Chitosan as a flocculant for pre-hydrolysis liquor of kraft-based dissolving pulp production process. Carbohydrate Polymers, 86(4), 1630-1636.

Sannino A., Demitri C., Madagheile M. (2009). Biodegradable Cellulose-based Hydrogels: Design and Applications. Materials, 2, 353-373

Scholtz, S., & Auffarth, G. U. (2012). Fifty years of soft contact lenses: Life and impact of Prof. Otto Wichterle. Acta Ophthalmologica, 90, 58.

Sewalt, V. J., Oliveira, W. D., Glasser, W. G., Fontenot, J. P. (1996). Lignin Impact on Fibre Degradation: 2--A Model Study Using Cellulosic Hydrogels. Journal of the Science of Food and Agriculture, 71(2), 204-208.

Shen, X., Berton, P., Shamshina, J.L., Rogers, R.D. (2016). Preparation and comparison of bulk and membrane hydrogels based on Kraft- and ionic-liquid-isolated lignins. Green Chemistry, 18, 5607-5620

Shewan, H.M, Stokes, J.R. (2013). Review of techniques to manufacture micro-hydrogel particles for the food industry and their applications. Journal of Food Engineering, 119(4), 781-792

Sixta, H. (2006). Handbook of Pulp, vol. 1, Wiley-VCH: Weinheim

Smook, G. (2002). Handbook for pulp and paper technologists, 3rd ed., Angus Wilde Publications Inc.: Vancouver

Song, X., Chen F., Liu, S. (2016). A Lignin-containing Hemicellulose-based Hydrogel and its Adsorption Behavior. BioResources, 11(3), 6378-6392

Spasojevic, D., Zmejkoski, D., Glamoclija, J., Nikolic, M., Sokovic, M., Milosevic, V., Jaric, I., Stojanovic, M. (2016). Lignin model compound in alginate hydrogel: a strong antimicrobial agent with high potential in wound treatment. International Journal of Antimicrobial Agents, 48, 732-735

Stewart, D. (2008). Lignin as a base material for materials applications: Chemistry, application and economics. Industrial crops and products, 27(2), 202-207.

Sun, Y., Ma, Y., Fang, G., Li, S., Fu, Y. (2016a). Hydrolysis lignin-g-PAA hydrogel. BioResources, 11(3), 5731-5742

Sun, Y., Ma, Y., Fang, G., Ren, S., Fu, Y. (2016b). Controlled Pesticide Release from Porous Composite Hydrogels Based on Lignin and Polyacrylic Acid. BioResources

Sussman, C., Bates-Jensen, B. M. (2007). Wound care: a collaborative practice manual. Lippincott Williams Wilkins: New York.

Tejado, A., Pena, C., Labidi, J., Echeverria, J.M., Mondragon, I. (2007). Physico-chemical characterization of lignins from different sources for use in phenol-formaldehyde resins synthesis. Bioresource Technology 98, 1655–1663

Thakur V.K., Thakur M.K. (2015). Recent advances in green hydrogels from lignin: a review. International Journal of Biological Macromolecules, 72, 834-847

Thielemans, W., Can, E., Morye, S. S., Wool, R. P. (2002). Novel applications of lignin in composite materials. Journal of Applied Polymer Science, 83(2), 323-331.

Tomani, P. (2010). The lignoboost process. Cellulose chemistry and technology, 44(1-3), 53-58

Uliniuc, A., Popa, M., Hamaide, T., Dobromir, M. (2012). New approaches in hydrogel synthesis—Click chemistry: A review. Cellulose Chemistry and Technology, 46(1), 1.

Uraki, T., Imura, T., Kishimoto, T., Ubukta, M. (2004). Body temperature-responsive gels derived from hydroxypropylcellulose bearing. Carbohydrate Polymers, 123-130

Uraki, T., Imura, T., Kishimoto, T., Ubukta, M. (2006). Body temperature-responsive gels derived from hydroxypropylcellulose bearing lignin II: absorption and release behaviour. Cellulose 13, 225-234

Vishtal, A. G., Kraslawski, A. (2011). Challenges in industrial applications of technical lignins. BioResources, 6(3), 3547-3568.

Vishtal, A., Kraslawski, A. (2011). Challenges in Industrial Applications of Technical Lignin. BioResources, 6(3), 3547-3568

Wagner, E.P. (2013). An Introduction to Polymer Processing, Morphology and Property Relationships through Thermal Analysis of Plastic Polyethylene Terephthalate (PET) Bottles. Department of Chemistry, University of Pittsburgh

Wang, M., Leitch, M., Xu, C. C. (2009). Synthesis of phenol–formaldehyde resol resins using organosolv pine lignins. European Polymer Journal, 45(12), 3380-3388.

White, E.M., Yatvin, J., Grubbs, J.B., Bilbrey, J.A., Locklin, J. (2013). Advances in smart materials: Stimuli-responsive hydrogel thin films. Part B: Journal of Polymer Science, 51(14), 1084-1099

Wu, H., Chen, F., Feng, Q., Yue, X. (2012). Oxidation and sulfomethylation of alkali-extracted lignin from corn stalk. BioResources, 7(3), 2742-2751

Yamoto, H., Amaike, H., Saitoh, H., Sano, H. (2000). Gel formation of lignin and biodegradation of the lignin gels by microorganisms. Materials Science and Engineering C, 7, 143-147

Yu, C., Wang, F., Zhang, C., Fu, S., Lucia, L.A. (2016). The synthesis and absorption dynamics of a lignin-based hydrogels for remediation of cationic dye-contaminated effluent. Reactive and Functional Polymers, 106, 137-142

Yu, G., Li, B., Wang, H., Liu, C., Mu, X. (2013). Preparation of Concrete Superplasticizer by Oxidation-Sulfomethylation of Sodium Lignosulfonate. BioResources, 8(1), 1055-1063.

Yu, Y., Lou, X., and Wu, H. (2008). Some Recent Advances in Hydrolysis of Biomass in Hot-Compressed Water and Its Comparisons with Other Hydrolysis Methods. Energy and Fuels, 22, 46-60

Zao, J., Zheng, K., Nan, J., Tang, C., Chen, Y., Hu, Y. (2017). Synthesis and characterization of lignosulfonate-graft-poly(acrylic acid)/hydroxyethyl cellulose semi-interpenetrating hydrogels. Reactive and Functional Polymers, 115, 28-35

Zhu Ryberg, Y. Z., Edlund, U., Albertsson, A. C. (2011). Conceptual approach to renewable barrier film design based on wood hydrolysate. Biomacromolecules, 12(4), 1355-1362.

Zohuriaan-Mehr, M. J., Kabiri, K. (2008). Superabsorbent polymer materials: a review. Iranian Polymer Journal, 17(6), 451.

3 EXPERIMENTAL METHODOLOGY

3.1 Materials

Mixed hardwood kraft lignin (LGN) was supplied by FPInnovations' pilot scale plant located in Thunder Bay, ON. N-isopropylacrylamide (NIPAAm, 97%), N,N'-methylenebisacrylamide (MBAAm, 99%), azobisisobutyronitrile (AIBN, 98%), acetone (97%), dimethyl sulfoxide-d_6 (DMSO, 99.9% atom D), and tetramethylthionine chloride (methylene blue, MB) were obtained from Sigma-Aldrich. Sulfuric acid (98%) and sodium hydroxide (97%) were also obtained from Sigma-Aldrich and diluted with deionized water to 20% and 10%, respectively.

3.2 Crosslinking reaction

In this set of experiments, 0.1 g of kraft lignin, 0.06 g of N,N'-methylenebisacrylamide and varying concentrations of N-isopropylacrylamide (1.2 – 2.4 g) were dissolved in a round bottom flask with deionized distilled water. Water was added into the flask until the total mass of 40 g (including the weight of the reactants) were placed in the reactor. The pH of the solutions was then adjusted with 20% sulfuric acid and 10% sodium hydroxide (to pH 2.0 – 3.0) before being purged with nitrogen gas for 30 minutes. The flask was placed in a water bath and heated to the desired temperature before adding 0.08 g of the azobisisobutyronitrilec (AIBN) initiator.

The reaction was then allowed to proceed at the steady state temperature (65^{o}C – 85^{o}C) with a constant flow of nitrogen gas and stirring at 220 rpm. This procedure was repeated for samples with and without lignin. Table 3.1 lists the reaction parameters.

Table 3.1. Reaction parameters

Level	Temperature, ^{o}C	Time, h	NIPAAm content, g	pH
1	65	3	1.2	2.0
2	75	4	1.8	2.5
3	85	5	2.4	3.0

After completion, the hydrogel samples were extracted from the flasks and rinsed with acetone to remove unreacted monomers. The hydrogels were then rinsed with water to prevent further degradation, and frozen overnight. Once completely frozen, they were freeze dried at -50^{o}C for over 24 hours in a Labconco FreeZone 1L freeze dryer.

3.3 Elemental analysis

The prepared freeze-dried hydrogel samples were ground to powder, and 0.002 g of powdered hydrogel was measured in silver vessels of the elemental analyzer. The samples were loaded into the Elementar Vario El Cube elemental analyzer where they were scorched at 1200^{o}C within a combustion chamber. The resulting gases were then reduced and analyzed for their nitrogen content.

3.4 ^{1}H nuclear magnetic resonance spectroscopy

The prepared freeze-dried hydrogel samples were ground to powder before being dissolved in 0.5 g of deuterated dimethyl sulfoxide (DMSO-d_6), and placed into a 5 mm, 500 MHz glass NMR tube. The sample-containing tubes were inserted into the magnet of a Varian Unity INOVA 500 MHz spectrometer. The ^{1}H NMR spectra of the samples were acquired at a

15^{o} pulse flipping angle, a 4.6 μm pulse width, a 2.05 acquisition time, and 1 s relaxation delay time.

3.5 Experimental design and statistical analysis

The Taguchi L9 orthogonal design was performed with four factors (each containing three levels) to investigate the effect of reaction parameters on the responses of yield and maximum swelling ratio. The four factors studied are the reaction temperature, time, N-isoproylacrylamide (NIPAAm) content and pH, as shown in Table 3.2. This Taguchi L9 model was applied for two separate experimental design experiments, the control and the lignin-based hydrogels. The range of analysis was optimized by evaluating the signal-to-noise (SN) ratio to maximize the responses of each model. The results of the applied SN ratio, which is elaborated in the discussion section, determined samples 3C and 6C, as well as 2L and 9L, to be produced under the optimum conditions for the control and lignin-based hydrogels, respectively.

Table 3.2. Taguchi L9 orthogonal design parameters

Run	Temperature, ^{o}C	Time, h	NIPAAm content, g	pH
1	65	3	1.2	2.0
2	65	4	1.8	2.5
3	65	5	2.4	3.0
4	75	3	1.8	3.0
5	75	4	2.4	2.0
6	75	5	1.2	2.5
7	85	3	2.4	2.5
8	85	4	1.2	3.0
9	85	5	1.8	2.0

3.6 Yield

After completing the reaction, the prepared hydrogel samples were left in their respective round bottom flasks used during the reactions, and the remaining water was drained. The flasks containing the samples were then dried overnight at 60^{o}C to remove excess moisture. Once dried, the samples were removed, and left to cool for 30 minutes before recording their final weight. The weight of the hydrogel was determined by subtracting the recorded weight by the weight of the empty flask. The weight of the dried hydrogel was then divided by the initial weight of the reactants and initiator added before the start of the reaction, as such:

$$\text{Yield}(\%) = \frac{W_{\text{Hydrogel}}}{W_{\text{LGN}} + W_{\text{NIPAAm}} + W_{\text{MBAAm}} + W_{\text{AIBN}}} \times 100\% \quad (3.1)$$

Where $W_{Hydrogel}$ is the total dry weight of the hydrogel (g), and W_{LGN}, W_{NIPAAm}, W_{MBAAm}, W_{AIBN} are the initial weight of kraft lignin, N-isopropylacrylamide, N,N'-methylenebisacrylamide, and azobisisobutyronitrile, respectively.

3.7 Swelling ratio

The dried hydrogel samples were cut and divided into samples weighing approximately 0.2 g. The dried samples (with a known weight) were placed into tea infusers purchased from the market, and immersed into 200 mL of deionized water for 24 hours.

The weight of the infusers containing the hydrogels were measured periodically over 24 hours. This was conducted by removing the infusers from water, allowing them to drain, and wiping the excess water before placing them on the balance. The infusers were then placed back in the water-containing beaker.

To determine the weight of the swollen hydrogels, the total weight was subtracted from the dry weight of the tea infuser. The swollen weight of the hydrogel samples was then subtracted and divided by its dry weight to determine the amount of water contained per gram of hydrogel, also known as swelling ratio, Q:

$$Q = \frac{W_{swollen} - W_{dry}}{W_{dry}} \tag{3.2}$$

Where $W_{swollen}$ is the weight of the swollen hydrogel, and W_{dry} is the initial weight of the dry hydrogel.

3.8 Brunauer–Emmett–Teller (BET) analysis

The surface area of the hydrogel particles was determined by using a Quantachrome surface area analyzer, Nova 2200e, instrument. The dried hydrogels were first ground to a

powder and passed through multiple sieves. The size fraction between 150 μm and 300 μm was selected to allow for a less size variation within the sample for more accurate analysis. For each test, 0.05 g of the powdered sample were measured. The specific surface area of the samples was then analyzed according to Branuer-Emmett-Teller (BET) method via adsorption-desorption isotherms using nitrogen gas at -180 °C with relative pressure range of 0.01 to 0.99.

3.9 Fourier transform infrared spectroscopy

Fourier Transform Infrared Spectroscopy (FTIR) analysis was conducted for all selected hydrogel samples, reactants, and initiator. Approximately 0.001 g of dried powdered samples were analyzed using a Bruker Tensor 37 (Germany, ATR accessory). The IR spectra was recorded in transmittance mode within the wavelength range of 500 cm^{-1} and 4000 cm^{-1} with a 4 cm^{-1} resolution.

3.10 Absorption equilibrium

The absorption isotherm model of the hydrogels was investigated using methylene blue dye. First, a calibration curve was developed to relate the concentration of methylene blue to its absorbance at a wavelength of 664 nm using a Genesys 10S UV-Vis spectrometer (Thermo Scientific). The recorded absorbance was plotted with respect to the predetermined concentration for which the linear correlation exhibited a slope 0.25 (R^2=0.99).

In each experiment, approximately 0.2 g of the hydrogel sample was stirred at 100 rpm for 3 days in a 100 mL solution of methylene blue with a predetermined concentration. Afterwards, 2 mL of the methylene blue solution was diluted in a 25mL volumetric flask. The absorbance of the diluted solution was recorded, and the corresponding concentration was

obtained using the calibration curve. The equilibrium absorption capacity of methylene blue, q_e, was calculated using Eq. (3.3):

$$q_e = \frac{(C_0 - C_e)V}{m} \tag{3.3}$$

Where C_0 and C_e are the initial and equilibrium concentrations of methylene blue, V is the total volume of the solution, and m is the mass of the hydrogel.

3.11 Focused beam reflectance measurement

The swelling behavior of the powdered hydrogels were analyzed using a Mettler Toledo FBRM Particle Track. The dried hydrogels were ground to a powder and passed through multiple sieves to distribute the particles. The size fraction between 150 µm and 300 µm was selected to allow for less size variation within the sample in this analysis. For each test, 0.05 g of the powdered sample were used.

The FBRM probe and attached stirrer were fixed vertically in a beaker containing 200 mL of distilled water. The stirrer was set to 100 rpm and the powdered hydrogel sample was added. After adding, the hydrogels absorbed water and their size enlarged. The FBRM was used to monitor this size changes, and the FBRM software measured the 'unweighted' chord length distribution at 10 second intervals and calculated the number of counts for six size ranges: less than 10, 10 to 50, 50 to 150, 150 to 300, 300 to 1000, and greater than 1000 microns.

3.12 Thermogravimetric analysis

The dried powdered hydrogel samples were placed in a desiccator overnight before undergoing thermal analysis using a thermogravimetric analyzer (TGA i-1000 series, Instrument

Specialist Inc.). Approximately, 0.008 g of sample was heated at a constant flow rate of nitrogen (35 mL/min) from room temperature to 700ºC at a rate of 10ºC/min.

3.13 Differential scanning calorimetry

The thermal behaviour of the dried powdered hydrogels was examined using a differential scanning calorimeter (DSC), TA instrument Q2000, and RC standard cell. The samples were first placed in a desiccator overnight to remove excess moisture, and 0.007 g of sample was measured onto a Tzero aluminium pan. The hydrogels were heated within the range of 50ºC and 275ºC at a rate of 5ºC/min, and a constant flow rate of nitrogen (50mL/min).

3.14 Rheology

The TA Instruments' Discovery HR-2 hybrid rheometer, with a peltier temperature control system, was used for analyzing the viscoelastic properties of control and lignin-based hydrogels that were selected from the experimental design. The upper geometry was a 40mm steel parallel plate with a gap of 1 mm and a loading gap of 60 mm. The dynamic oscillatory measurements were carried out at a constant temperature of 25ºC, unless stated otherwise. In addition, all hydrogel samples utilized for these tests were saturated in deionized water. The hydrogel was loaded onto the peltier plate, which covered the surface area of the parallel plate. Approximately, the same amount of the hydrogel sample with similar thickness was loaded on the Peltier plate for each test. The details and conditions applied for each rheological test in this study are explained in the results section.

3.14.1 Frequency sweep

Rheological measurements were carried out at a shear stress of 0.2 Pa throughout the frequency range of 0.2 and 20 Hz (1.267 to 125.7 rad/s).

3.14.2 Amplitude sweep

Mechanical spectra were obtained at a constant frequency mode of 10 rad/s over a strain rate range of 0.01 and 1000%.

3.14.3 Temperature ramp

Rheological measurements were recorded at a constant strain rate of 2%, with a low frequency of 10 rad/s over a temperature range of 0 and 50ºC. The temperature ramp rate was 5ºC/min.

3.14.4 Structure recovery

The structure recovery of the hydrogel samples was determined by an oscillatory step change at a constant frequency of 10 rad/s. The samples underwent a 1% deformation for 60 seconds before undergoing 100% deformation over the following 60 seconds. Subsequently, the strain rate was again reduced to 1% to monitor the structural recovery of the deformed hydrogel.

4 RESULTS AND DISCUSSION

4.1 Free radical polymerization

The free radical polymerization mechanism of the lignin-based hydrogels is demonstrated in Figure 4.1. Azobisisobutyronitrile (AIBN) first undergoes thermal decomposition to generate radicals, which initiates the polymerization. Figure 4.1(a) demonstrates the thermal decomposition of the azo compounds with the addition of heat, producing two 2-cyanoprop-2-yl radicals and nitrogen gas. Since the bond strength between azo compounds is high, this dissociation can be attributed to the formation of nitrogen as a stable molecule (Odian, 2004).

In Figure 4.1(b), the 2-cyanoprop-2-yl radicals form the crosslinked network structure by attacking the carbon double bonds found in the end groups of N-isopropylacrylamide and N,N'-methylenebiscrylamide. This allows for the formation of radicals at the end of the segment enabling the propagation step. The 2-cyanoprop-2-yl radicals may also abstract hydrogen from the hydroxyl group located on lignin's aromatic ring. This creates a free radical site on the oxygen atom, which then forms an epoxy group (Odian, 2004). The radical polymerization is most commonly terminated through the combination of two active chains (Carraher et al., 2002). This may result in smaller homopolymers, which are similar in structure as the crosslinked hydrogels. In addition, termination may occur via interaction with the pH adjustment chemicals present in solution (i.e., sulfuric acid and sodium hydroxide). As a result, additional homopolymers may formed if these chemicals react readily with 2-cyanoprop-2-yl radicals.

(a)

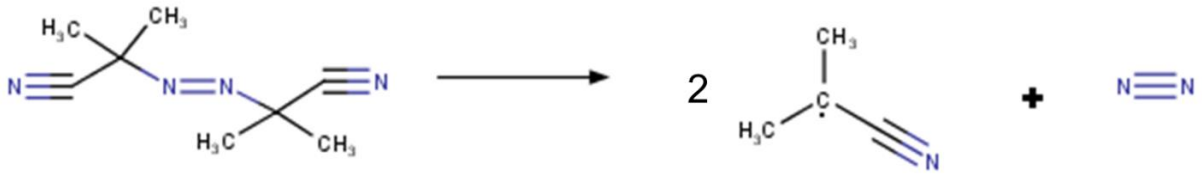

(b)

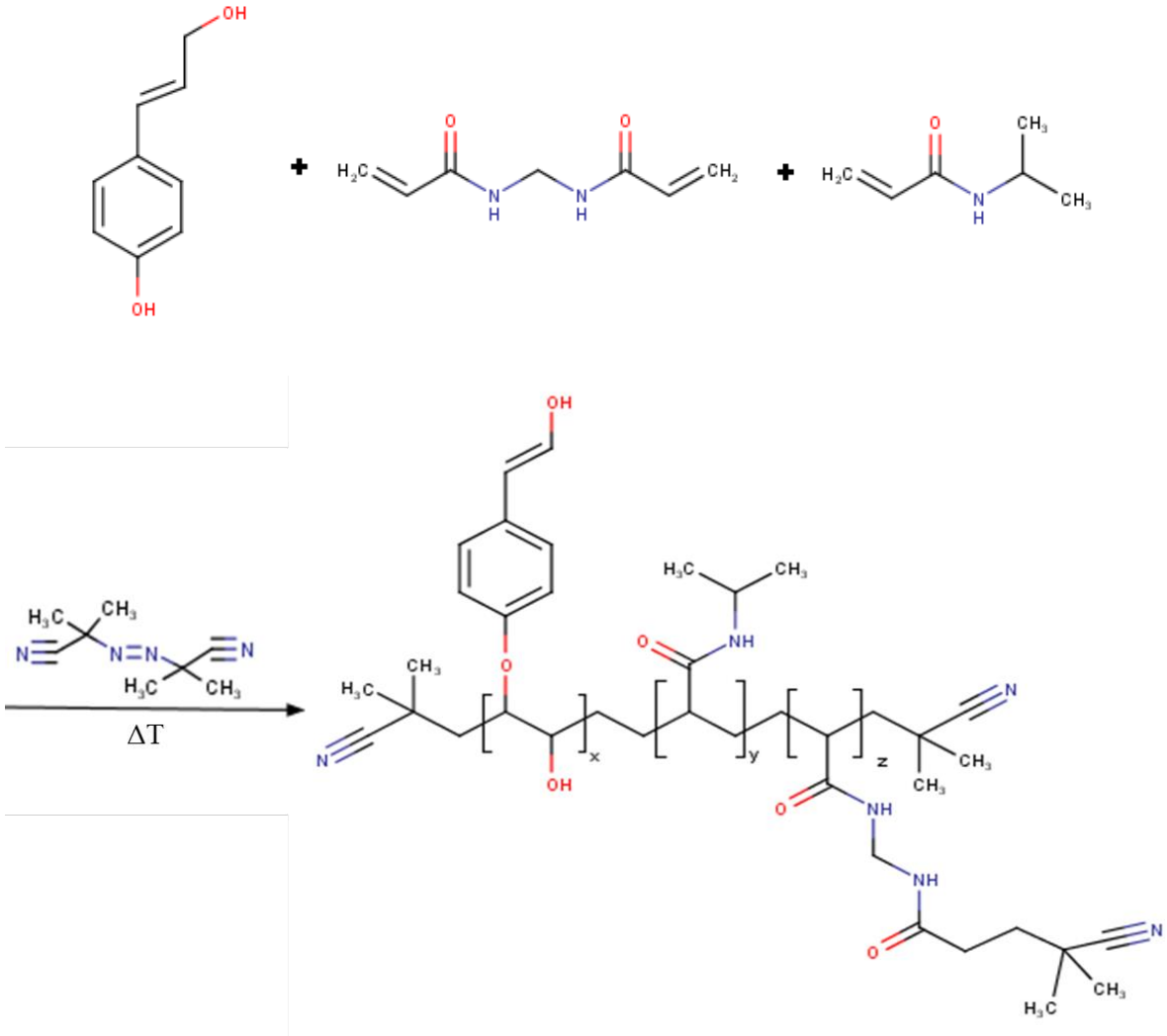

Figure 4.1. Radical polymerization reaction of the lignin-based hydrogels: (a) Decomposition of AIBN initiator, (b) Crosslinking reaction mechanism

4.2 Nitrogen content

Figure 4.2 shows the nitrogen content of the hydrogel samples. Control samples have a slightly higher nitrogen content (an average of 11.4 wt.%) compared to that of the lignin-based hydrogels (an average of 10.6 wt.%). This difference is most likely due to the addition of lignin, which reduces the overall percentage of the nitrogen-based compounds within the hydrogel.

In addition, the overall nitrogen content for the control and lignin-based hydrogels does not exhibit a significant change between runs. This most likely means that the degree of crosslinking of the hydrogels is similar with respect to its bulk mass.

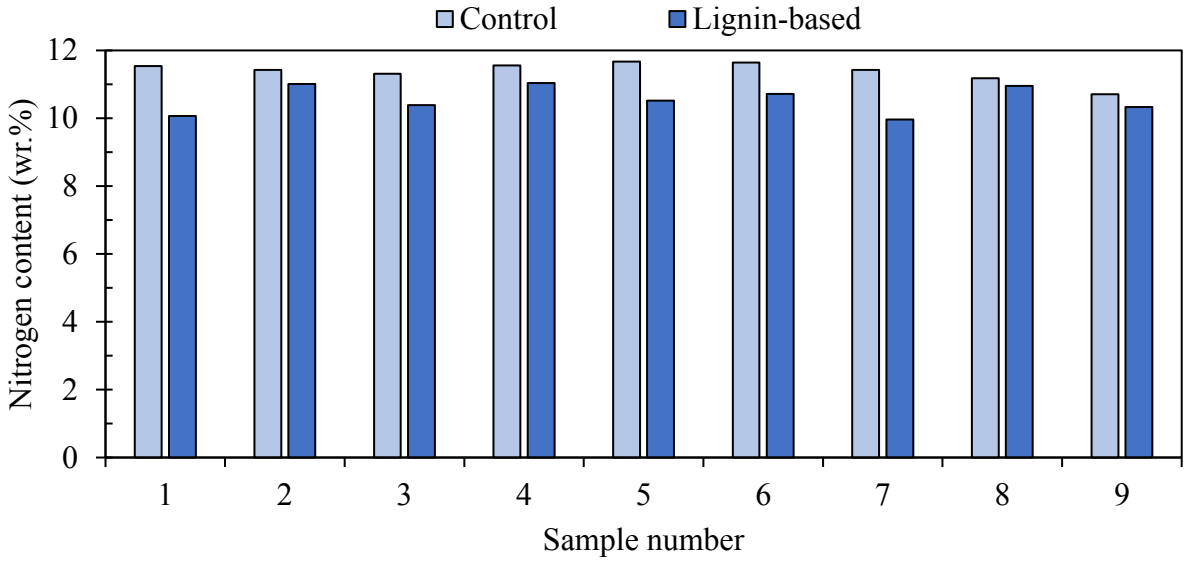

Figure 4.2. Nitrogen content of the control and lignin-based hydrogels

4.3 ^{1}H nuclear magnetic resonance spectroscopy

Figure 4.3 illustrates the ^{1}H NMR spectrum for the lignin-based hydrogels. The peak at 1.15 ppm corresponds to two methyl protons of the N-isopropyl group (A). The proton of the N-isopropyl group (E) is present at 4.1 ppm. These large peaks are dominant over the others due to

the large content of N-isopropylacrylamide within the hydrogels (Kim & Kadla, 2010; Zhang et al., 2009). The functional groups for lignin are depicted by a cluster of small peaks from 5 to 8 ppm which may be due to the aromatic rings present in kraft lignin. These peaks are relative, and may be compared in contrast to the DMSO (D) peak, since the concentration DMSO-d_6 solvent is known (Kim & Kadla, 2010).

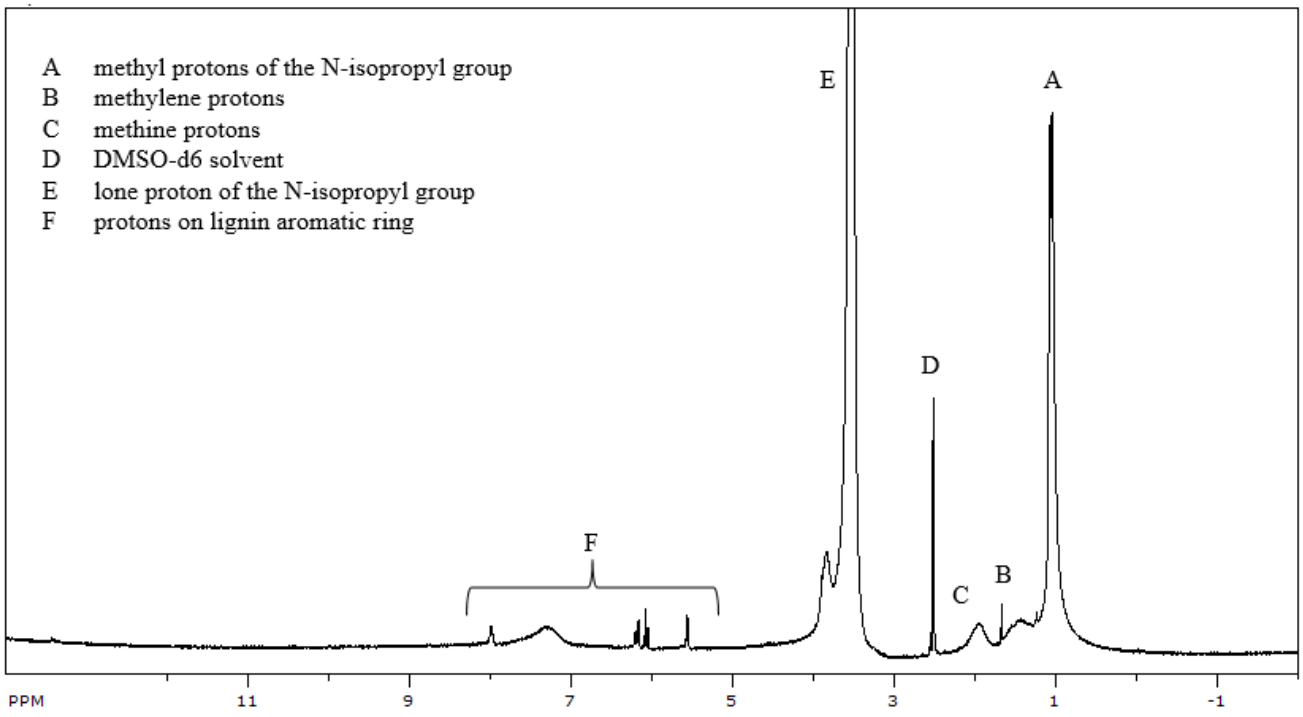

Figure 4.3. ^{1}H NMR spectrum for lignin-based hydrogels

4.4 Effect of reaction conditions

Design of experiments (DOE) allows to study the joint effects of selected factors on a response. These factors can be observed in both quantitative and qualitative levels ranging from low to high. Traditional DOE models normally utilize two-level factors and assumes a linear response to determine potential interactions. However, non-linear effects may also be studied through surface designs such as central composite or Box-Behnken designs (Montgomery,

2013). Although classical DOE are useful in predicting an optimal target value for process characteristics, they do not offer a rapid understanding of the process. Another approach to DOE is Taguchi orthogonal design, which allows for the selection of three or more levels and focusses on studying the non-linear effects between factor levels. The Taguchi approach studies all the main effects and some important interactions with a reduced samples size. In addition, this model is capable of reducing the variability around a target value and determining its associated loss (Antony, 2006). Thus, the Taguchi method is a suitable model to support a multivariate analysis with multiple levels without the need of an increased number of experiments.

Preliminary studies were executed to determine the parameters studied in the Taguchi L9 model. The hydrogels were found to react only above 65ºC, but were found to react too rapidly at very high temperatures. In addition, the hydrogels were found to require a minimum of 3 hours for the formation of the gel, but the reaction was not found to improve after 5 hours. Finally, preliminary reaction studies also found that the hydrogels were formed more readily at low pH values (below pH 3.0). For these reasons, the temperature, time, and pH factors varied between 65ºC to 85ºC, 3 to 5 hours, and pH 2 to 3, respectively.

The N-isopropylacrylamide, N,N'-methylenebisacrylamide, and lignin concentrations were based on the studies developed by Feng et al. (2011). Preliminary swelling studies determined that swelling increased with increasing lignin content, but only up to 1:12 ratio of lignin to N-isopropylarylamide, respectively. This behavior is most likely due to the increased hydrophobicity of lignin (Peng & Chen, 2011). For the experimental design, the N-isoprylacrylamide dosage was doubled to determine the effect of varying its concentration. Furthermore, the azobisisobutyronitrile initiator concentration was also selected via trial and

error trials for the production of the hydrogels; the formation of the hydrogels was formed only above 0.08 g, but were found to crosslink too rapidly at high concentrations.

The statistical hypothesis of a model represents a probability distribution of its parameters. This may be specified as either a null hypothesis or alternative hypothesis. The null hypothesis occurs when a pair of means are equal, indicating that there is no effect in the response. The alternative hypothesis, on the other hand, indicates a difference between the pair of means, meaning that there is a level of significance within the obtained data (Montgomery, 2013). The level of significance and the effect size for a set of data may be determined by performing an analysis of variance (ANOVA).

In the case of the Taguchi L9 orthogonal design presented in Table 3.2, multivariate analysis (MANOVA) was applied to determine whether there are differences between levels and factors. Contrary to performing multiple ANOVAs, which accounts for only one response at a time, accounting for the multiple responses during this analysis reduces the type I error associated with breaking the variance. A type I error occurs when the null hypothesis is rejected when it is in fact true (Montgomery, 2013). In other words, performing a MANOVA allows for a more accurate prediction on whether there is significance associated with varying factor levels, since the variance is shared between responses. The alternative hypotheses for the various factors in the Taguchi L9 orthogonal model are stated as:

Hypothesis 1. The reaction temperature has a significant effect on **(a)** yield, and **(b)** maximum swelling ratio.

Hypothesis 2. The reaction time has a significant effect on **(a)** yield, and **(b)** maximum swelling ratio.

Hypothesis 3. The amount of N-isopropylacrylamide has a significant effect on **(a)** yield, and **(b)** maximum swelling ratio.

Hypothesis 4. The pH of the reaction medium has a significant effect on **(a)** yield, and **(b)** maximum swelling ratio.

Table 4.1 demonstrates the results of the MANOVA for the responses of both the control and lignin-based hydrogels. The P-value essentially reports the level of significance associated with the response. In other words, the probability to reject the null hypothesis. A 95% confidence interval was selected for this model, meaning that the response is deemed significant if the P-value falls below 0.05 (Montgomery, 2013). According to the presented results, all the stated hypotheses are corroborated except for hypothesis 1(b) and 4(b) for the control samples. The MANOVA essentially specifies that there is no significant effect on reaction temperature and time with respect to the control hydrogels' maximum swelling ratio with a confidence of 50.2% and 32.9%, respectively.

The observed power of rejection for these hypotheses demonstrates a relatively low confidence, meaning that they may be more susceptible to a Type II error. This is defined as the failure to reject the null hypothesis when it is true, in which case both these hypotheses may have been deemed insignificant when in fact there is a significant effect present (Montgomery, 2013).

Although the MANOVA is effective at determining whether a factor has a significant effect on the response, it does not identify where these differences lie when considering multiple levels. For this purpose, a Post Hoc analysis was used to better analyze the results of the experimental data (Demšar, 2006). Thus, Tukey's Test was selected as an effective model to compare all possible pairs of means and determine where they differ within the data (Tukey,

1949; Demšar, 2006). Figure 4.4 and Figure 4.5 helps to better illustrate these differences for both the control and lignin-based hydrogel models, respectively.

For simplicity, the previously stated hypotheses will be analyzed first for the control hydrogels, followed by for the lignin-based hydrogels. It is important to note that both the control and lignin-based samples are considered as separate models, and that the MANOVAs are not related to one another. In addition, unlike classical DOE models, which uses a sequential approach to study every present interaction within the model, the Taguchi method only studies the main effects and a few important interactions (Antony, 2013). For this reason, the effect of an individual factor on the response may be difficult, in some cases, to identify since additional factors may be present.

Table 4.1. Multivariate analysis of the Taguchi L9 orthogonal model for the control and lignin-based hydrogels

Source	Dependent variable	Sum of squares		Degrees of freedom		Mean square		F-value		P-value		Partial eta squared		Observed power	
		Cntrl	Lgn	Cntrl	Lgn	Cntrl	Lgn	Cntrl	Lgn	Cntrl	Lgn	Cntrl	Lgn	Cntrl	Lgn
Model	Yield	344.83	2852.78	8	8	43.10	356.60	21.37	80.10	0.000	0.000	0.950	0.986	1.000	1.000
	Max. S.R.	1863.78	777.82	8	8	232.97	97.23	8.91	20.53	0.002	0.000	0.888	0.948	0.993	1.000
Temperature	Yield	45.95	69.07	2	2	22.98	34.54	11.39	7.84	0.003	0.011	0.177	0.635	0.955	0.852
	Max. S.R.	182.85	133.27	2	2	91.43	66.63	3.50	14.07	0.075	0.002	0.437	0.758	0.502	0.983
Time	Yield	98.86	1956.94	2	2	49.43	978.47	24.51	222.24	0.000	0.000	0.845	0.980	1.000	1.000
	Max. S.R.	1190.64	183.67	2	2	595.32	91.83	22.77	19.39	0.000	0.001	0.835	0.812	0.999	0.998
NIPAAm content	Yield	30.36	378.66	2	2	15.18	189.33	7.53	43.00	0.012	0.000	0.626	0.905	0.837	1.000
	Max. S.R.	378.24	157.85	2	2	189.12	78.92	7.23	16.67	0.013	0.001	0.617	0.787	0.822	0.993
pH	Yield	169.66	448.11	2	2	84.83	224.05	42.05	50.89	0.000	0.000	0.903	0.919	1.000	1.000
	Max. S.R.	112.06	303.03	2	2	56.03	151.52	2.14	32.00	0.173	0.000	0.323	0.877	0.329	1.000
Pure error	Yield	18.15	39.62	9	9	2.02	4.40								
	Max. S.R.	235.28	42.61	9	9	26.14	4.73								
Corrected total	Yield	362.98	2892.41	17	17										
	Max. S.R.	2099.06	820.43	17	17										

Max. S.R. = Maximum swelling ratio

For the control samples, Table 4.1 indicates that temperature presents a significant effect on yield, $F(2,17)=11.39$, $p=0.003$, $\eta^2=0.177$, thus corroborating hypothesis 1(a). In addition, the size of this effect may be determined by the partial eta squared (η^2); 0.01 indicating a small effect, 0.06 a medium effect and 0.14 a large effect. In this case, temperature presents a large effect on yield as the partial eta squared falls above 0.14. According to Tukey's test, however, this effect is only present between 75°C and 85°C, for which Figure 4.4(a) indicates a slight rise in yield. This is most likely due to reaction kinetics; a higher temperature having resulted in an increased rate of reaction. With higher temperatures, the cleavage of the azo compounds occurs more rapidly, thus increasing the concentration of radicals present in solution (Omidian, 2004).

Hypothesis 2 is also validated, both yield, $F(2,17)=24.51$, $p<0.001$, $\eta^2=0.845$, and maximum swelling ratio, $F(2,17)=22.77$, $p<0.001$, $\eta^2=0.835$, presenting a large effect between 4 and 5 hours. An increase in yield and maximum swelling ratio is also shown in Figure 4.4(b) between 4 and 5 hours, indicating that longer reaction times allow for better conversion, as well as greater crosslinking.

Yield, $F(2,17)=7.53$, $p=0.012$, $\eta^2=0.626$, was found to be significantly improved when increasing the N-isopropylacrylamide content from 1.2 g to 2.4 g, a higher reactant content leading to better hydrogel production. This large effect also exhibits a slight drop at 1.8 g of N-isopropylacrylamide in Figure 4.4(c), which is most likely caused by other interactions such as the variation of temperature, time, and pH. The maximum swelling ratio, $F(2,17)=7.23$, $p=0.013$, $\eta^2=0.617$, also exhibits a large effect between 1.8 g and 2.4 g, thus corroborating hypothesis 3. Since N-isopropylacrylamide directly contributes to the swelling ability of the hydrogel, this reinforces that an increase in reactant concentration improves the formation of the polymer network.

Since radicals are highly reactive, an increase in hydronium ions caused by a decrease in pH would ultimately result in the radicals engaging in faster and more frequent termination. The opposite effect, however, was observed, Figure 4.4(c) illustrating a decrease in yield, $F(2,17)=42.05$, $p<0.001$, $\eta^2=0.903$, from pH 2.5 to pH 3.0. Therefore, as the concentration of sulfate ions in the reaction mixture increases, the hydrogens within the terminated polymer chains are most likely abstracted, which, in turn, reinitiates the propagation step (Su, 2013). As a result, hypothesis 4(a) is validated, although no significant effect is demonstrated for the maximum swelling ratio. Since swelling ratio is essentially a measure of crosslinking degree, the second propagation step most likely consists of the hydrogen abstraction of smaller polymer chains; thus, small groups are added to the polymer, increasing the overall yield, but perhaps the crosslinked structure of the network (Thakur & Thakur, 2015; Su, 2013).

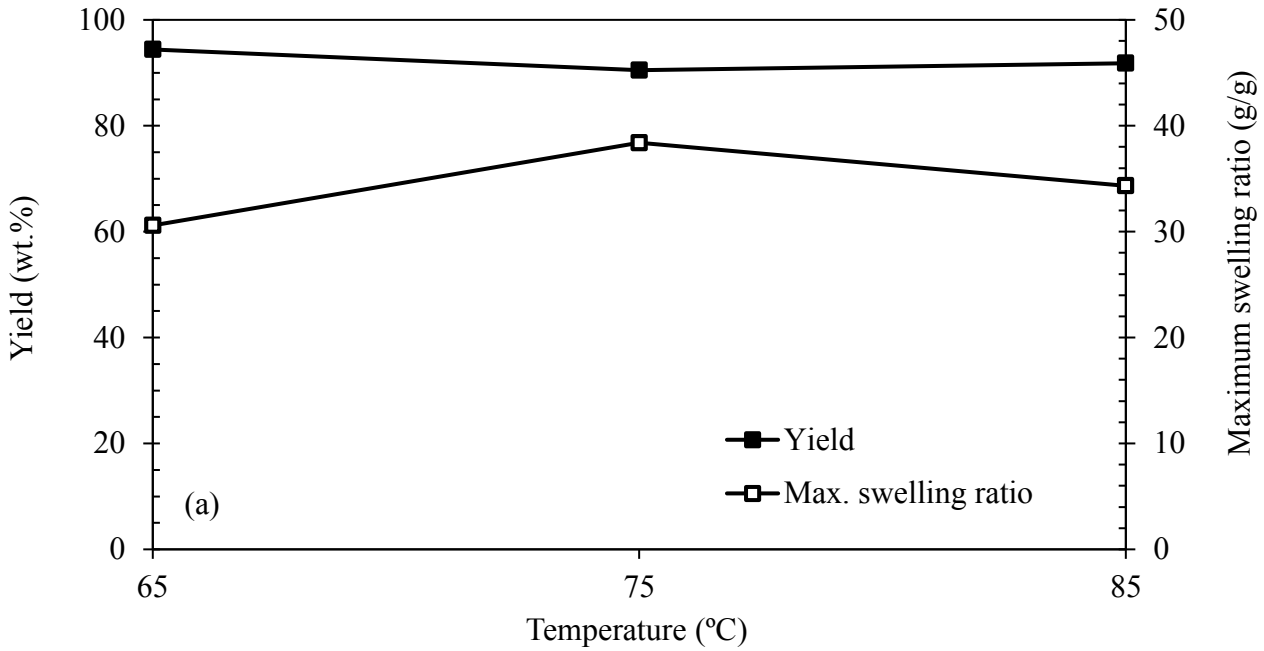
100
80
60
40
20
0
50
40
30
20
10
0
Yield (wt.%)
Maximum swelling ratio (g/g)
Yield
Max. swelling ratio
(a)
65
75
85
Temperature (ºC)

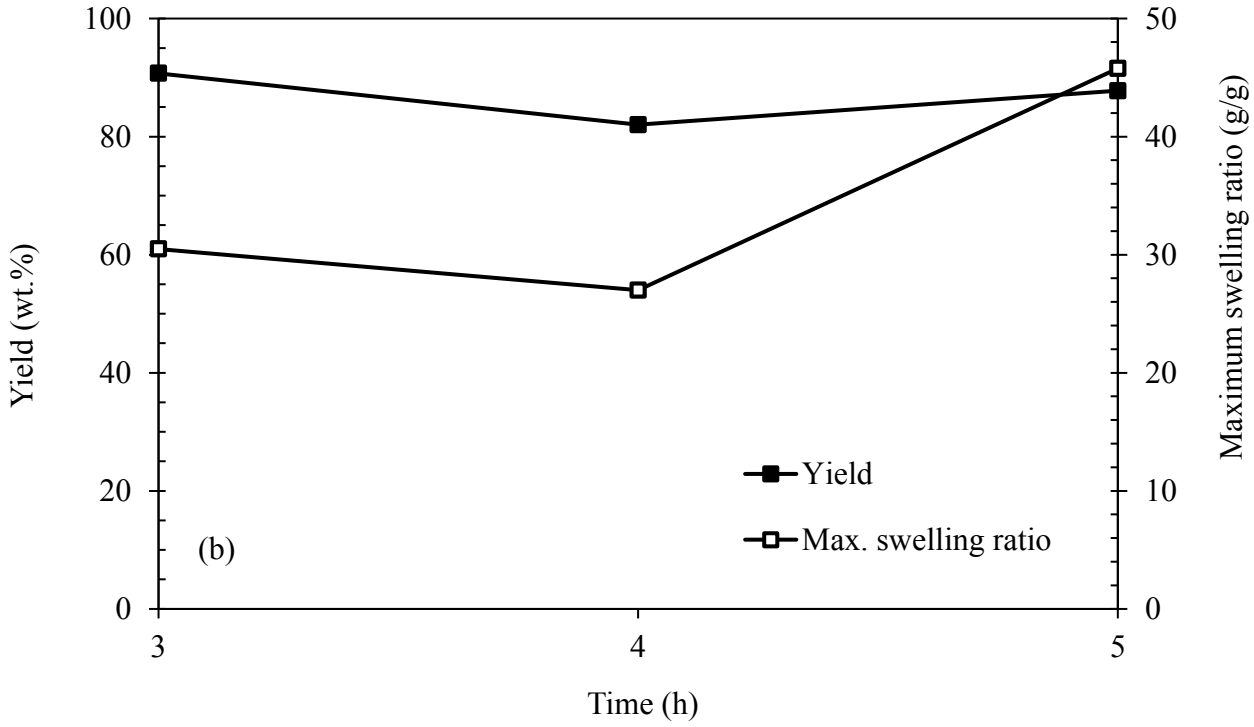
100
80
60
40
20
0
50
40
30
20
10
0
Yield (wt.%)
Maximum swelling ratio (g/g)
Yield
Max. swelling ratio
(b)
3
4
5
Time (h)

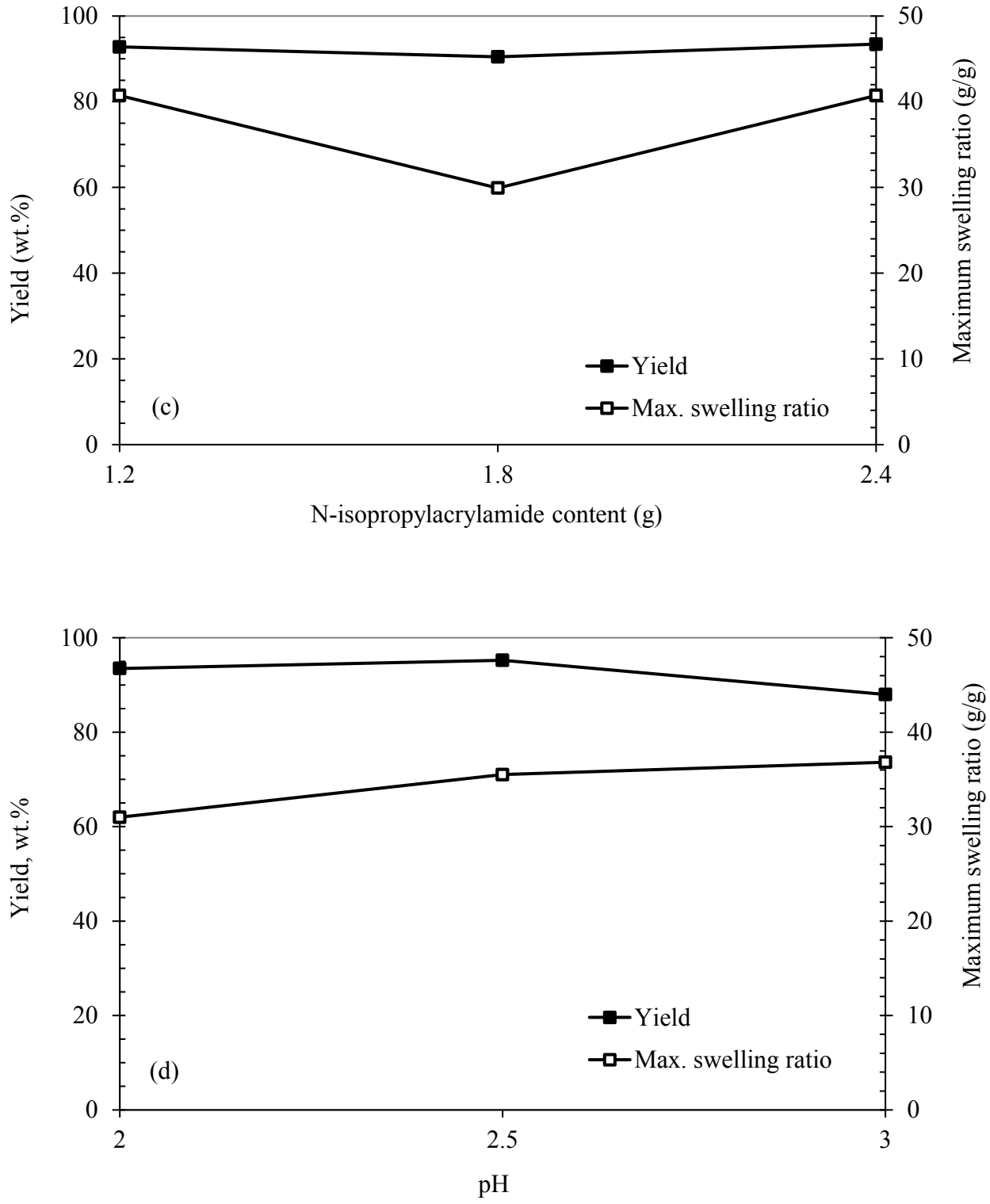

Figure 4.4. The effect of responses on control hydrogel samples with respect to (a) temperature, (b) time, (c) N-isopropylacrylamide content, and (d) pH

Figure 4.5 demonstrates the effect of the studied reaction conditions on yield and swelling capacity for the lignin-based hydrogels. Similarly to the control samples, a large effect in temperature was observed for the yield of the lignin-based hydrogels, $F(2, 17)=7.84$, $p=0.011$, $\eta^2=0.635$, between 75°C and 85°C. The maximum swelling ratio, $F(2, 17)=14.07$, $p=0.002$, $\eta^2=0.076$, also followed the same trend in Figure 4.5(a), increasing significantly from 75°C to 85°C. A decrease in swelling performance was observed at 75°C, however, was most likely induced by additional interacting factors. This overall consistent behavior with the control samples is attributed to the same phenomena and facts explained above, meaning that temperature of the reaction essentially has the same effect on hydrogel production with or without the presence of lignin.

In addition, reaction time demonstrates a consistent behavior between the control and lignin-based samples with respect to yield, $F(2, 17)=222.24$, $p<0.001$, $\eta^2=0.980$, from 4 to 5 hours. The time extension allows for additional crosslinking to occur in the reaction, resulting in a higher product yield. On the other hand, Figure 4.5(b) depicts the maximum swelling ratio as increasing between 3 to 4 hours, but decreasing from 4 to 5 hours. This trend differs from that of Figure 4.4(b), which continues to increase over time. Since crosslinking performance does not improve after reacting for 4 hours, it can be stipulated that lignin is more readily grafted onto the hydrogel between 4 to 5 hours, and thereby increases yield. This is most likely due to lignin having a more stable configuration than N-isopropylacrylamide and N,N'-methylenebisacrylamide, which are more readily reacted.

Figure 4.5(c) illustrates a significantly large decrease in yield, $F(2, 17)=43.00$, $p<0.001$, $\eta^2=0.905$, with increasing N-isopropylacrylamide content. As with the control samples, however, there is a greater drop in yield that occurs at 1.8 g of N-isopropylacrylamide, which is most

likely due to the presence of additional interactions. The maximum swelling ratio, $F(2,17)=16.67$, $p=0.001$, $\eta^2=0.787$, on the other hand, demonstrates a significant effect with respect to N-isopropylacrylamide content from 1.8 to 2.4 g. This is the same trend that occurred for the control samples, since the N-isopropylacrylamide greatly contributes to the swelling ability of the hydrogel. Similarly, yield was also shown to increase from 1.8 g to 2.4g of N-isopropylacrylamide. As with the control hydrogels, an increase in monomer would result in a overall higher yield of product.

According to the results from Tukey's test, yield, $F(2,17)=50.89$, $p<0.001$, $\eta^2=0.919$, and the maximum swelling ratio, $F(2,17)=32.00$, $p<0.001$, $\eta^2=0.877$, exhibit a significant effect between pH 2.0 and pH 2.5. An overall increase in yield illustrated in Figure 4.5(d) is attributed to the same phenomena explained previously for the control sample. The opposite trend is observed for the maximum swelling ratio, which may be attributed to an increase in grafted lignin onto the polymer network (Feng et al., 2011).

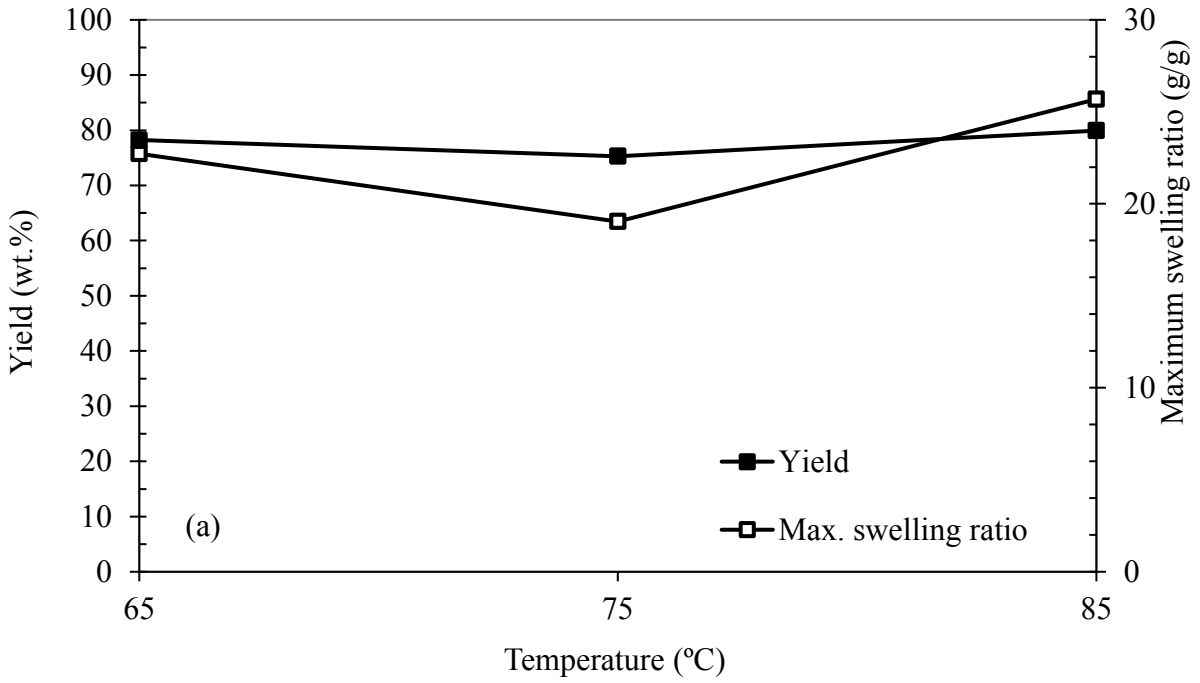
100
90
80
70
60
50
40
30
20
10
0
Yield (wt.%)
30
20
10
0
Maximum swelling ratio (g/g)
Yield
Max. swelling ratio
(a)
65
75
85
Temperature (ºC)

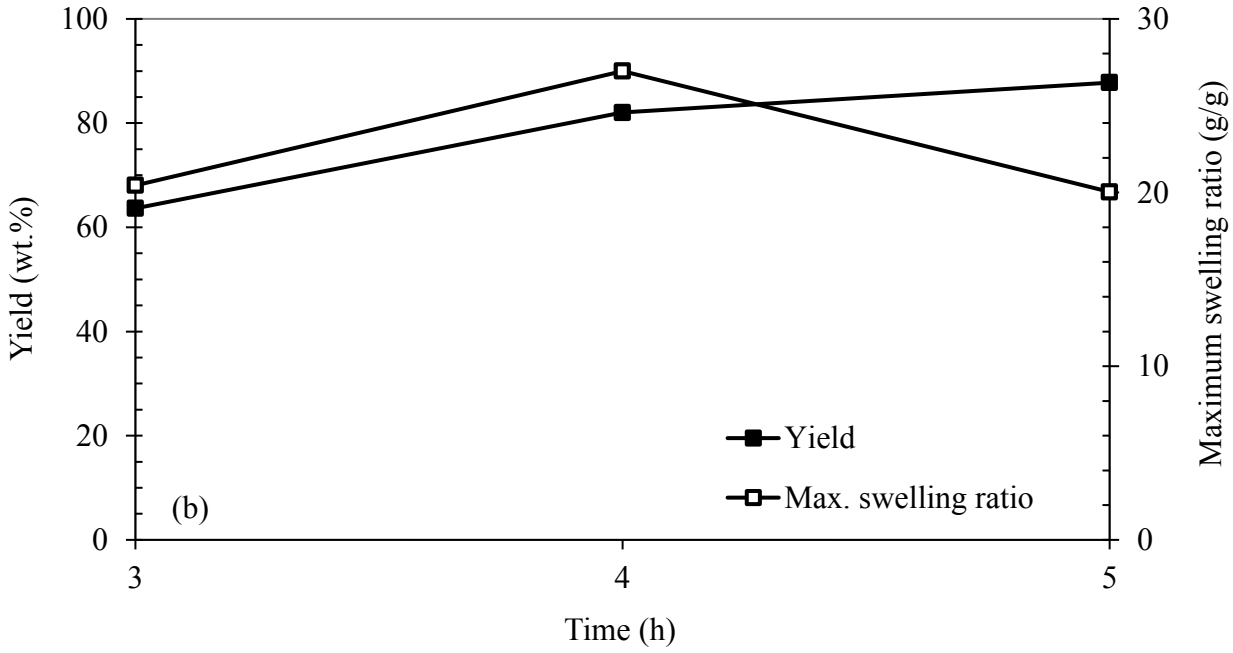
100
80
60
40
20
0
Yield (wt.%)
30
20
10
0
Maximum swelling ratio (g/g)
Yield
Max. swelling ratio
(b)
3
4
5
Time (h)

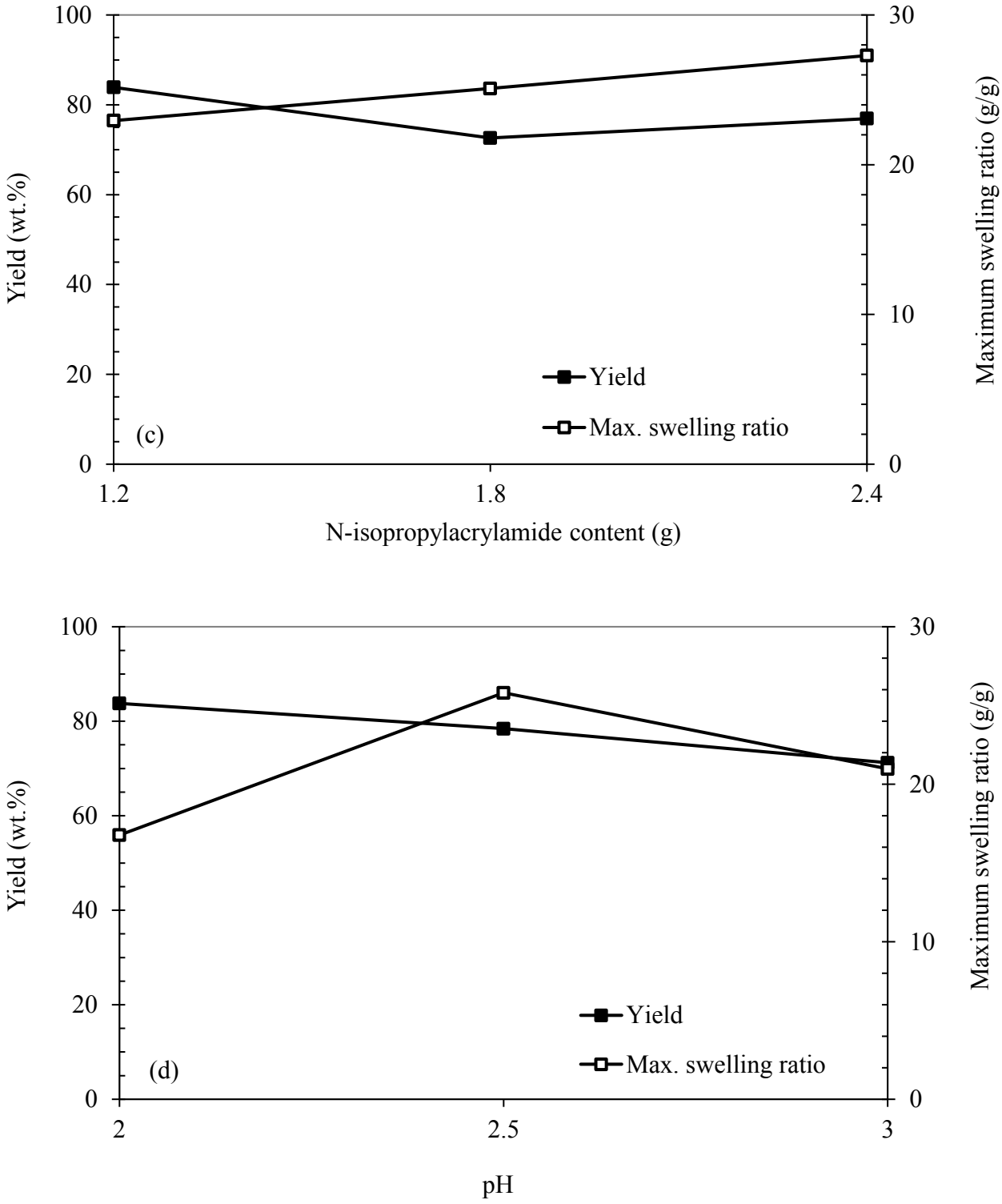

Figure 4.5. The effect of responses on lignin-based hydrogel samples with respect to (a) temperature, (b) time, (c) N-isopropylacrylamide content, and (d) pH

Table 4.2 compares the means and standard deviations for both responses, as well as the associated coefficients. The responses exhibited a low coefficient of variation, meaning that there was not much dispersion within the distribution of the obtained data. In other words, the obtained data is considered as precise and repeatable (Brown, 1998). This is further supported by the reliability analysis presented in Table 4.3, for which the intraclass correlation coefficient (ICC) was selected as a reliability index. Since the data was collected by a single researcher, the ICC was based on the single measure model where the estimator remains constant and does not depend on whether interactions are present. The reported ICC was found to range between 0.78 to 0.97, indicating a strong reliability for all responses (Koo & Li, 2016).

Table 4.2. Descriptive statistics

Dependent variable	Standard deviation		Mean		95% Confidence Interval				Coefficient of variation (%)	
					Lower Bound		Upper Bound			
	Cntrl	Lgn	Cntrl	Lgn	Cntrl	Lgn	Cntrl	Lgn	Cntrl	Lgn
Yield	1.42	2.10	92.22	77.77	91.46	76.65	92.97	78.89	1.54	2.70
Max. S. R,	5.11	2.18	34.44	22.48	31.71	21.32	37.17	23.64	14.84	9.68

Max. S. R. = Maximum swelling ratio

Table 4.3. Reliability analysis

Dependent variable	Intraclass correlation coefficient		95% Confidence Interval			
			Lower Bound		Upper Bound	
	Cntrl	Lgn	Cntrl	Lgn	Cntrl	Lgn
Yield	0.90	0.97	0.63	0.89	0.98	0.99
Max. S. R.	0.78	0.90	0.28	0.55	0.94	0.98

Max. S.R. = Maximum swelling ratio

In order to determine which sample run exhibits the best responses, the Taguchi method uses a performance statistic known as the signal-to-noise (SN) ratio. It is important to note that Taguchi method does not provide the optimum value, but rather the best value from the range of results (Alao & Konneh, 2011). Essentially, the SN ratio is used to determine process robustness, combining both the mean and variability of the response as a single performance measure. Since the goal for this experiment was to maximize the response values, the larger-the-better (LB) SN ratio equation, Eqn. (4.1), was selected (Alao & Konneh, 2011):

$$S/N_{LB} = -10 \log\left[\frac{1}{n}\sum_{i=1}^{n}\frac{1}{y_i}\right] \tag{4.1}$$

Where n is the number of experiments, and y_i is the collected experimental data. The optimal level can then be determined by selecting the largest SN ratio from each of the performance parameters (Alao & Konneh, 2011).

Table 4.4 lists signal to noise ratios for selected control and hydrogel samples along with their responses (yield and maximum swelling ratio). The SN values, which maximized both these responses, were found to be highest for 3C, followed by 6C. The lignin-based model, on the

other hand, exhibited a higher SN ratio for 2L and 9L. The SN ratios for both models were found to differ due to the addition of lignin, which presented adverse effects with respect the swelling capacity.

Since the control and lignin-based samples are essentially separate models, it is not possible to relate the SN ratios to one-another. Thus, the sample size was reduced to the two best SN ratios of each model, and compared to their counterpart, for a total of 8 samples. Hence, future analyses will only take into consideration samples 2C, 2L, 3C, 3L, 6C, 6L, 9C, and 9L.

Table 4.4. Signal-to-noise ratio for the responses of the control and lignin-based hydrogels

Run	Control			Lignin-based		
	Yield (wt.%)	Max. swelling ratio (g/g)	S/N_{LB}	Yield (wt.%)	Max. swelling ratio (g/g)	S/N_{LB}
1	94.68	21.41	32.41	76.09	15.41	24.62
2	93.88	19.78	31.75	77.86	32.59	26.30
3	94.65	50.59	39.01	80.7	20.19	25.41
4	82.96	32.30	35.59	49.33	24.08	25.66
5	91.2	33.86	36.05	84.57	14.00	24.67
6	97.32	49.02	38.85	91.93	19.03	25.25
7	94.48	37.74	36.91	65.49	21.76	25.58
8	86.34	27.56	34.41	83.63	34.39	25.61
9	94.6	37.71	36.91	90.67	20.91	25.74

4.5 Fourier transform infrared spectroscopy

The FTIR spectra for all the raw materials and hydrogel samples are shown in Figure 4.6 and 7, respectively.

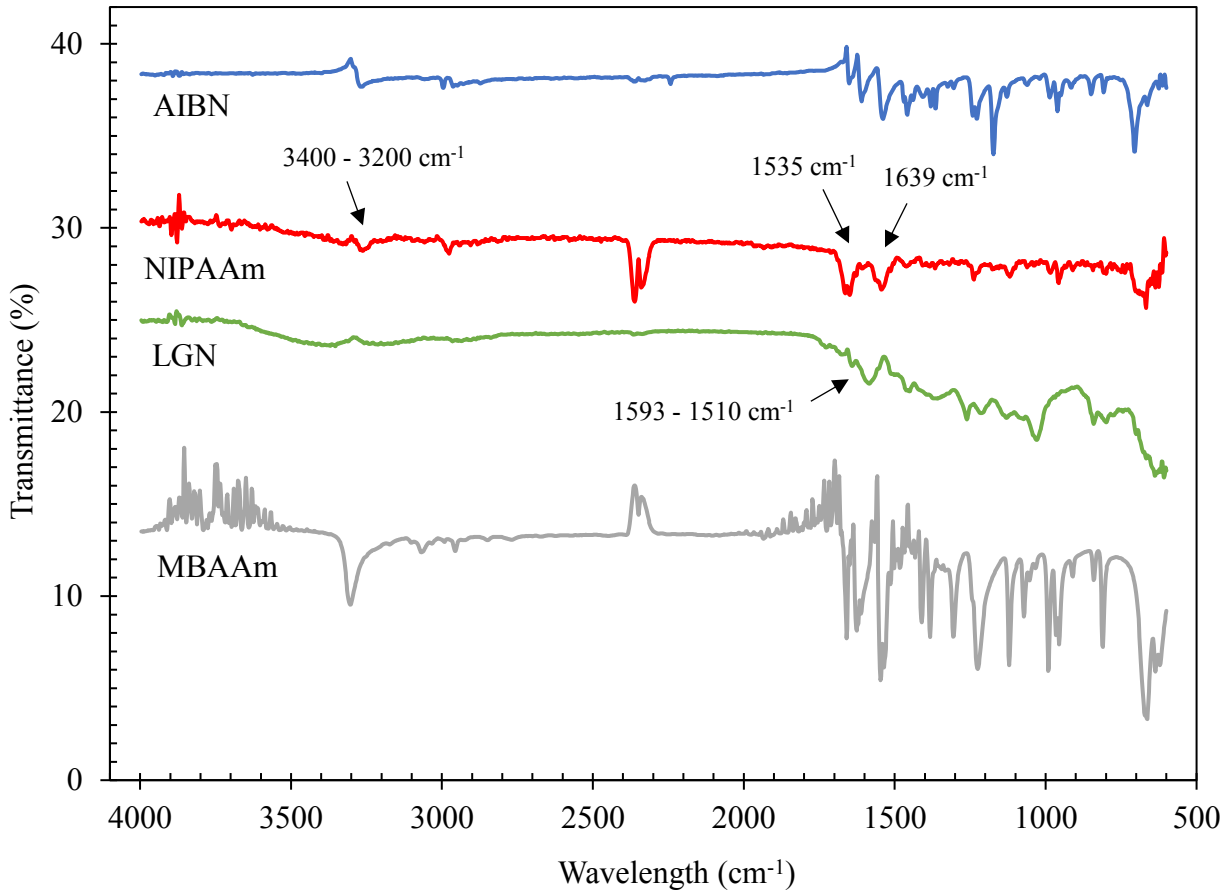

Figure 4.6. FTIR analysis of the AIBN initiator, kraft lignin (LGN), N-isopropylacrylamide (NIPAAm), and N,N'-methylebisacrylamide (MBAAm)

The bands located between 1535 cm^{-1} and 1639 cm^{-1} are attributed to the amide groups found in N-isopropylacrylamide, as well as in N,N'-methylenebiscrylamide and AIBN (Feng et al, 2014; Ling & Lu, 2009). These compounds also exhibit a broad spectrum between 3400 cm^{-1} to 3200 cm^{-1}, indicating the stretching of the N-H bond (Yang et al., 2011; Feng et al., 2014).

According to Mohan & Fatehi (2015), the presence of kraft lignin's aromatic compounds yields a broad peak between 1593 cm^{-1} and 1510 cm^{-1}, these peaks being attributed to the benzene ring vibrations. There are also absorption peaks present at 1130 cm^{-1} and 1171 cm^{-1}, which correspond to the stretching C-O of the primary alcohol and ether of kraft lignin, respectively (Feng et al., 2014).

In addition, the C=O and C=C stretching may be depicted by the bands located at approximately 1200 cm^{-1} and 1500 cm^{-1}, respectively. The CH stretching of methyl or methylene groups are also shown to be present in the peaks between 2300 cm^{-1} and 2400 at cm^{-1} (Mohan & Fatehi, 2015). In addition, all hydrogels were found to have similar peaks. However, the peaks at 1535 cm^{-1} and 1639 cm^{-1} were most intense for all samples, indicating the presence of N-isopropylacrylamide. For this reason, the peaks for N-isopropylacrylamide overshadow the lignin aromatic peaks at 1593 cm^{-1} and 1510 cm^{-1}.

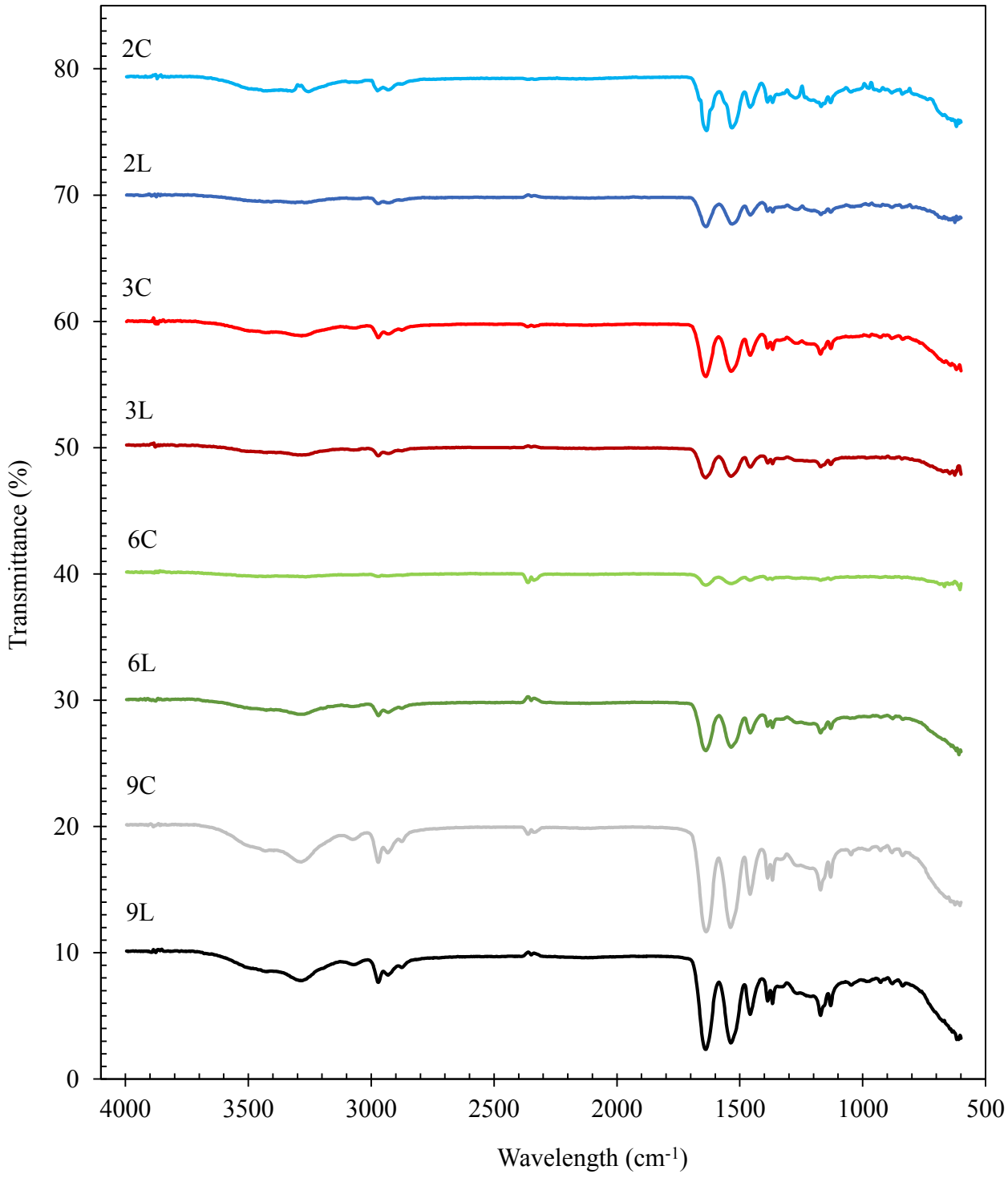

Figure 4.7. FTIR analysis for the control and lignin-based hydrogels

4.6 Surface properties and swelling behavior

The surface area properties of the selected samples are shown in Table 4.5. The control samples were found to have higher surface area, pore volume, and pore size compared to the lignin-based hydrogels, which explains their high affinity to absorb water. This is because the diffusion occurs over a larger surface area, increasing flux. In addition, the pore size and pore volume has a great effect on swelling capacity as it allows for the absorption of water; larger pores can accommodate higher contents of water. This indicates that the hydrogel has well-developed crosslinked structure (Feng et al., 2011).

Table 4.5. Surface properties of control and lignin-based hydrogels

Sample	Surface area (m^2/g)	Total pore volume (cm^3/g)	Average pore size (A°)
2C	49.62	0.058	24.9
2L	44.56	0.048	22.1
3C	44.73	0.053	22.7
3L	41.34	0.043	20.8
6C	42.48	0.052	22.4
6L	40.73	0.043	20.6
9C	46.94	0.056	23.8
9L	42.65	0.047	22.1

The swelling behavior of the selected lignin-based hydrogels are illustrated in Figure 4.8. This analysis will only focus on the lignin-containing hydrogels since the control samples were found to swell within the minutes disabling analysis.

-

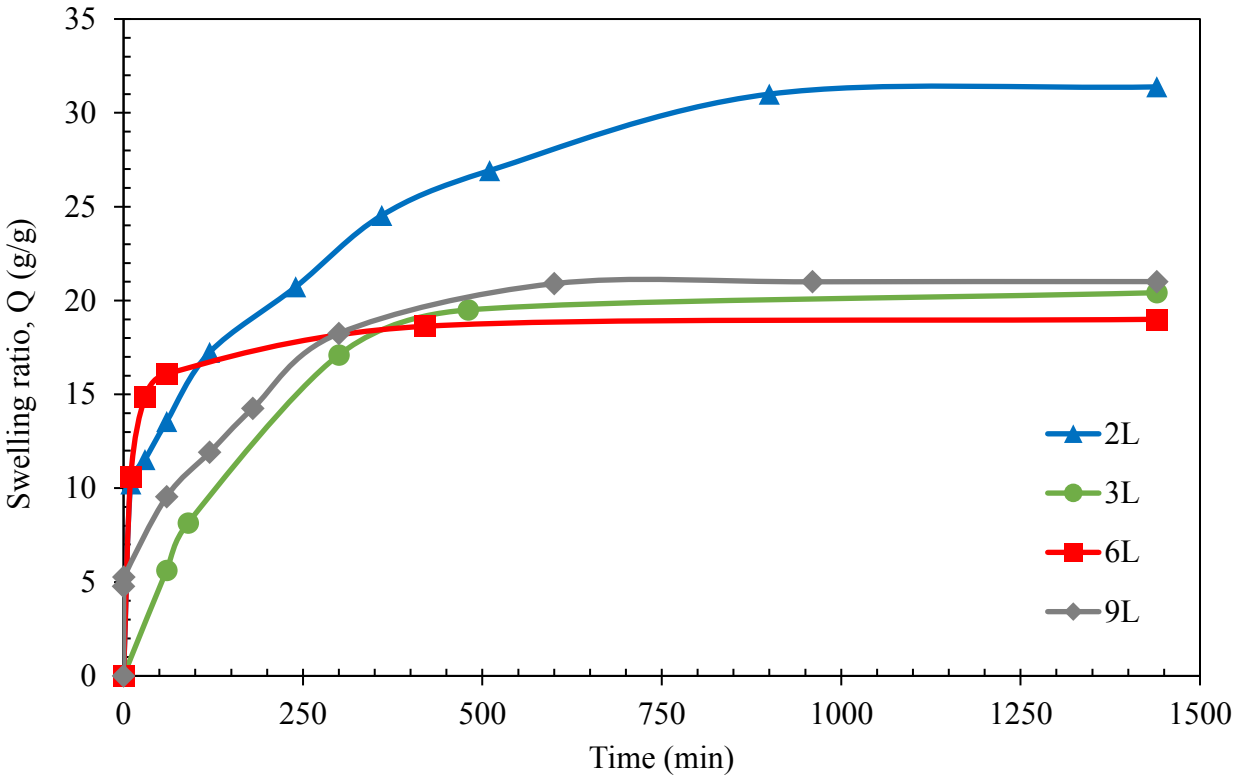

Figure 4.8. Swelling ratio of lignin-based hydrogels

The swelling capacity of the gels were found to largely depend on reaction parameters such as temperature, time, N-isopropylacrylamide concentration and pH. Sample 6L was shown to exhibit the higher swelling rate, followed by 9L, 3L, and 2L, respectively. According to Table 4.5, the pore volume and pore size for sample 2L was found to be greatest, allowing for a higher capacity of water to be retained. Sample 6L, on the other hand, demonstrated the lowest pore size and pore volume, since it exhibited the lowest maximum swelling ratio. It is also likely that the increased composition of a hydrophobic moiety such as lignin would ultimately lead to a less hydrophilic gel, therefore decrease the overall swelling capacity (Feng et al., 2011). When

comparing 3L and 9L, however, it was found that these samples had similar porosities, and these samples exhibit similar swelling capacities, as shown Figure 4.8.

Furthermore, sample 2L had increased surface areas in comparison with the other samples, which could attest to their kinetic of swelling. The larger surface area would allow for more water to enter at a faster rate. Based on the results in Figure 8 and Table 4.5, the presence of lignin might improve the swelling rate, but would hamper the overall water absorbency of hydrogels.

The mechanism of water diffusion was also studied using the the Ritger-Peppas equation, Eqn. (4.2), to determine the driving force for swelling (Khare & Peppas, 1995):

$$Q_t/Q_e = kt^n \tag{4.2}$$

Where Q_t and Q_e are the amounts of water absorbed at time t and at equilibrium, respectively, k is the proportionality constant, t is swelling time, and n is the diffusional exponent (Liang et al., 2013; Khare & Peppas, 1995; Wilson et al., 2014). Fickian diffusion, or Case I diffusion, is observed when n=0.5, meaning that the transport of the penetrant behaves according to Fick's Law of diffusion (Chen, 2005). For n<0.5, diffusion is deemed to be pseudo-Fickian (Hodkingson, 2000). In addition, certain polymers exhibit a different sorption behavior, for which the mechanical deformation of the glassy region of the polymer dominates the controlling rate of diffusion. This, in combination with the diffusivity of the penetrant, are referred to as Case II diffusion, where n=1.0 (Thomas & Windle, 1982; Chen, 2005). Anomalous sorption behavior may also be present at 0.5<n<1.0, indicating the presence of Case I and Case II diffusion (Chen, 2005; Thomas & Windle, 1982). Eq. (4.3) can also be manipulated by applying a logarithm in order to obtain a linear correlation:

$$\ln\left({}^{Q_t}/_{Q_e}\right) = \text{nlnt} + \text{lnk} \quad (4.3)$$

Using Eq. (3.4), the diffusion parameters were calculated, where n is the slope of the line and lnk is the intercept and listed in 8. The diffusion coefficient, n, for the investigated lignin-based hydrogels were found to be less than 0.5, illustrating that they follow a pseudo-Fickian diffusion behavior (Fu & Kao, 2009). The proportionality constant, k, which relates to the structure of the hydrogel network, was found to directly relate to the rate of swelling (Liang et al., 2013). In other words, a higher k value would ultimately result in a higher swelling rate since it is a multiplier to time. The calculated proportionality constant in Table 4.6 for the hydrogels may be compared with Figure 4.8; 6L exhibits the highest k value as it has the highest swelling rate, reaching its maximum swelling capacity within 5 hours. The k values for samples 2L, 9L, and 6L decreased in that order, which is consistent with their swelling rates.

Table 4.6. Diffusion parameters of lignin-based hydrogels

Sample	Diffusional exponent, n	Proportionality constant, k (min^{-n})	R^2
2L	0.256	0.159	0.977
3L	0.421	0.059	0.864
6L	0.106	0.501	0.815
9L	0.341	0.103	0.930

The kinetic of swelling was also studied. The pseudo-first order and pseudo-second order models were selected to determine the swelling dynamics of the lignin-based hydrogels, for Eqn. (4.4) and (4.5) were used, respectively (Feng et al., 2014):

$$\frac{1}{Q_t} = \frac{k_1}{Q_e t} + \frac{1}{Q_e} \quad (4.4)$$

$$\frac{t}{Q_t} = \frac{t}{Q_e} + \frac{1}{k_2 Q_e} \quad (4.5)$$

Where k_1 and k_2 are the pseudo-first order and pseudo-second order rate constants, respectively (Feng et al., 2014). Eqn. (4.4) and (4.5) were applied to the experimental data to determine the equation of best fit. Table 4.7 demonstrates that the swelling behavior of the lignin-based hydrogels followed the pseudo-second order kinetic model. The predicted equilibrium swelling ratio was found to be closer to the experimental data, with an average percent error of 5.9%. Moreover, the pseudo-second order rate constant was found to be an order of magnitude greater for sample 6L, indicating that this hydrogel exhibited a significantly rapid swelling rate.

Table 4.7. Pseudo-first order and pseudo-second order kinetic parameters of lignin-based hydrogels

Sample	$Q_{e,exp}$ (g/g)	Pseudo-first order			Pseudo-second order		
		$Q_{e,calc}$ (g/g)	$k_1 \times 10^{-3}$ (min)	R^2	$Q_{e,calc}$ (g/g)	$k_2 \times 10^3$ (min^{-1})	R^2
2L	31.38	21.47	0.20	0.706	33.08	0.41	0.983
3L	20.42	27.91	1.69	0.990	22.67	0.40	0.994
6L	19.00	18.73	0.08	0.995	19.12	5.49	1.000
9L	21.01	15.99	0.36	0.781	22.41	0.70	0.997

4.7 Absorption isotherm studies

The Langmuir and the Freundlich isotherm models were used to analyze the absorption behavior of the control and lignin-based hydrogels. The Langmuir model, as shown in Eqn. (4.6), assumes monolayer, or homogeneous, absorption. In other words, the thickness of the absorbed layer is essentially one molecule, for which the absorption can only occur at fixed localized sites (Langmuir, 1918, Vijayaraghavan et al., 2006). The Freundlich isotherm, on the other hand, accounts for multilayer absorption. This model, expressed by Eqn. (4.7), assumes heterogeneous surface, for which there is a non-uniform distribution of absorption (Hameed & Foo, 2010).

$$q_e = \frac{C_e q_o K_L}{C_e K_L + 1} \tag{4.6}$$

$$q_e = K_F C_e^{1/n} \tag{4.7}$$

Where q_e is the equilibrium absorbance capacity, q_0 is the monolayer absorbance capacity, C_e is the equilibrium concentration, n is the absorption intensity and, K_L and K_F are the Langmuir and Freundlich isotherm constants, respectively.

The obtained coefficients for both isotherm models are expressed in Table 4.8 and Table 4.9 for the control and lignin-based hydrogels, respectively. For both cases, the hydrogels were found to favor the Freundlich model, meaning that the ratio methylene blue absorbed onto the given mass of the hydrogels was not constant at different solution concentrations (Ahmaruzzaman, 2008). The presence of all absorption sites, each with a respective bond energy, quantifies the absorption capacity. The sites having stronger binding affinity are readily occupied, this absorption process following an exponential trend (Chen et al., 2011).

Table 4.8. The isotherm parameters for the control hydrogels

Isotherm model		2C	3C	6C	9C
Langmuir	Q_o (mg/g)	0.13	5.06	6.95	23.71
	K_L (L/mg)	$1.12x10^{-4}$	0.14	0.14	1.50
	R^2	0.34	0.23	0.02	0.03
Freundlich	N	0.23	0.74	0.93	1.21
	K_F ($mg^{1-(1/n)}$ $L^{1/n}$/g)	$2.89x10^{-8}$	0.02	0.09	0.19
	R^2	0.97	0.74	0.27	0.63

Table 4.9. The isotherm parameters for the lignin-based hydrogels

Isotherm model		2L	3L	6L	9L
Langmuir	Q_o (mg/g)	55.52	150.32	6.90	143.21
	K_L (L/mg)	9.95	48.19	0.24	45.33
	R^2	0.25	0.06	0.36	0.06
Freundlich	N	0.88	1.39	0.67	1.59
	K_F ($mg^{1-(1/n)}$ $L^{1/n}$/g)	0.18	1.03	0.02	1.43
	R^2	0.76	0.58	0.75	0.75

4.8 Focused beam reflectance measurement

The swelling behavior of the powdered hydrogels were also studied to determine how differently produced hydrogels would have different swelling capabilities. The size and shape of the particles was recorded over time by measuring the chord length (Petrak et al., 2015). The median in the FBRM results for the control and lignin-based hydrogels are illustrated in Figure 4.9.

The hydrogels were found to reach their maximum swelling much sooner compared to absorption test due to their smaller size (and thus surface area) in FBRM analysis. This is because mass transfer occurs more rapidly over a smaller surface area (Geankopolis, 2003). Furthermore, the control hydrogels were found to swell only slightly, indicating the partial destruction of the polymer network structure. It is observable that the time extension increased the chord length of hydrogel particles, but this increase was rapid for lignin based hydrogels. It is also seen that the overall size of hydrogels was similar (100-125 μm), but sample 9L reached to this size in a slower pace than did other lignin-based hydrogel samples.

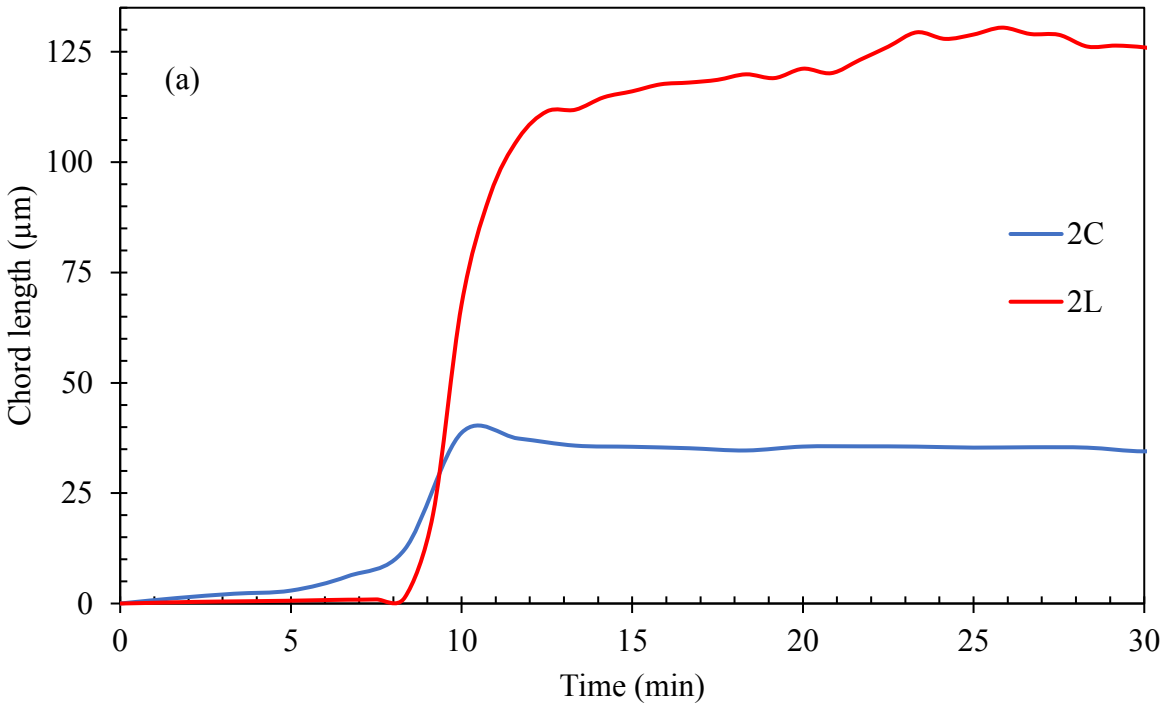
(a)
Chord length (µm)
Time (min)
2C
2L
0
25
50
75
100
125
0
5
10
15
20
25
30

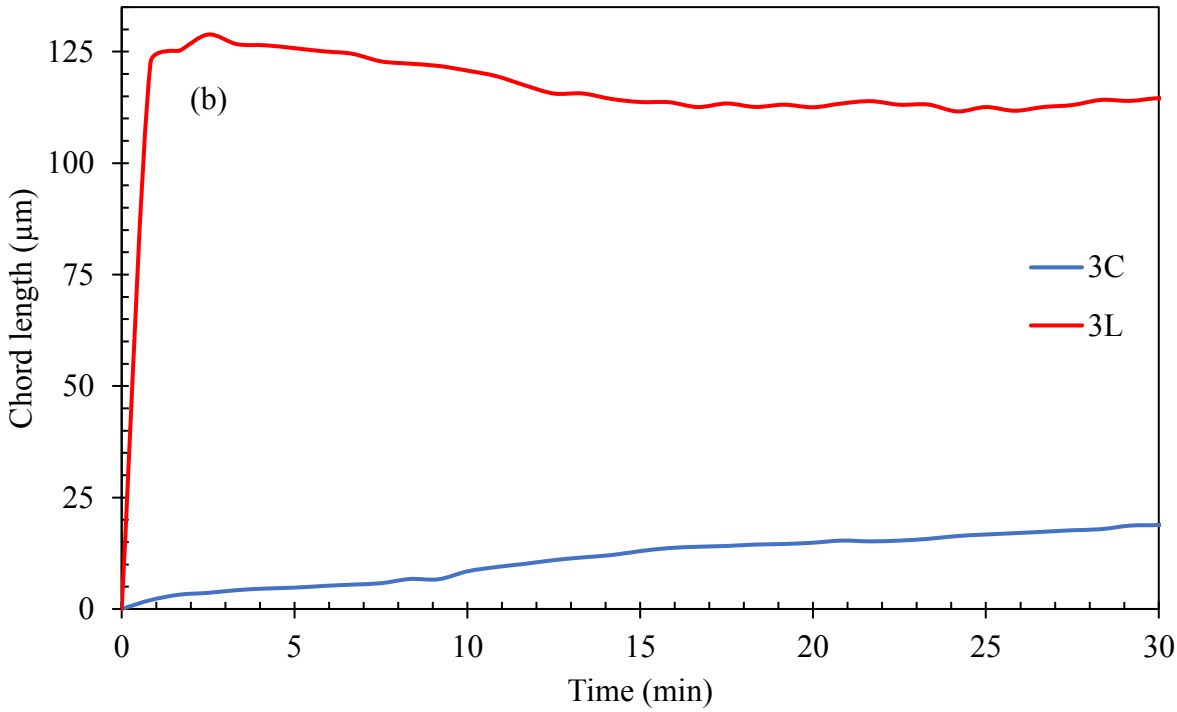
(b)
Chord length (µm)
Time (min)
3C
3L
0
25
50
75
100
125
0
5
10
15
20
25
30

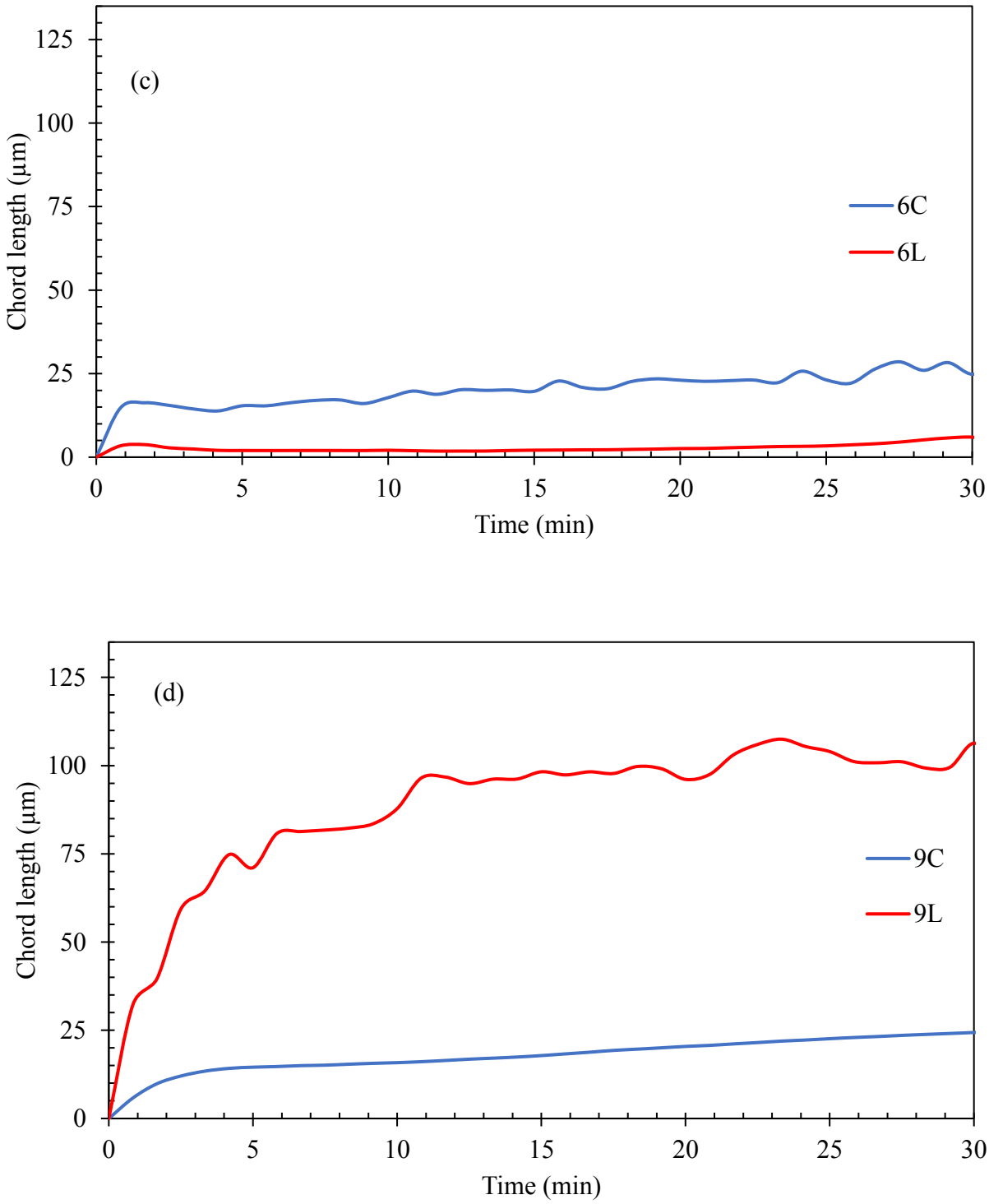

Figure 4.9. FBRM of control and lignin-based hydrogels: (a) 2C and 2L, (b) 3C and 3L, (c) 6C and 6L, and (d) 9C and 9L

4.9 Thermogravimetric analysis

The thermal decomposition behavior of the initiator, as well as all the reactants involved in the radical polymerization of the hydrogels are presented in Figure 4.10. AIBN is shown to exhibit a high rate of degradation from 60^{o}C to 135^{o}C according to Figure 4.10(a), indicating that AIBN is readily decomposed during the reaction. In other words, the selected reaction temperatures, 65^{o}C to 85^{o}C, may be considered ideal for free radical polymerization using AIBN. Figure 4.10(a) also plots the weight loss rate, or weight loss derivative, for which a significant peak is observed at 122.2^{o}C. At this temperature, AIBN exhibits its most significant decomposition, meaning that higher temperatures would results in immediate degradation of the initiator.

Figure 4.10(b) illustrates that lignin exhibits an initial weight loss of 12.9% due to residual moisture. Afterwards, lignin demonstrates a higher thermal stability in comparison to the other samples, a desirable property for additional end-use applications (Wu et al., 2012). Above 200^{o}C, lignin exhibits a gradual decrease in weight loss, and plateaus at a 55% weight loss above 600^{o}C. This is because the thermal breakdown of lignin occurs via two competing reaction paths; that is, the intramolecular condensation and the thermal depolymerization (Varfolomeev et al., 2015). This also supported by the weight loss derivative, which demonstrates a very gradual maximum between 200^{o}C and 600^{o}C.

N,N'-methylenebiscrylamide also demonstrates good thermal stability, as shown Figure 4.10(c). At 198^{o}C, the monomer exhibited a significant decrease in weight loss of approximately 4%, but was found to stabilize between 200^{o}C and 320^{o}C at 93.7% of its total weight. This initial weight loss may be attributed to the decomposition of the aliphatic alkenes groups. Between 320^{o}C and 500^{o}C, N,N'-methylenebiscrylamide reaches its melting point and undergoes another

considerable weight loss (66%), due to the breakdown of the remaining carboxylic and amine groups (Avşar et al., 2017). It should also be noted that N,N'-methylenebiscrylamide does not completely degrade within the studied range, but rather reaches a minimum weight of 19.1%.

N-isopropyacrylamide, however, whose weight loss begins at 60^{o}C, exhibits a much lower thermal stability. The melting point for N-isopropyacrylamide is between 60^{o}C and 63^{o}C, indicating that its decomposition is due to melting. Thus, the breakdown of the monomer structure should also occur readily in solution. Figure 4.10(d) also demonstrates a rapid rate of degradation at 162.9^{o}C, for which the weight loss rate curve exhibits a sharp peak, and a complete decomposition is achieved at approximately 190^{o}C.

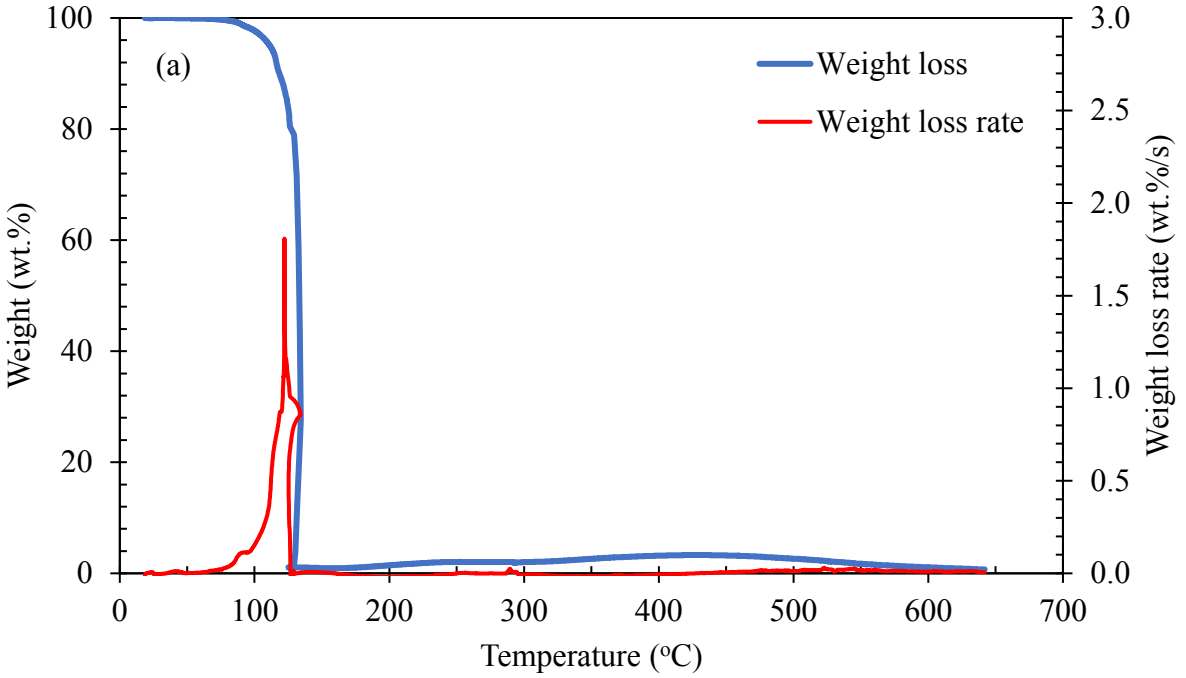
(a)
Weight loss
Weight loss rate
Weight (wt.%)
Weight loss rate (wt.%/s)
Temperature (°C)
0
20
40
60
80
100
0.0
0.5
1.0
1.5
2.0
2.5
3.0
0
100
200
300
400
500
600
700

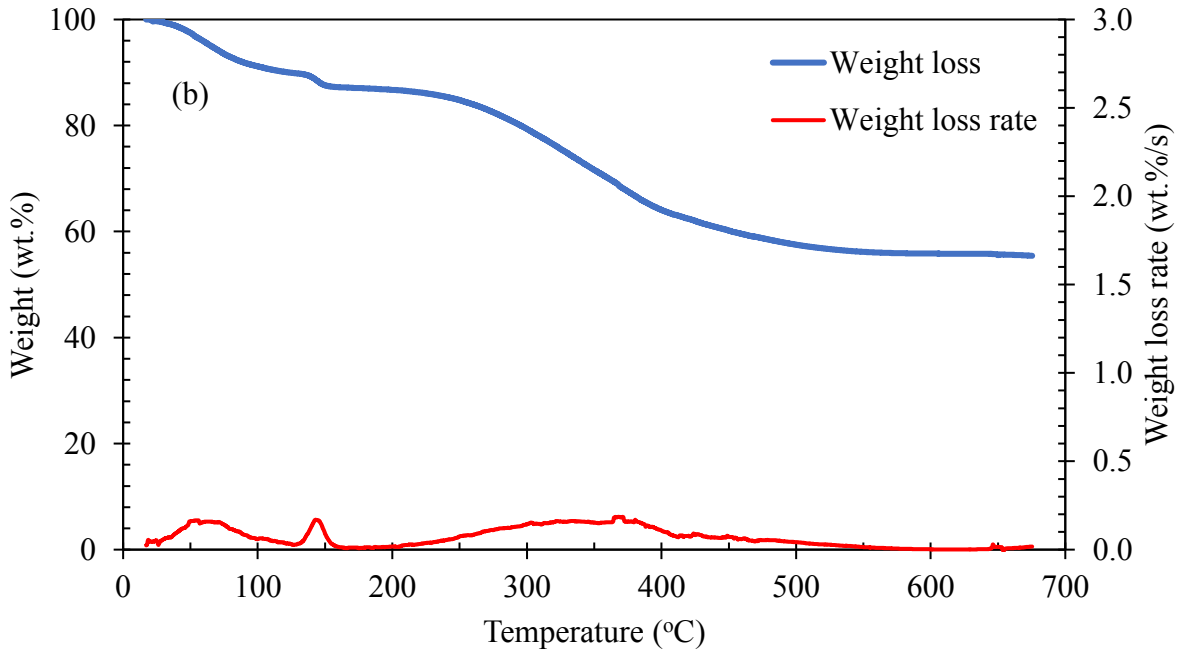
(b)
Weight loss
Weight loss rate
Weight (wt.%)
Weight loss rate (wt.%/s)
Temperature (°C)
0
20
40
60
80
100
0.0
0.5
1.0
1.5
2.0
2.5
3.0
0
100
200
300
400
500
600
700

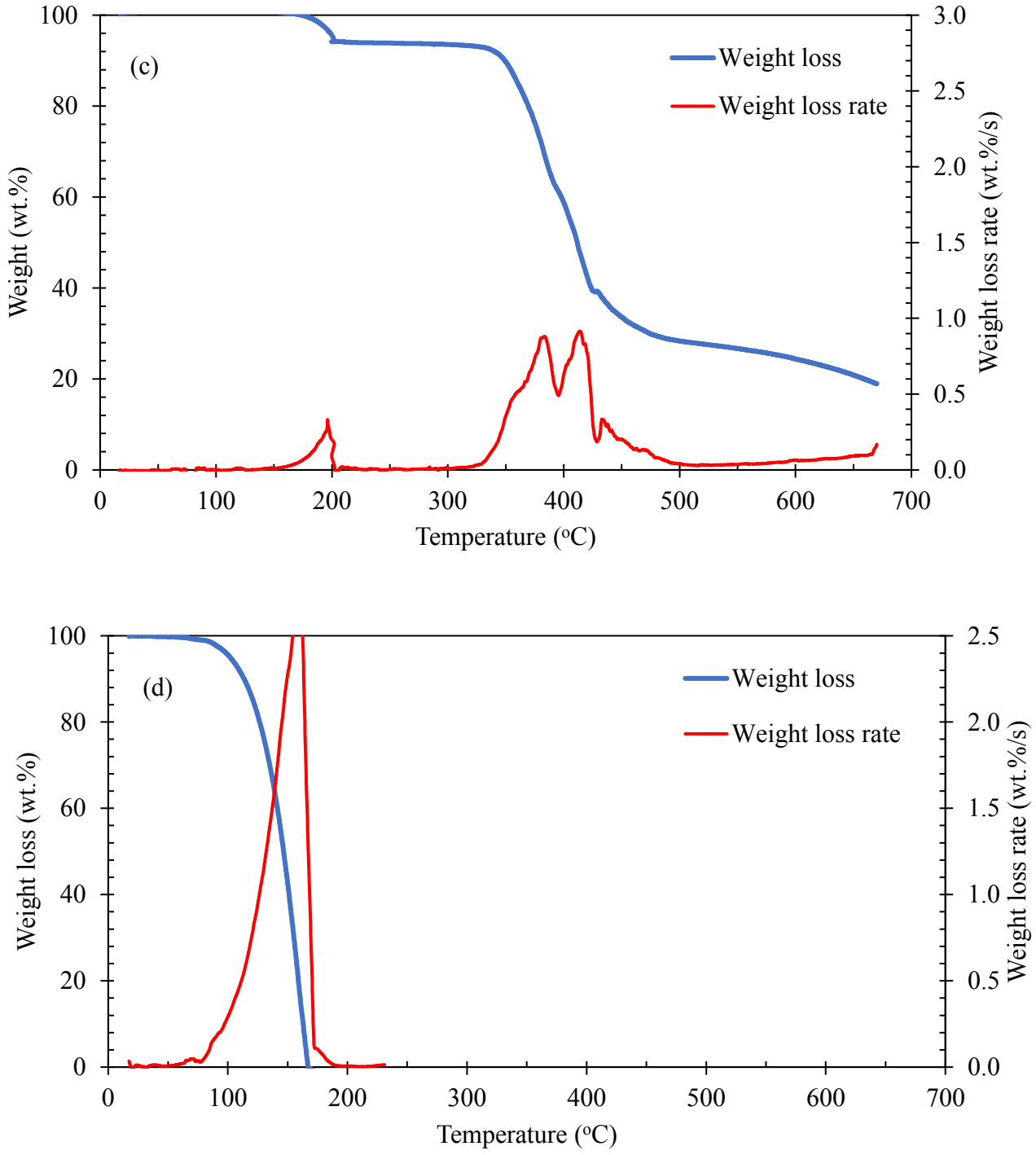

Figure 4.10. TGA of the initiator and reactants: (a) AIBN (b) kraft lignin (c) N,N'-methylebisacrylamide (d) N-isopropylacrylamide

The thermal stability of the hydrogels demonstrates a similar thermal behavior to that of N,N'-methylenebiscrylamide, indicating that it is largely present within the polymer matrix. According to Zarzyka et al. (2014), the incorporation of N,N'-methylenebiscrylamide allows for a higher crosslinking density, which in turn decreases the chain mobility within the gels. Therefore, since N,N'-methylenebiscrylamide is the limiting reagent and contributes highly to crosslinking, it can be assumed that it was readily consumed during the thermal decomposition reaction. The overall thermal stability of the hydrogels, however, is not as high as the N,N'-methylenebiscrylamide depicted in Figure 4.10(c). This is most likely due to the incorporation of N-isopropylacrylamide, which exhibit lower decomposition temperatures.

According to Figure 4.11, sample 2C was the most thermostable, followed by 3C, 6C, and 9C, respectively. This suggests that lower reaction temperatures could have resulted in a better conversion of N,N'-methylenebiscrylamide, since this monomer gives the hydrogel its thermostability.

Figure 4.12 shows the thermal behavior of lignin-based hydrogels. It is seen that the incorporation of lignin resulted in a slightly more thermostable polymer than the control samples. Sample 6L is demonstrated to be the most resistant to temperature, as it incorporated the highest amount of lignin during reaction. Samples 2L and 3L are shown to have a similar thermostability, whereas 9L is shown to have the lowest thermostability. This could be due the higher incorporation of N,N'-methylenebiscrylamide, which was less thermally stable than other components of the hydrogels.

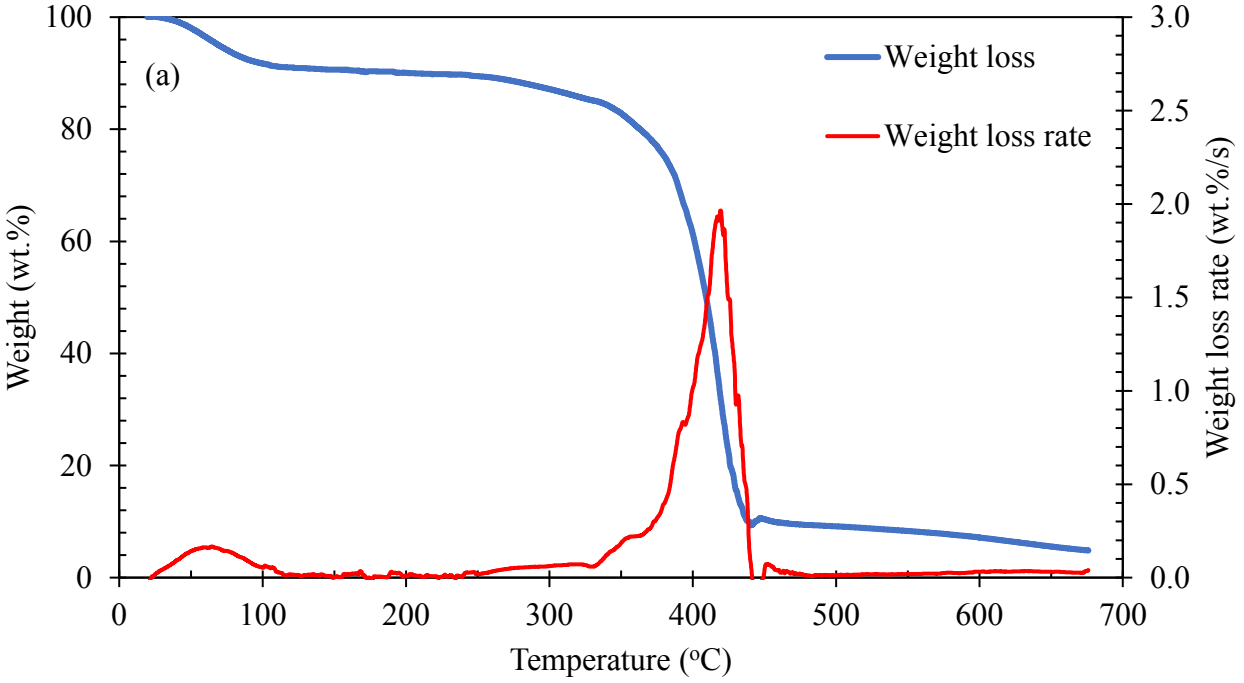
(a)
Weight loss
Weight loss rate
Weight (wt.%)
Weight loss rate (wt.%/s)
Temperature (°C)
100
80
60
40
20
0
3.0
2.5
2.0
1.5
1.0
0.5
0.0
0
100
200
300
400
500
600
700

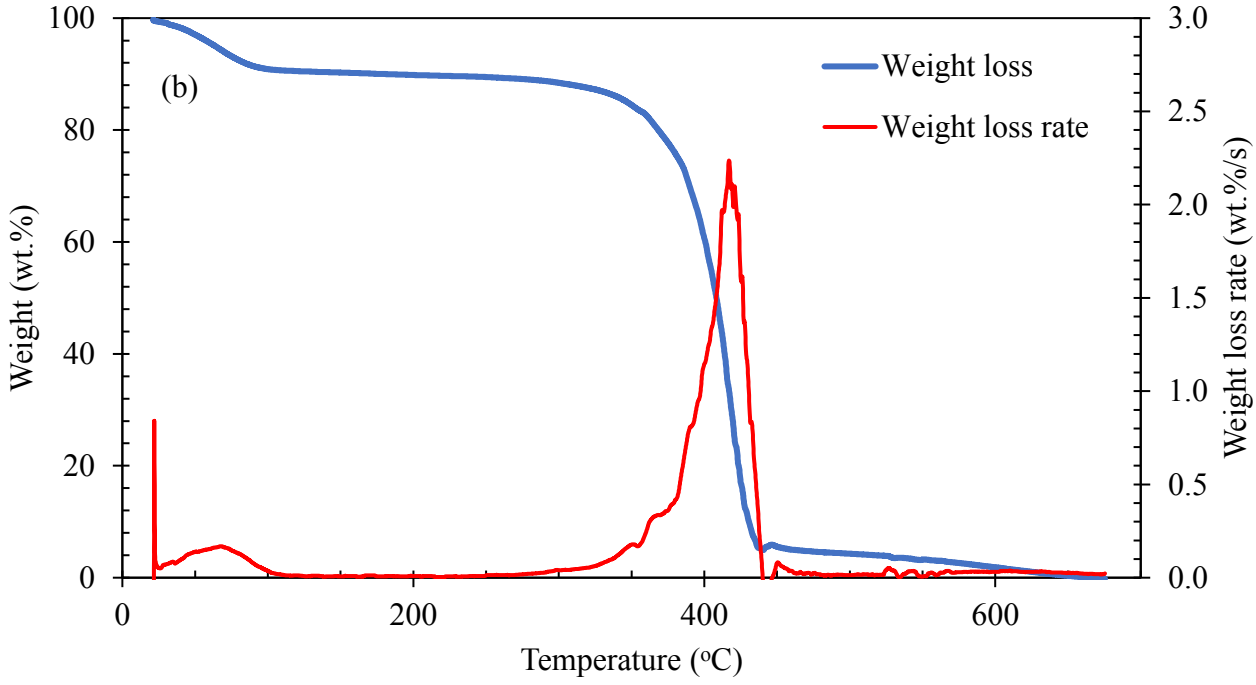
(b)
Weight loss
Weight loss rate
Weight (wt.%)
Weight loss rate (wt.%/s)
Temperature (°C)
100
80
60
40
20
0
3.0
2.5
2.0
1.5
1.0
0.5
0.0
0
200
400
600

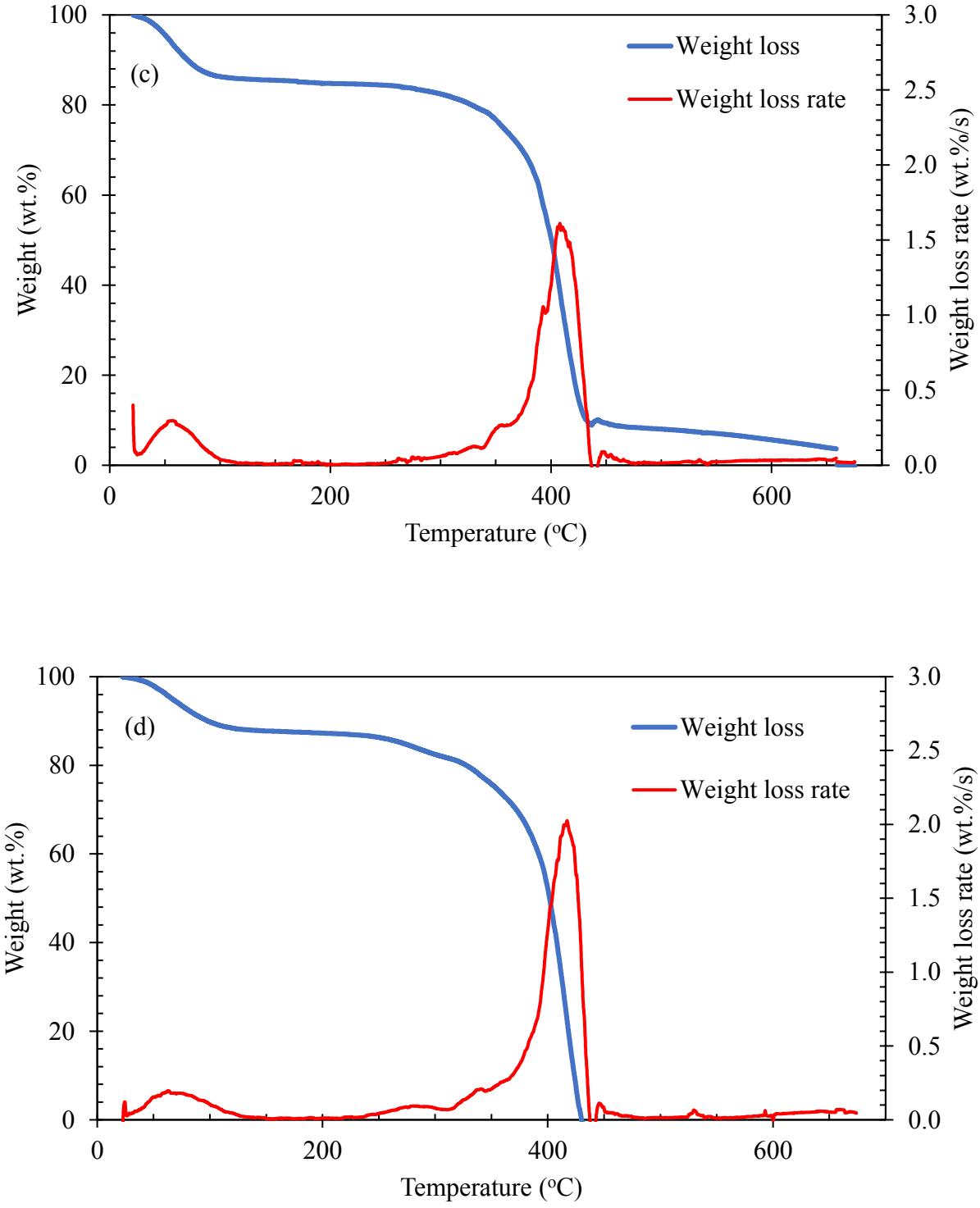

Figure 4.11. TGA of control hydrogels: (a) 2C, (b) 3C, (c) 6C, and (d) 9C

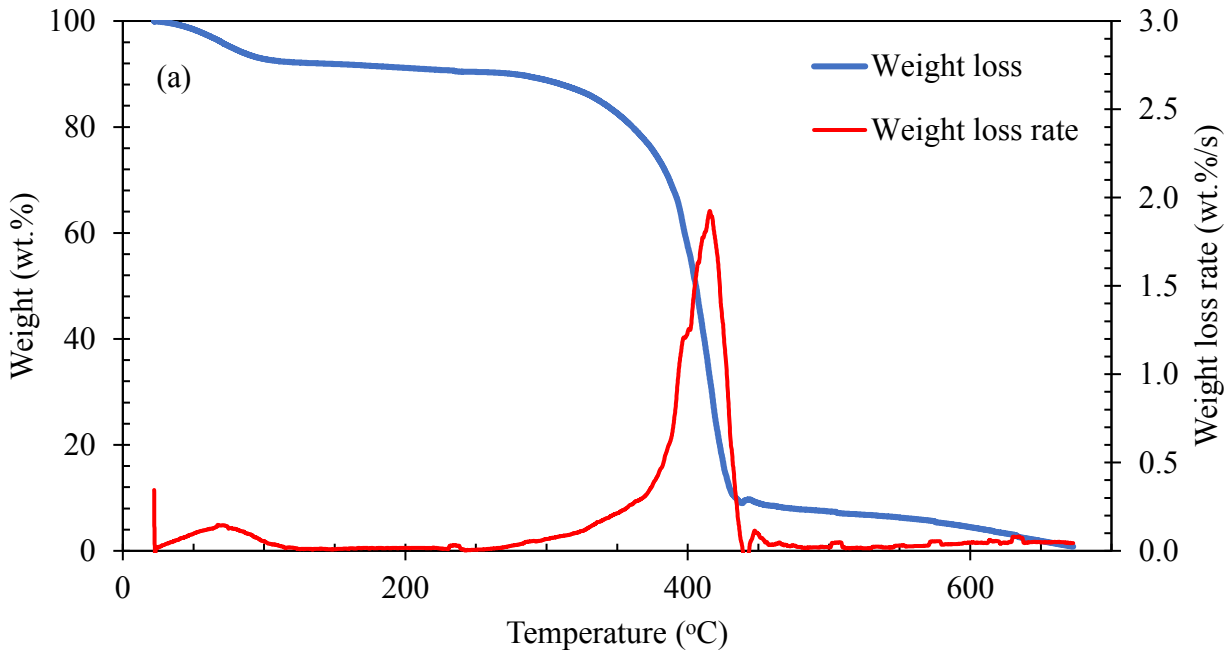
(a)
Weight loss
Weight loss rate
Weight (wt.%)
Weight loss rate (wt.%/s)
Temperature (°C)
100
80
60
40
20
0
3.0
2.5
2.0
1.5
1.0
0.5
0.0
0
200
400
600

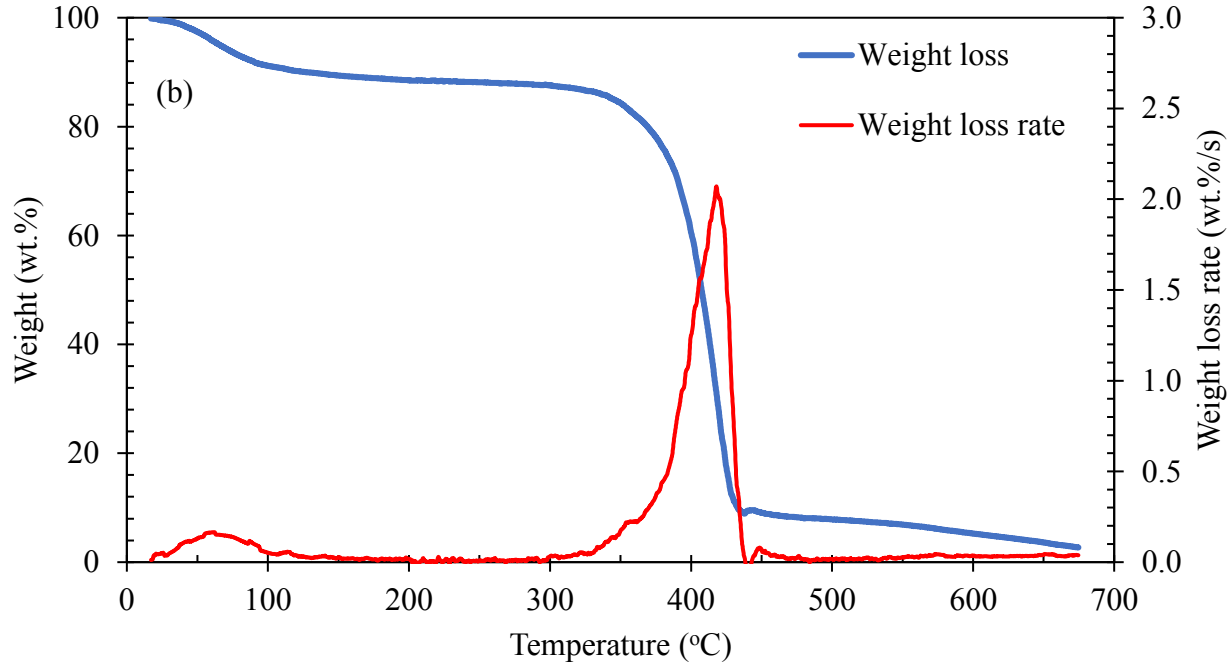
(b)
Weight loss
Weight loss rate
Weight (wt.%)
Weight loss rate (wt.%/s)
Temperature (°C)
100
80
60
40
20
0
3.0
2.5
2.0
1.5
1.0
0.5
0.0
0
100
200
300
400
500
600
700

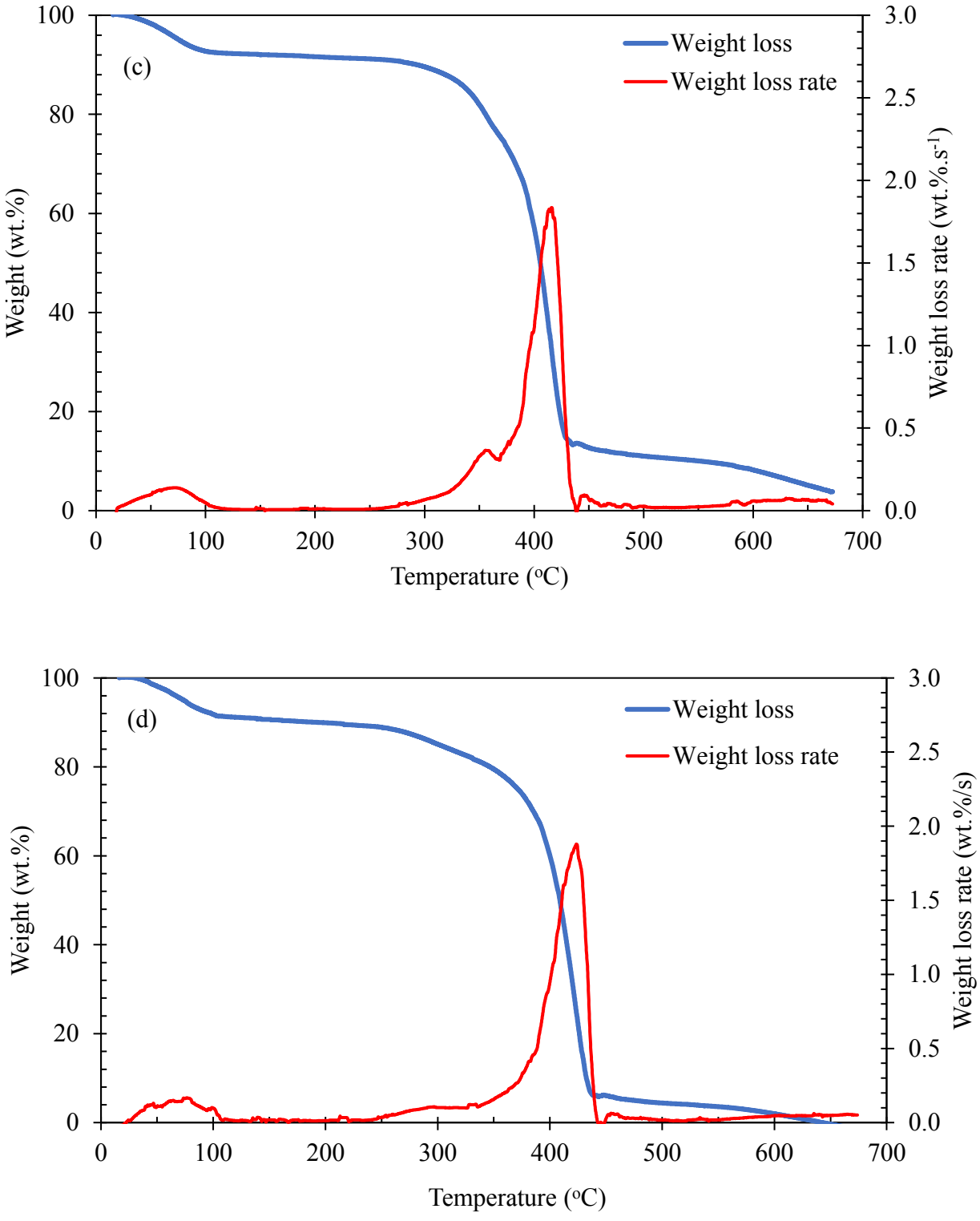

Figure 4.12. TGA of lignin-based hydrogels: (a) 2L, (b) 3L, (c) 6L, (d) 9L

4.10 Differential scanning calorimetry

Figure 4.13 illustrates the results of DSC analysis. It is seen that all of the selected samples are shown to exhibit a baseline shift, associated to the glass transition temperature (T_g). This is the temperature at which the vibrationally inactive chains within the amorphous regions of the polymer undergo long-range segmental motion (Jadhav et al., 2009).

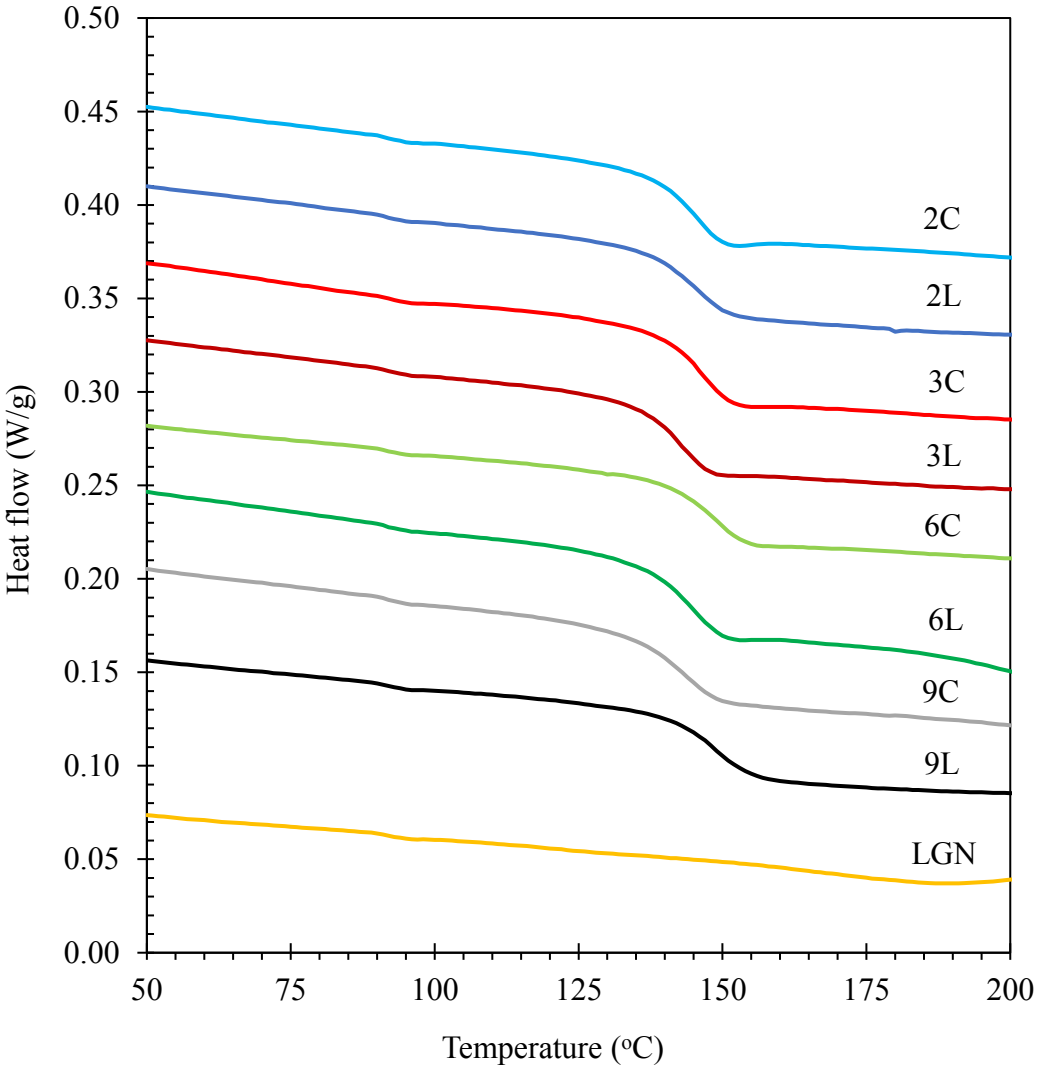

Figure 4.13. DSC of the control hydrogels, lignin-based hydrogels, and kraft lignin

Based on the results in Figure 13, the T_g of the samples were determined and listed in Table 11. The control and lignin-based hydrogels exhibit a T_g between 141.45ºC and 148.60ºC. This is found to be higher than the reported T_g of the linear poly(N-isopropylacrylamide) homopolymer (control samples), which exhibits this baseline shift between 85ºC and 130ºC (Geever et al., 2006; Erbil et al., 2004). As explained earlier, this overall increase in T_g for the crosslinked hydrogels is most likely due to the incorporation N,N'-methylenebiscrylamide (Avşar et al., 2017). The samples having a reduced amount of N-isopropylacrylamide resulted in a higher T_g. Regarding the control samples, 2C, 3C and 9C were found to have similar values for T_g as they were produced with high amounts of the N-isopropylacrylamide (1.8 to 2.4 g). Consequently, sample 6C, which only incorporated 1.2 g of the monomer, resulted in a higher T_g. The lignin-based samples also followed the same behavior, with 6L having the highest T_g. The addition of lignin did not increase the T_g when compared with the control samples, further indicating that N,N'-methylenebisacrylamide was responsible for the thermal stability of the hydrogels (Avşar et al., 2017). Kraft lignin is shown to exhibit the highest T_g at 159.25ºC, a high thermal stability and amorphous composition (Carraher, 2013). This is comparable to the reported T_g values for lignin in this analysis, which range between 80ºC and 220ºC depending on its source and treatment (Kadla et al., 2002; Kadla & Kubo, 2004; Raschip et al., 2013).

In Figure 4.13, a small exothermic region may be observed following the T_g, which is most likely due to the tendency for polymers to form micelles when subjected to segmental mobility (Carraher, 2013). This is due the decrease in heat capacity, which polymers exhibit at the T_g, induced by this relaxation process (Schawe, 2002). The associated heat capacity for all selected samples were found to range from 0.262 J/g ºC to 0.532 J/g ºC, as shown in

Table 4.10.

Table 4.10. Glass transition and heat capacity of the control hydrogels, lignin-based hydrogels, and kraft lignin

Sample	Glass transition temperature, T_g (°C)	Heat capacity, ΔC_p (J/g °C)
2C	143.56	0.398
2L	145.53	0.485
3C	144.48	0.526
3L	142.40	0.532
6C	148.60	0.288
6L	146.59	0.321
9C	143.09	0.262
9L	141.45	0.427
LGN	159.25	0.369

4.11 Rheology

The crosslinked structure of hydrogels can be characterized by applying dynamic oscillatory measurements. In other words, a sinusoidal oscillation with a given deformation and frequency may be inputted onto a material to obtain sinusoidal output for strain. Oscillatory measurements are applied for materials that exhibit purely viscoelastic properties such as crosslinked polymers and gels (Passauer et al., 2011). Their viscoelastic properties may be characterized by storage modulus (G'), which describes the material's elasticity, and loss modulus (G''), which is attributed to viscosity. The elastic component characterizes a material's

solid-like ability to store energy (its stiffness), whereas the viscous component is the liquid-like capability to dissipate energy (Seddiki & Aliouche, 2013; Rodriguez et al., 2003).

4.11.1 Frequency sweep

Figure 4.14 illustrates the effect of frequency on storage (G') and loss (G'') modulus, as well as on dynamic viscosity (η), for both the control and lignin-based hydrogel samples. Some loss modulus values were unable to be measured accurately at low frequencies and are thus analyzed from 6.30 rad/s (Okay & Oppermann, 2007). For all cases, the storage modulus is greater than that of the loss modulus, indicating that the hydrogel samples exhibit more elastic properties. This behavior is typical for gels as the solid-like mechanical properties of their crosslinked structure are more dominant than the viscous properties attributed to the small amorphous part of the polymer network (Passauer et al., 2011). In addition, both the storage and loss modulus were found to increase with increasing shear frequency, allowing for more energy to be dissipated. Although frequency is shown to influence the moduli curves, its dependence is not largely significant, indicating that the hydrogels have a well-structured three-dimensional network (Van Den Bulcke et al., 2000). Furthermore, the dynamic viscosity is also shown to linearly decrease with increasing frequency, an attribute typical to gels (Passauer et al., 2011).

In general, the amount of energy dissipated was found to be slightly greater for the control samples than the lignin-based samples. This may be due to the incorporation of lignin resulting in a less crosslinked structure. In other words, the network structure of the control samples is more tightly crosslinked, and are therefore better able to dissipate energy. Figure 4.14 (a) and (b) illustrated a large difference in rheological properties between the 2C and 2L. A potential reason may be the low reaction temperature and short reaction time of this sample compared to the other samples studied. At reaction conditions for sample 2, the resulting yield

was found to be significantly lower for the lignin-based hydrogel samples compared to the control samples; 77.86% and 93.88%, respectively. Due to the large size of the lignin polymer, additional time may have been required for the lignin-based sample to achieve a similar degree for crosslinking as the control sample (Peng & Chen, 2011). As a result, the amount of energy dissipated from the lignin-based sample with an applied frequency would be significantly lower than its control sample counterpart. Samples 3C and 3L in Figure 4.14 (c) and (d) are also shown to have a large difference between them, also supporting that the same theory. Figure 14(e) and (f), on the other hand, demonstrates that samples 6C and 6L have more similar moduli. This is also the case for sample 9L and 9C, shown in Figure 4.14(g) and (h). Despite these differences, however, the rheological behavior for the lignin-based hydrogels were found to be relatively similar, the changes in moduli mainly occurring within the control samples. A potential reason could be that the composition variation of lignin within the hydrogel structures was not great enough to be visible in a frequency range of the test.

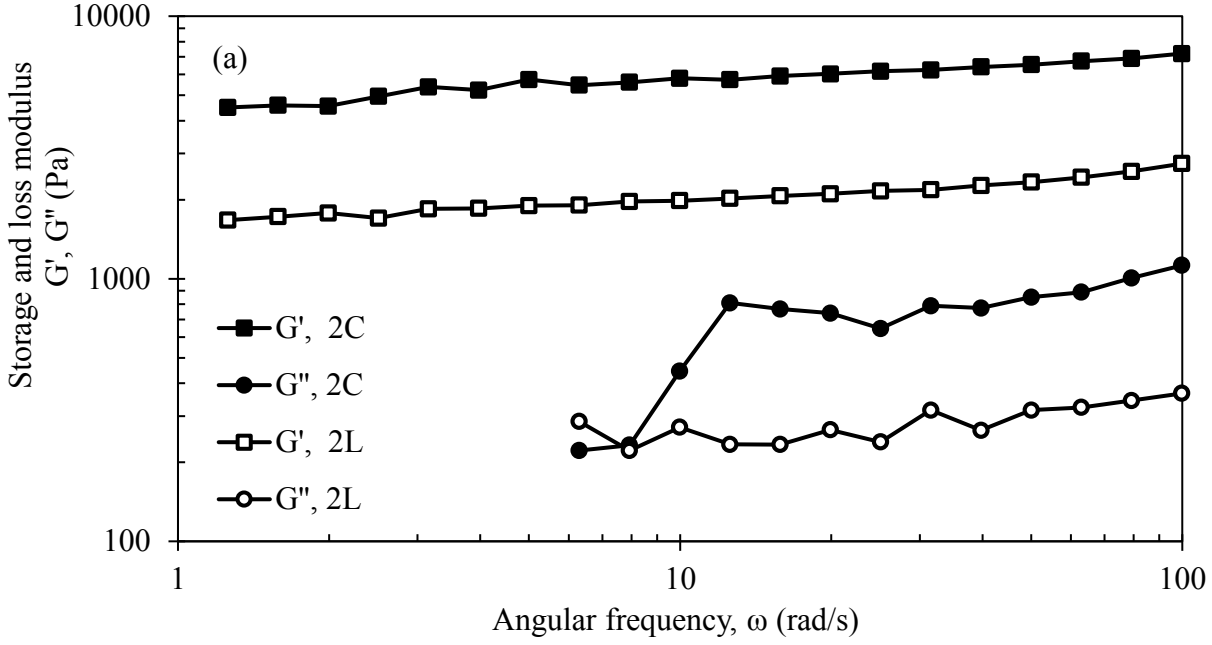
(a)
Storage and loss modulus
G', G" (Pa)
10000
1000
100
1
10
100
Angular frequency, ω (rad/s)
G', 2C
G", 2C
G', 2L
G", 2L

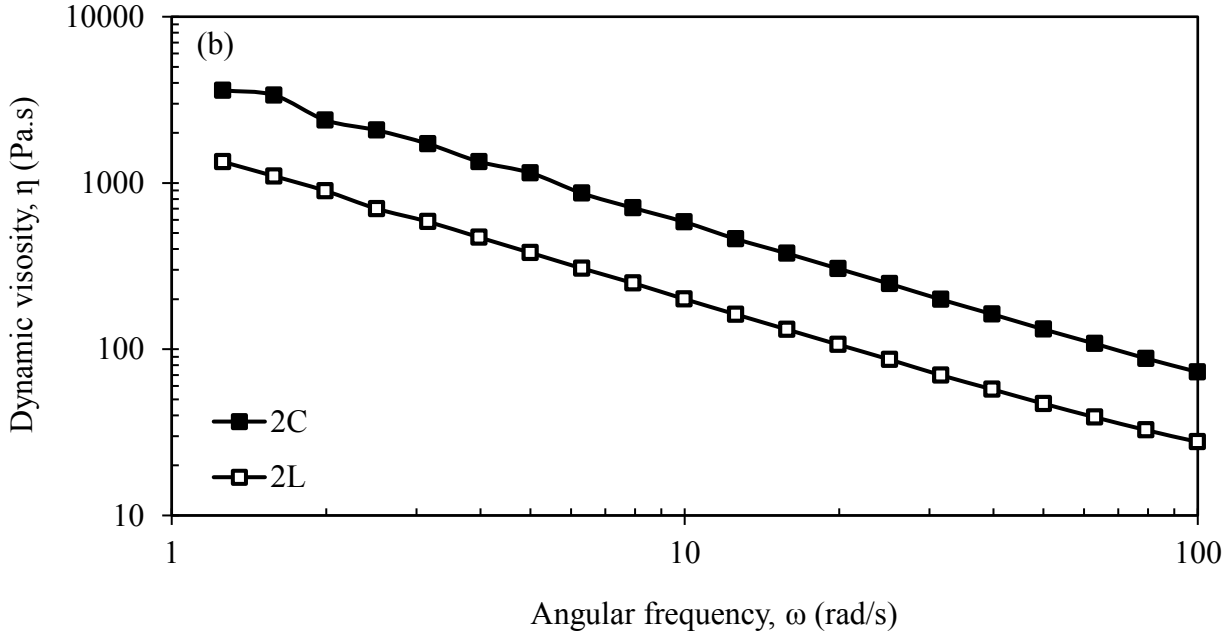
(b)
Dynamic visosity, η (Pa.s)
10000
1000
100
10
1
10
100
Angular frequency, ω (rad/s)
2C
2L

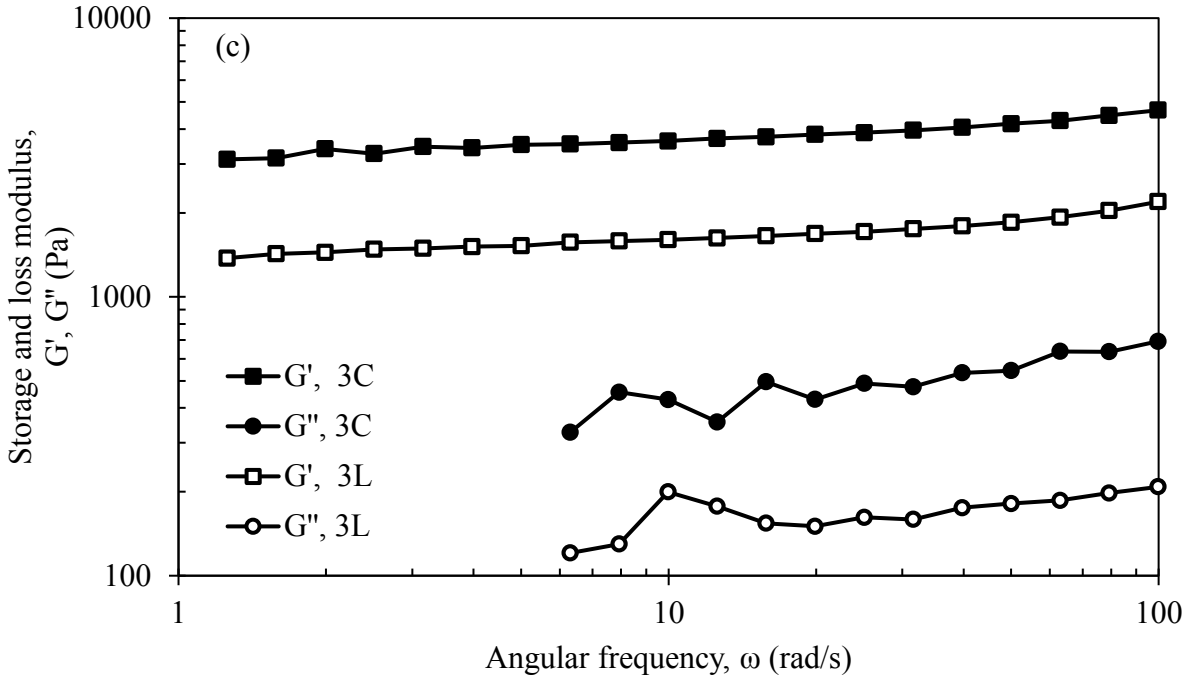
(c)
10000
1000
100
1
10
100
Storage and loss modulus, G', G'' (Pa)
Angular frequency, ω (rad/s)
G', 3C
G'', 3C
G', 3L
G'', 3L

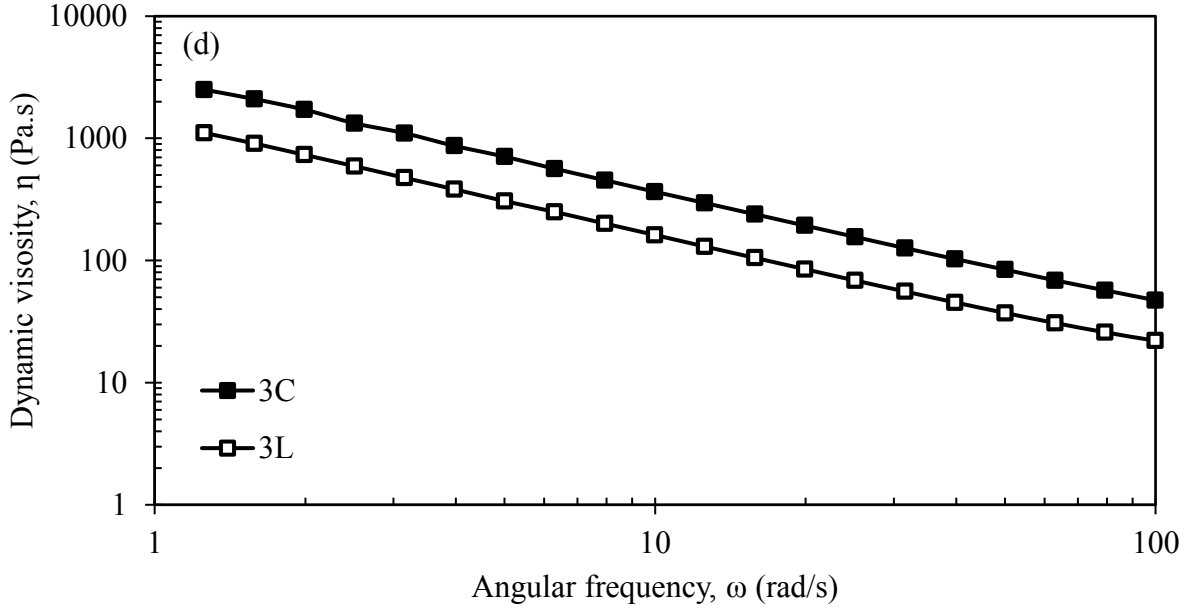
(d)
10000
1000
100
10
1
1
10
100
Dynamic visosity, η (Pa.s)
Angular frequency, ω (rad/s)
3C
3L

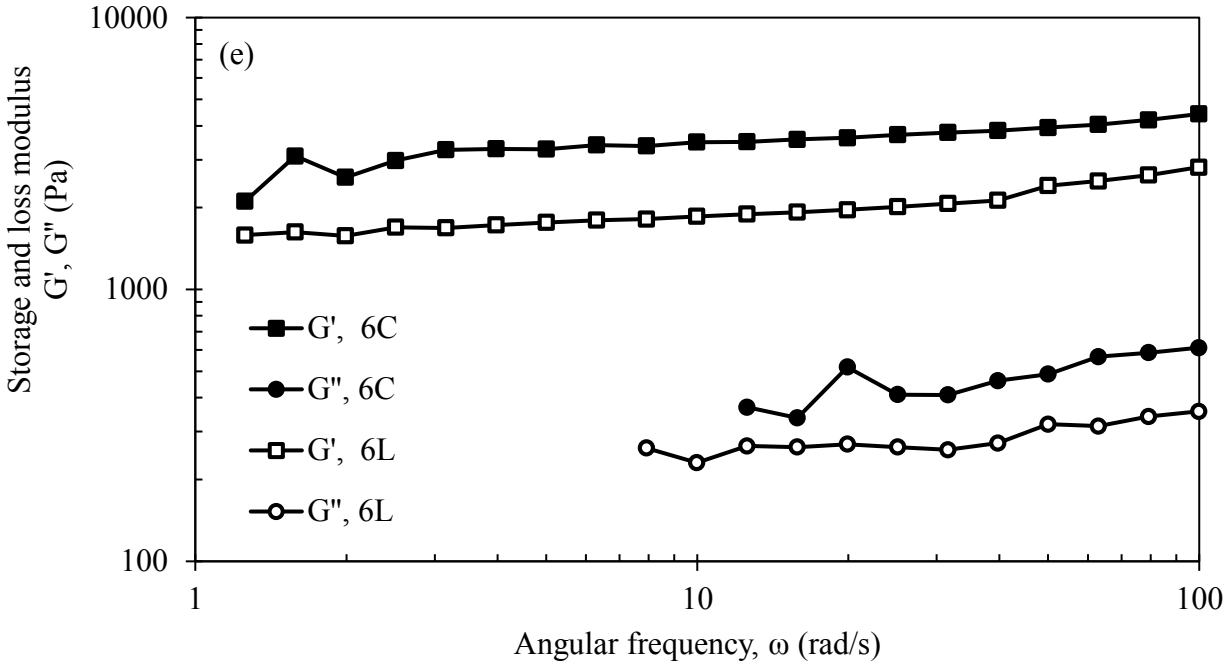
(e)
Storage and loss modulus
G', G" (Pa)
10000
1000
100
1
10
100
Angular frequency, ω (rad/s)
G', 6C
G", 6C
G', 6L
G", 6L

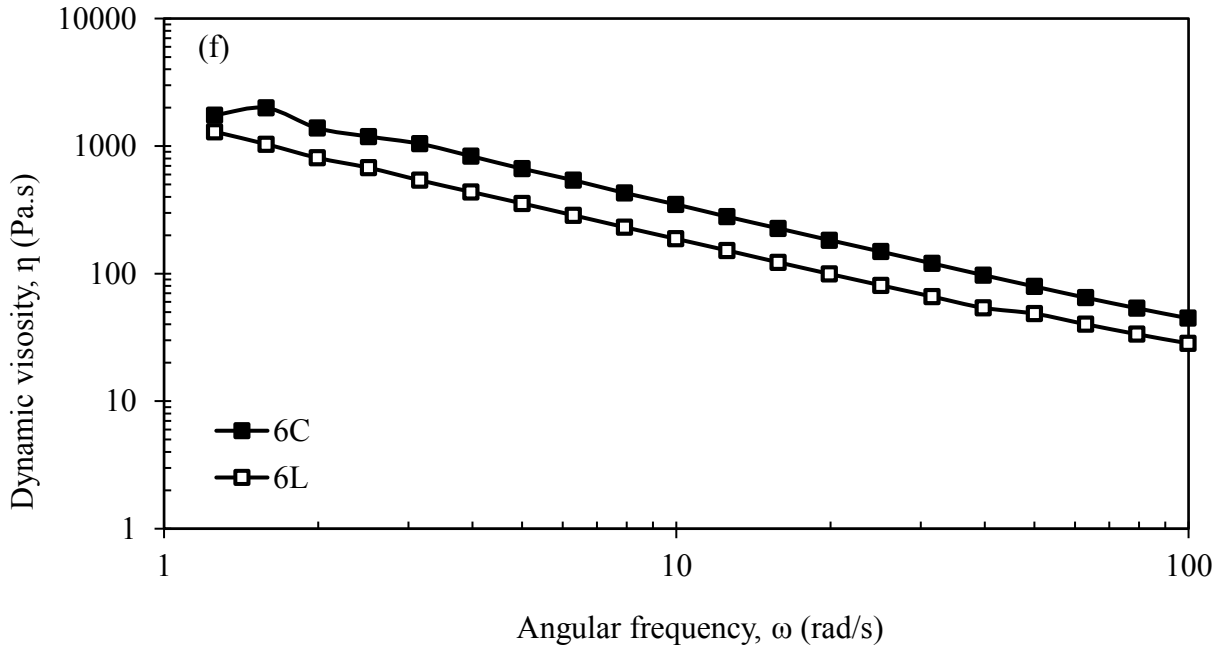
(f)
Dynamic visosity, η (Pa.s)
10000
1000
100
10
1
1
10
100
Angular frequency, ω (rad/s)
6C
6L

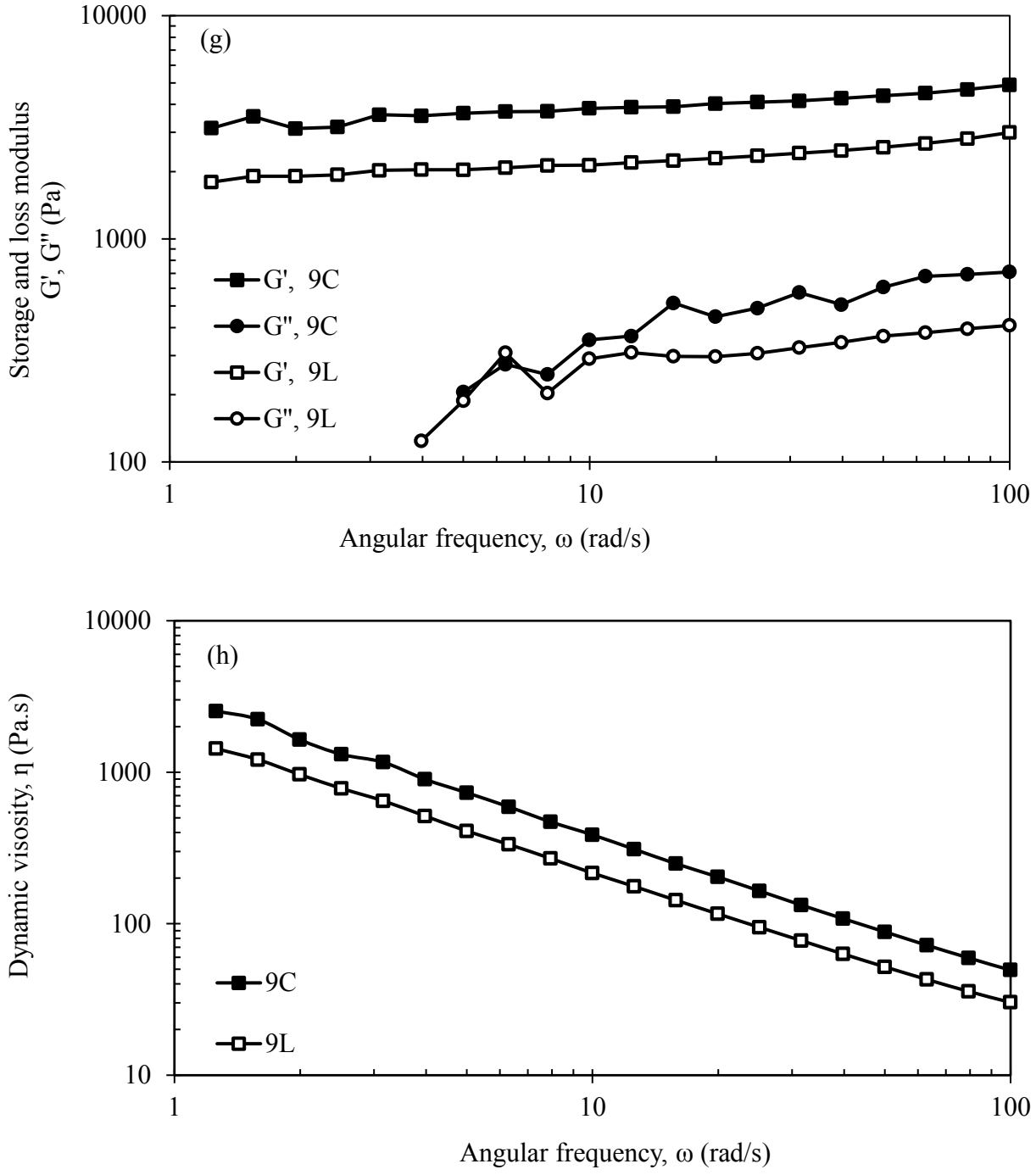

Figure 4.14. Frequency sweep of the control and lignin-based hydrogels: (a) Moduli of 2C and 2L (b) Dynamic viscosity of 2C and 2L, (c) Moduli of 3C and 3L, (d) Dynamic viscosity of 3C and 3L, (e) Moduli of 6C and 6L, (f) Dynamic viscosity of 6C and 6L, (g) Moduli of 9C and 9L, (h) Dynamic viscosity of 9C and 9L

4.11.2 Amplitude sweep

Figure 4.15 demonstrates the change in moduli with increasing strain. Generally, the hydrogels with identical reaction conditions were found to exhibit similar properties within the linear viscoelastic region (LVR). Within this region, as indicated within Figure 4.15(b), the strain applied does not exhibit a strong effect on the moduli, which serves as an indication of the hydrogels' rigidity (Ramazani-Harandi et al., 2006). In addition, the storage modulus is shown to exhibit a higher plateau, indicating that the samples' such as a viscoelastic solid (Han et al., 2014).

Above the LVR, the storage modulus is shown to significantly decrease with increasing strain, indicating a disturbance within the network structure. The loss modulus, on the other hand, slightly increases before rapidly decreasing after reaching 100% strain (or deformation). This maximum indicates the microscopic failure within the hydrogel network structure (Su & Okay, 2017). At this point, the storage and loss modulus exhibit a crossover where the hydrogel exhibits a phase change from primarily elastic to primarily viscous (Okay & Oppermann, 2007). This indicates the irreversible deformation of the three-dimensional network structure which gives the hydrogel its elasticity (Ricciardi, 2003; Seddiki & Aliouche, 2013). This is further elaborated in Figure 4.16.

For the most part, the crossover for the control samples was shown to occur at a lower strain rate compared to the lignin-based samples. This is most likely due to the increased mechanical properties of hydrogel via incorporation of lignin (Passauer et al., 2011). In addition, the LVR has a larger width for the lignin-based samples compared to the control samples, further supporting that the incorporation of lignin increases the samples' rigidity.

For the control samples, 3C was found to have the highest elastic moduli, indicating that the hydrogel is highly crosslinked. This is consistent with the data obtained from the swelling experiments, the high swelling ratio of 3C indicating a well-developed network structure. Sample 2C, with the lowest swelling ratio, was found to have the lowest elastic moduli. Hydrogel samples 6C and 9C, on the other hand, were found to exhibit trends similar to one another.

With respect to the lignin-based samples, 2L exhibited the highest storage modulus, followed by 9L. This behavior is similar to that of the control samples, which was also consistent with the previously obtained swelling capacities. This suggests that swelling ratio is an adequate performance measure for the crosslinked structure of the hydrogels. No significant difference could be observed, however, for samples 3L and 6L, as their maximum swelling capacities are similar.

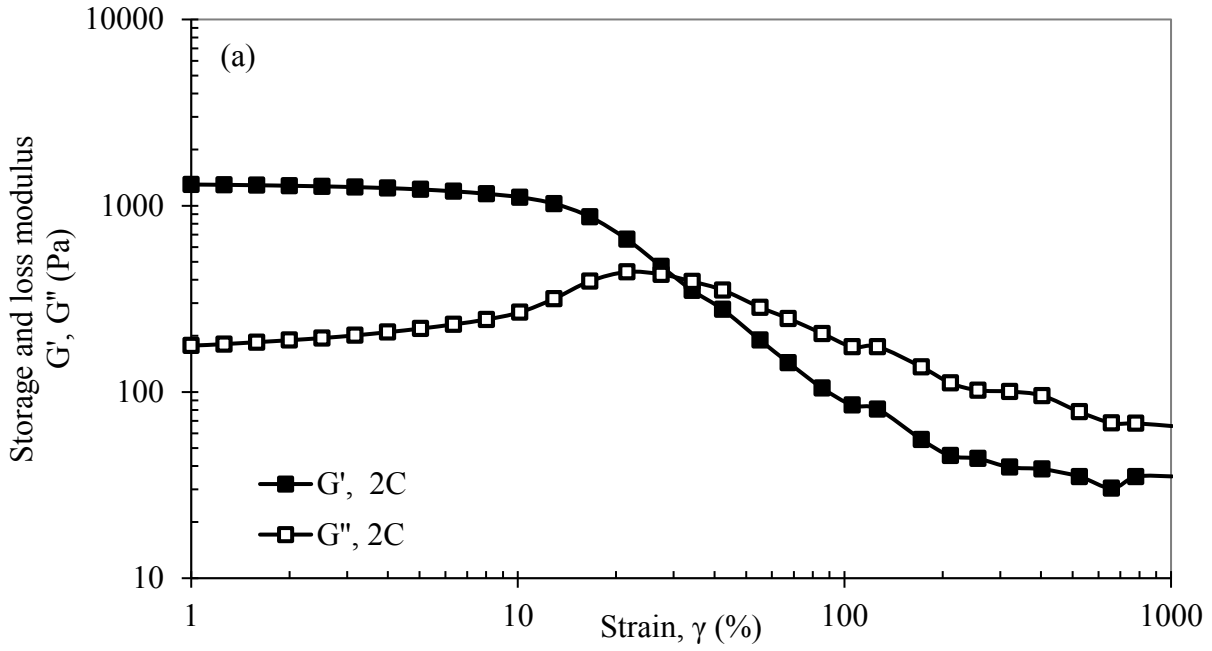
(a)
10000
1000
100
10
Storage and loss modulus
G', G" (Pa)
G', 2C
G", 2C
1
10
100
1000
Strain, γ (%)

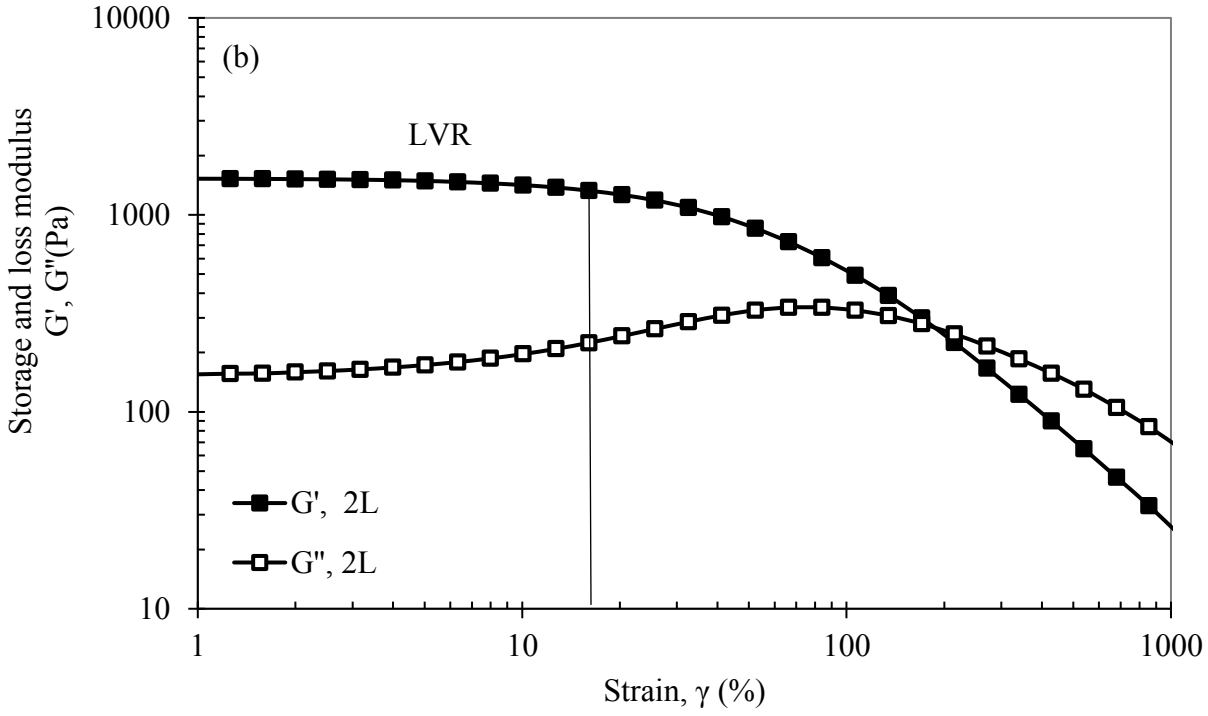
(b)
LVR
10000
1000
100
10
Storage and loss modulus
G', G"(Pa)
G', 2L
G", 2L
1
10
100
1000
Strain, γ (%)

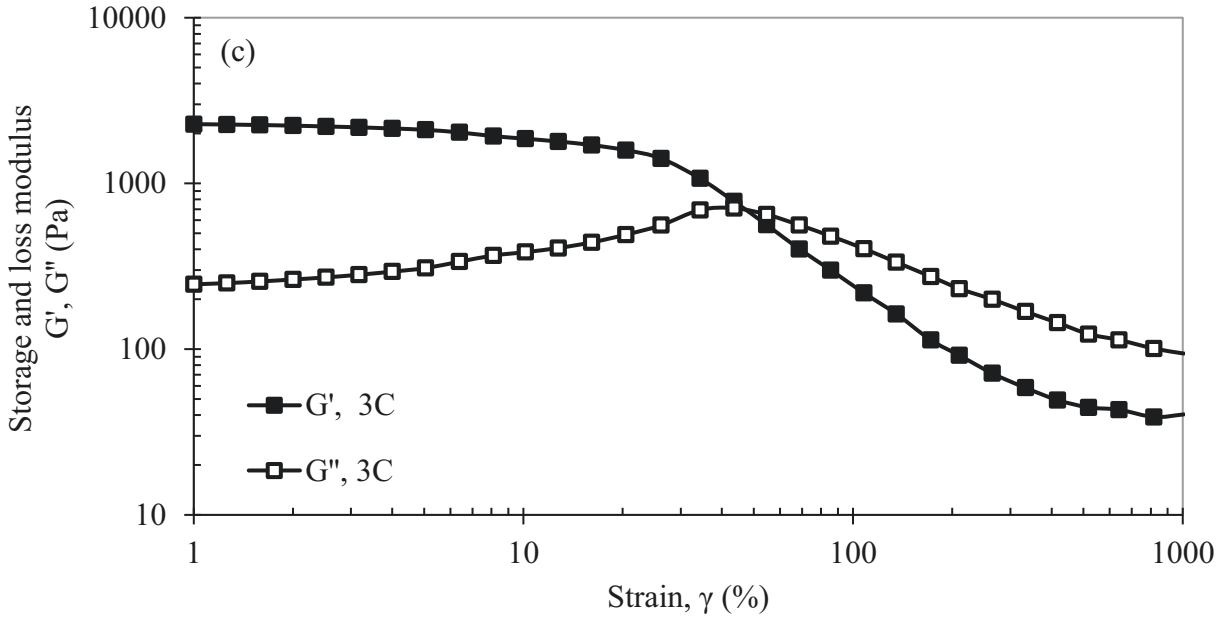
(c)
Storage and loss modulus G', G" (Pa)
10000
1000
100
10
1
10
100
1000
Strain, γ (%)
G', 3C
G", 3C

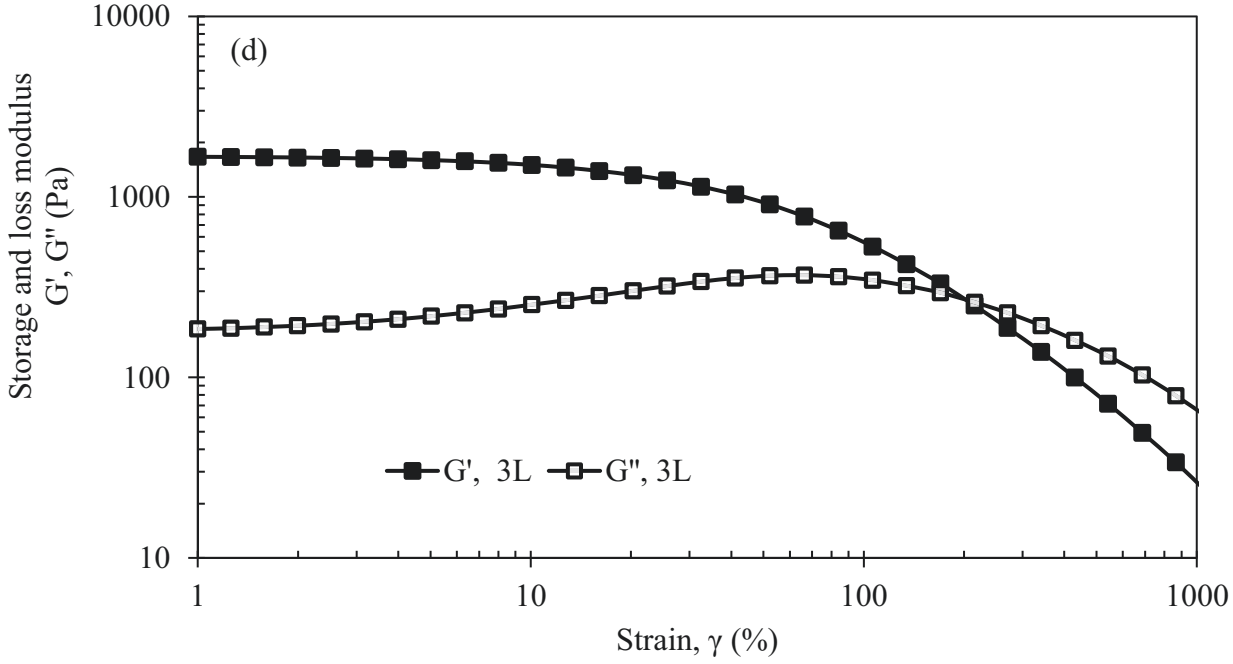
(d)
Storage and loss modulus G', G" (Pa)
10000
1000
100
10
1
10
100
1000
Strain, γ (%)
G', 3L
G", 3L

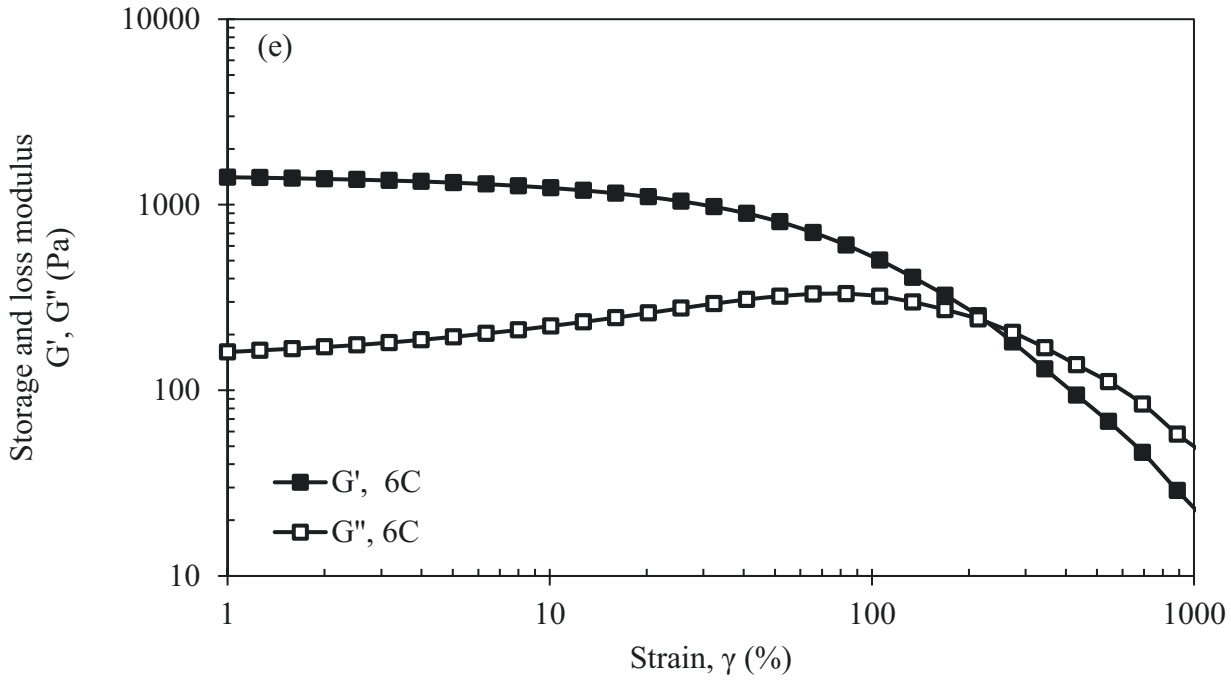
(e)
10000
1000
100
10
1
10
100
1000
Storage and loss modulus
G', G'' (Pa)
Strain, γ (%)
G', 6C
G'', 6C

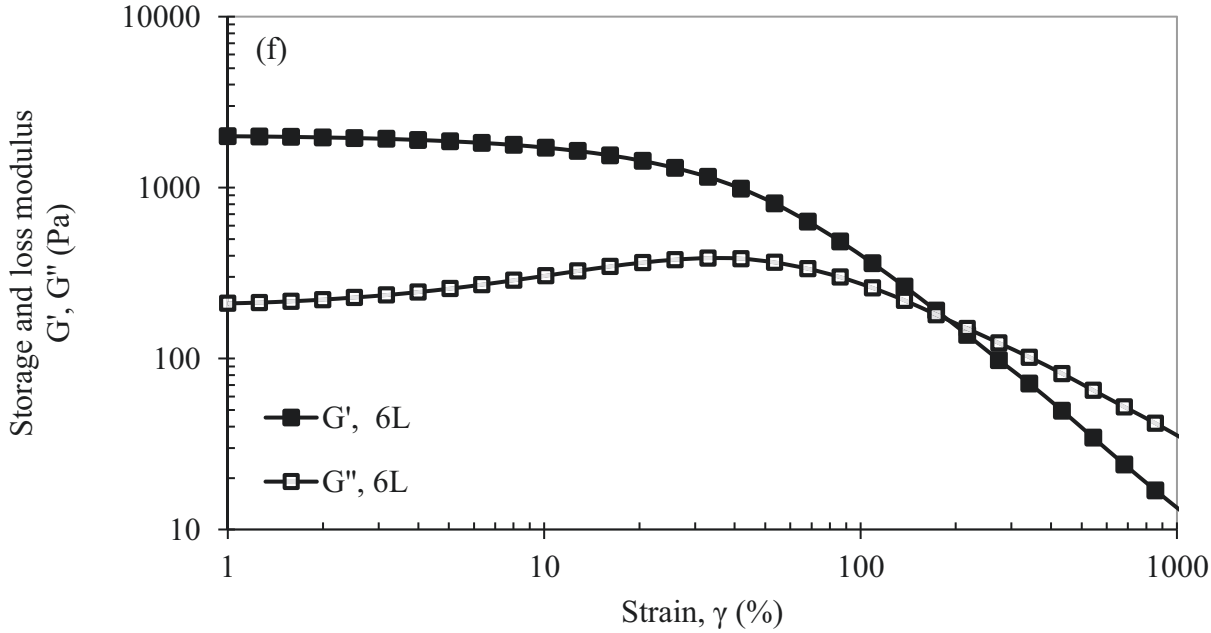
(f)
10000
1000
100
10
1
10
100
1000
Storage and loss modulus
G', G'' (Pa)
Strain, γ (%)
G', 6L
G'', 6L

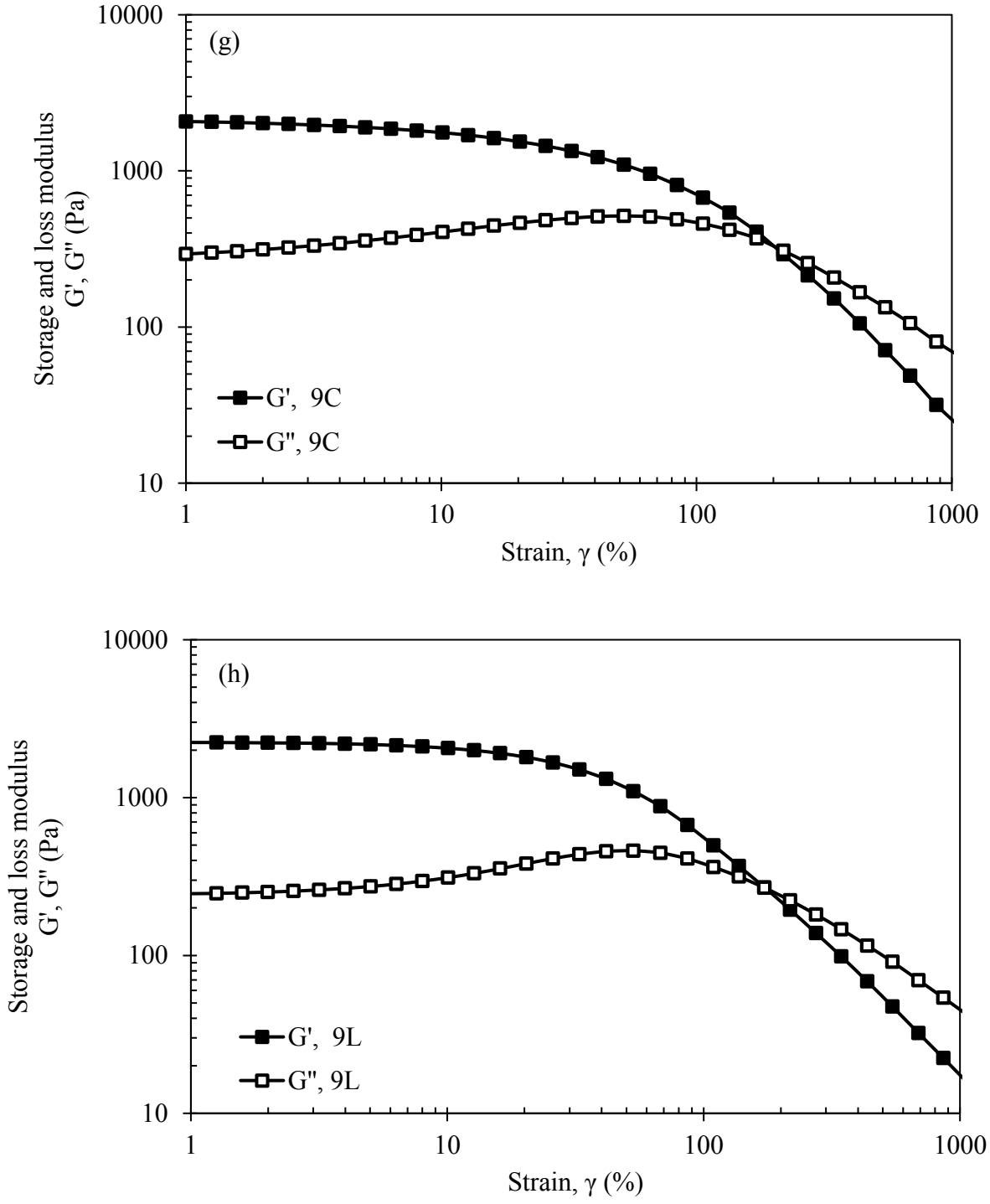

Figure 4.15. Strain amplitude sweep of the control and lignin-based hydrogels: (a) Strain of 2C, (b) 2L, (c) 3C, (d) 3L, (e) 6C, (f) 6L, (g) 9C, (h) 9L

The results in Figure 4.15 can also be plotted with respect to oscillation stress, as illustrated in Figure 4.16. The initial plateau designates the LVR, for which the change in moduli is denoted by the yield point (τ_y) as illustrated in Figure 4.16(b). As the moduli exhibits a crossover from mainly elastic to mainly viscoelastic, this crossover is known as the flow point (τ_f), as illustrated in Figure 4.16(b). These results for both these points are summarized in Table 4.11. For the control hydrogels, 9C was found to have the flow point at the highest oscillation strain, followed by 3C, 6C, and 2C, respectively. The high stability of sample 9C could have been a result in high reaction time, temperature, and N-isopropylacrylamide content, which could have led to an increase in crosslinking density. Furthermore, the lignin-based hydrogels were also found to follow the same behavior, the flow point occurring at the highest stress for 2L, 9L, 3L, and 6L, respectively. This is directly related to the maximum swelling capacity, which follows the same order, suggesting that swelling ratio is an accurate measure of crosslinking.

Table 4.11. Flow point and yield flow point for control and lignin-based hydrogels

Sample	Yield point, τ_y (Pa)	Flow point, τ_f (Pa)
2C	95.1	175.2
2L	216.1	628.9
3C	158.9	471.7
3L	169.6	293.1
6C	209.4	668.8
6L	144.3	474.2
9C	182.3	918.4
9L	312.2	668.9

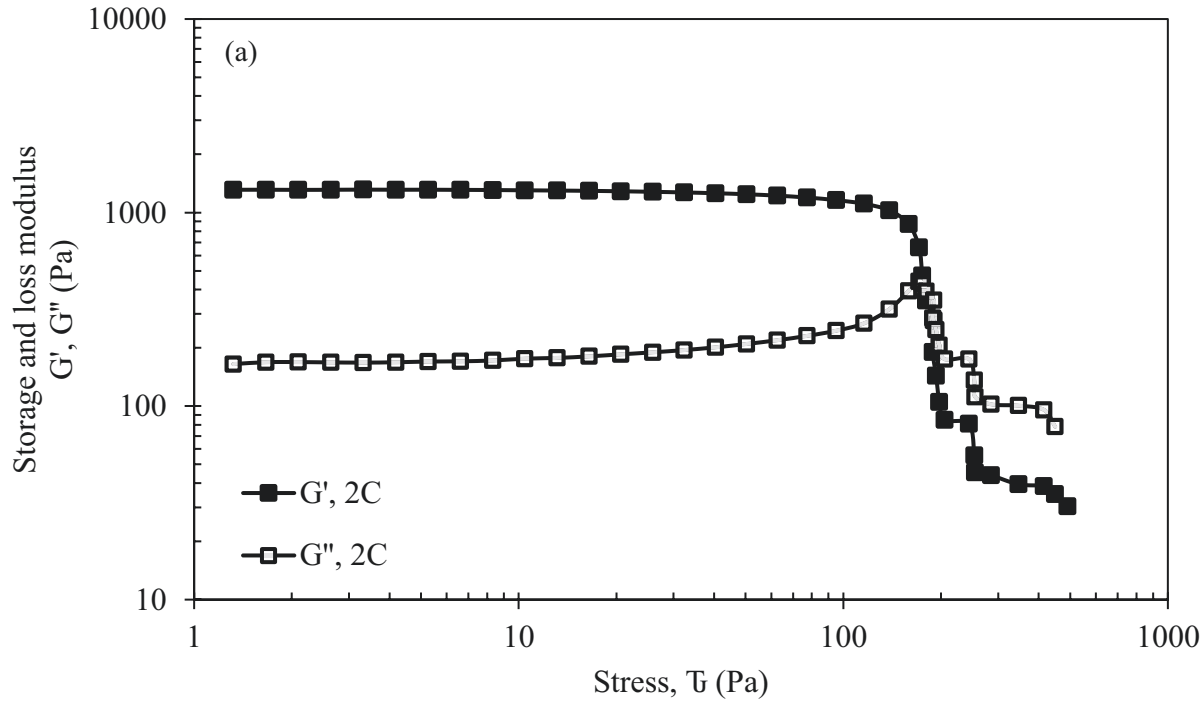
(a)
Storage and loss modulus
G', G" (Pa)
10000
1000
100
10
1
10
100
1000
Stress, τ (Pa)
G', 2C
G", 2C

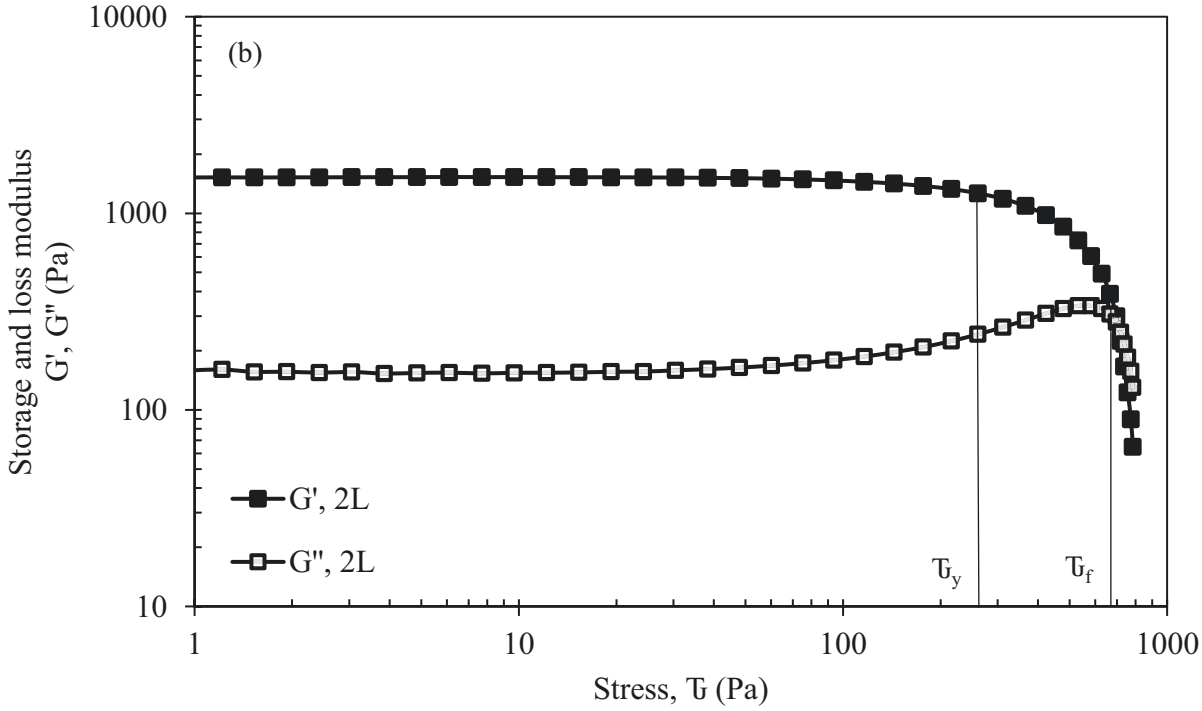
(b)
Storage and loss modulus
G', G" (Pa)
10000
1000
100
10
1
10
100
1000
Stress, τ (Pa)
G', 2L
G", 2L
τy
τf

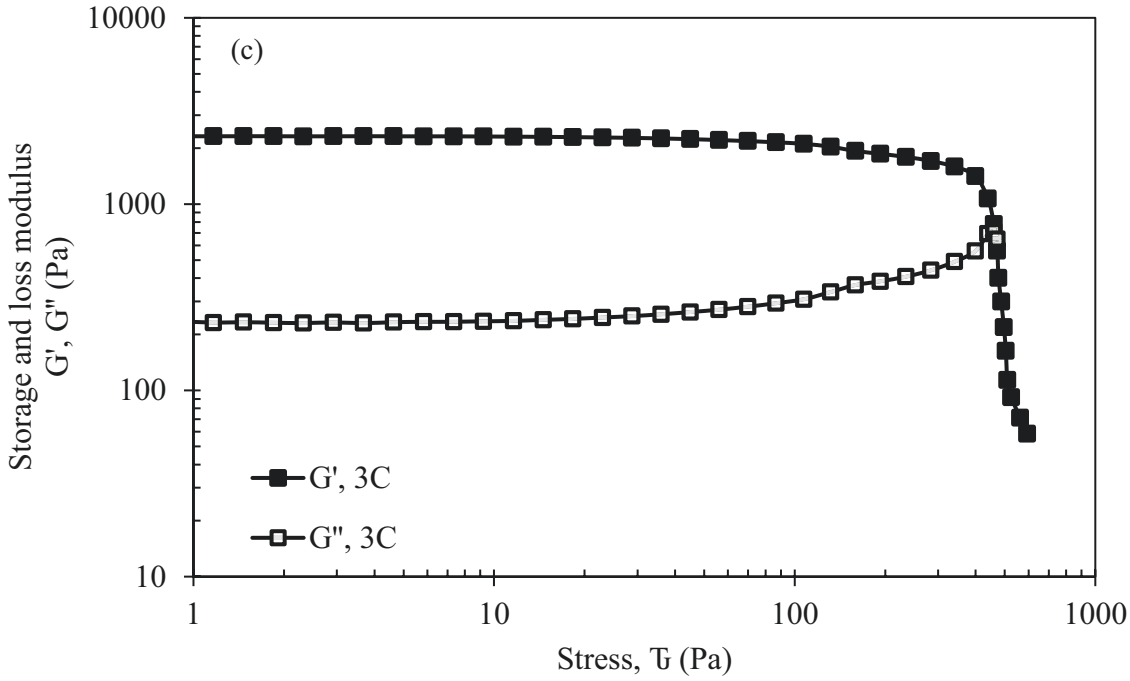
(c)
10000
1000
100
10
Storage and loss modulus
G', G" (Pa)
G', 3C
G", 3C
1
10
100
1000
Stress, Ꚍ (Pa)

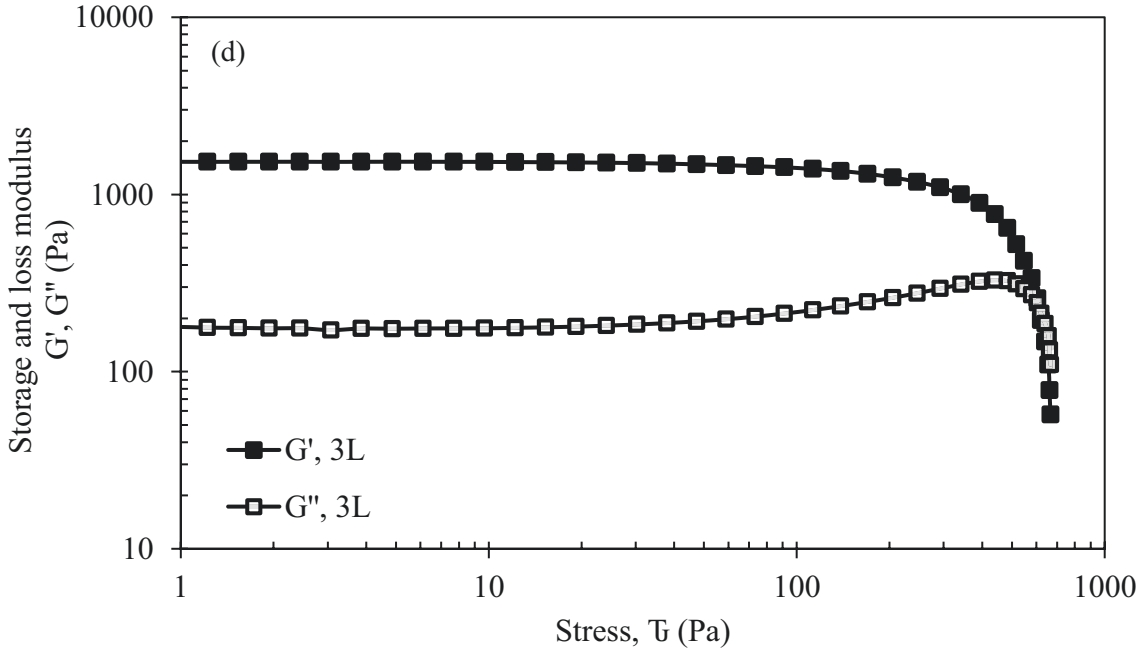
(d)
10000
1000
100
10
Storage and loss modulus
G', G" (Pa)
G', 3L
G", 3L
1
10
100
1000
Stress, Ꚍ (Pa)

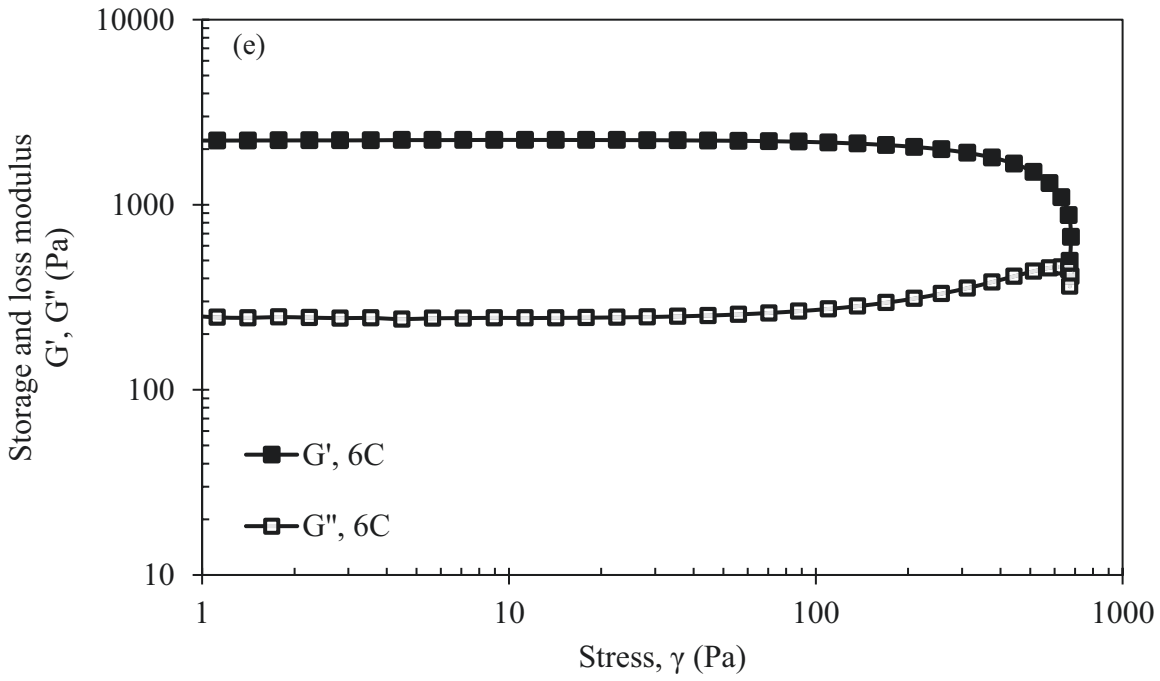
(e)
10000
1000
100
10
Storage and loss modulus
G', G" (Pa)
G', 6C
G", 6C
1
10
100
1000
Stress, γ (Pa)

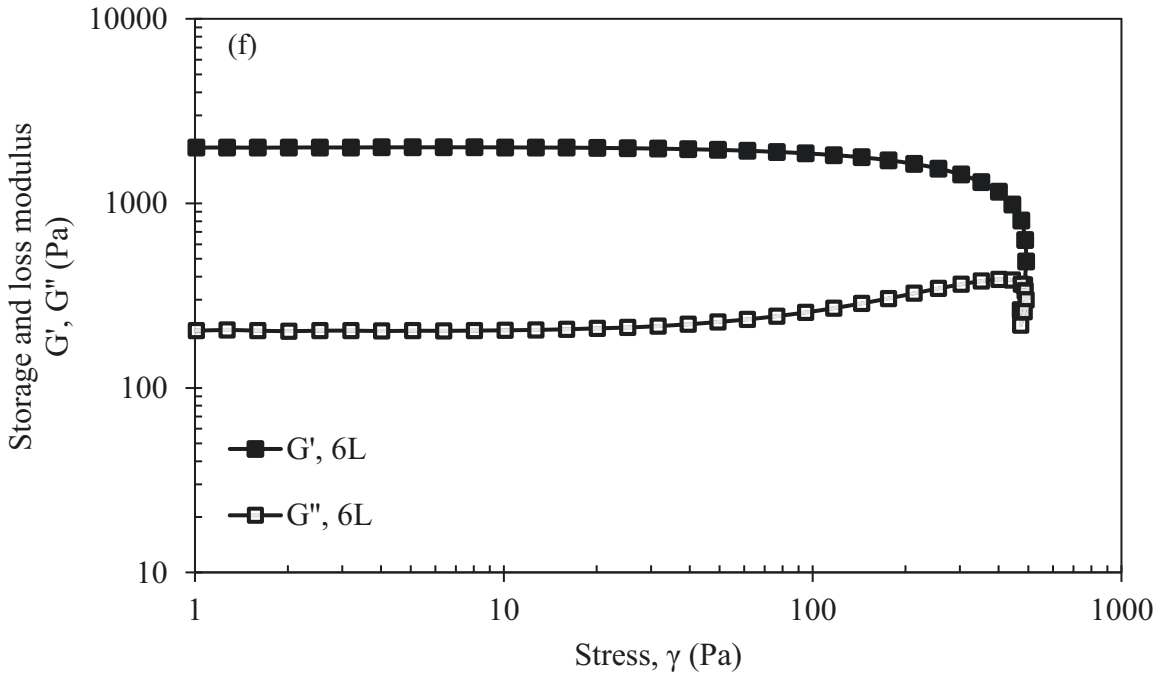
(f)
10000
1000
100
10
Storage and loss modulus
G', G" (Pa)
G', 6L
G", 6L
1
10
100
1000
Stress, γ (Pa)

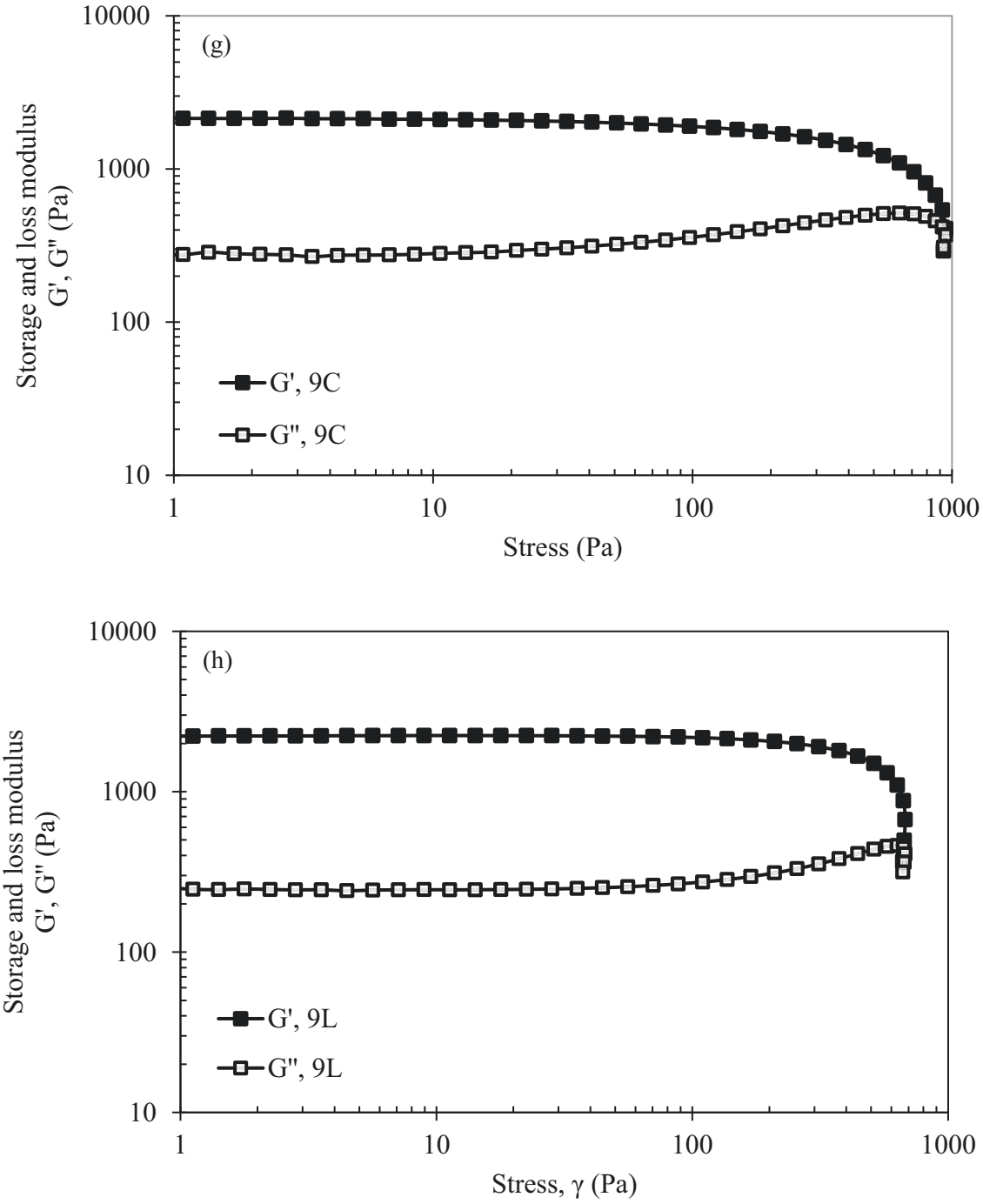

Figure 4.16. Stress amplitude sweep of the control and lignin-based hydrogels: (a) Strain of 2C, (b) 2L, (c) 3C, (d) 3L, (e) 6C, (f) 6L, (g) 9C, (h) 9L

4.11.3 Temperature ramp

Figure 4.17 demonstrates the thermal rheological properties for both the elastic and viscous modulus of the hydrogel samples. At low temperatures, the moduli curves are greater but decrease with increasing temperature. At approximately 34 to 37ºC, there is a slight valley in the moduli curves which is attributed to the lower critical solution temperature (LCST) of N-isopropylacrylamide (32ºC to 34ºC). At this temperature, the hydrogels undergo a reversible phase transition from their swollen state to a shrunken dehydrated state (Feng et al., 2011; Yang et al., 2011). Afterwards, the difference between the elastic and viscous moduli becomes smaller but does not reach a crossover temperature. In other words, the hydrogel samples do not exhibit a phase transition but rather undergo a plateau with increasing temperature, indicating thermal stability (Van De Bulcke et al., 2000).

The control samples (2C, 3C, 6C, and 9C) have a larger modulus than the lignin-based samples (2L, 3L, 6L, and 9L), indicating that the control samples have more elastic properties, even with increasing temperature. In addition, following the LCST, the gap between the elastic and viscous modulus decreases more significantly for the lignin-based hydrogels. This suggests that the lignin-based hydrogels more readily approach the sol-gel temperature (Niang et al., 2016).

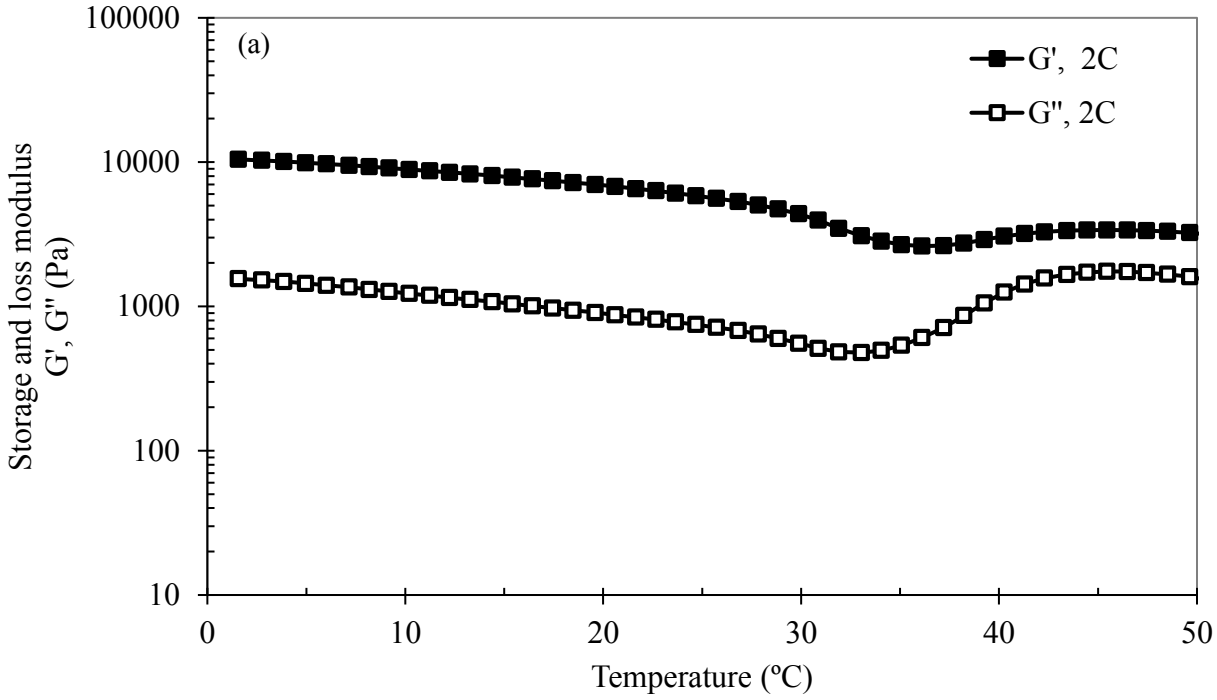
(a)
G', 2C
G", 2C
Storage and loss modulus G', G" (Pa)
100000
10000
1000
100
10
0
10
20
30
40
50
Temperature (ºC)

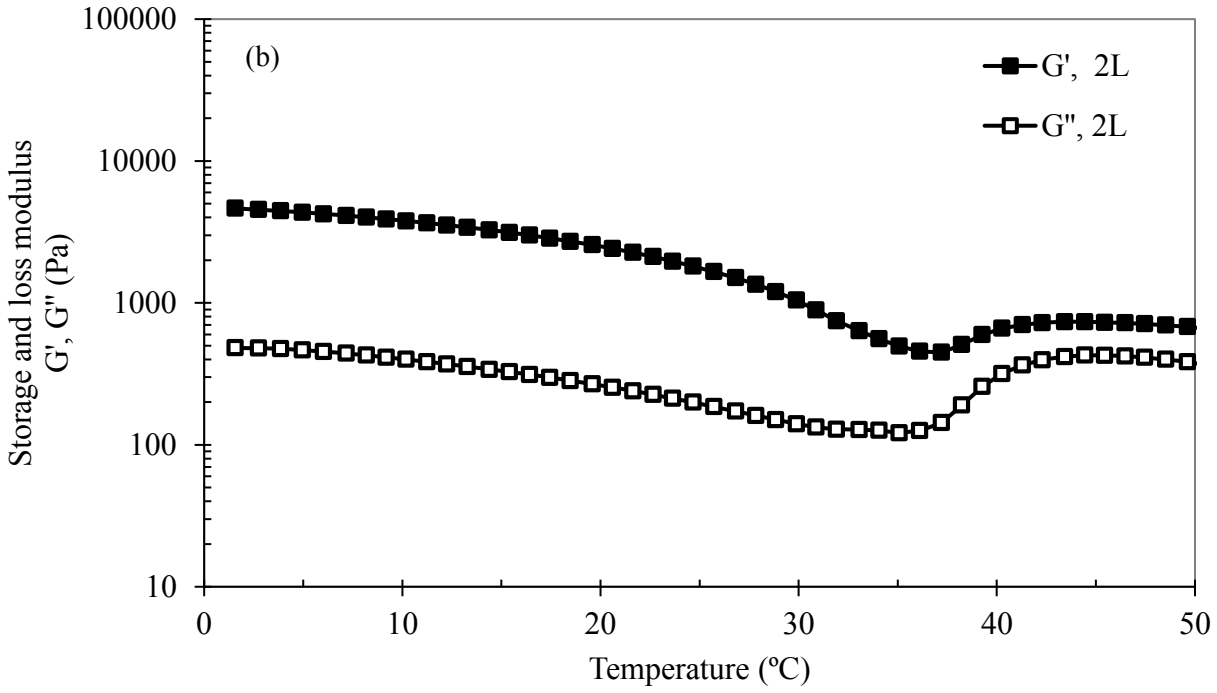
(b)
G', 2L
G", 2L
Storage and loss modulus G', G" (Pa)
100000
10000
1000
100
10
0
10
20
30
40
50
Temperature (ºC)

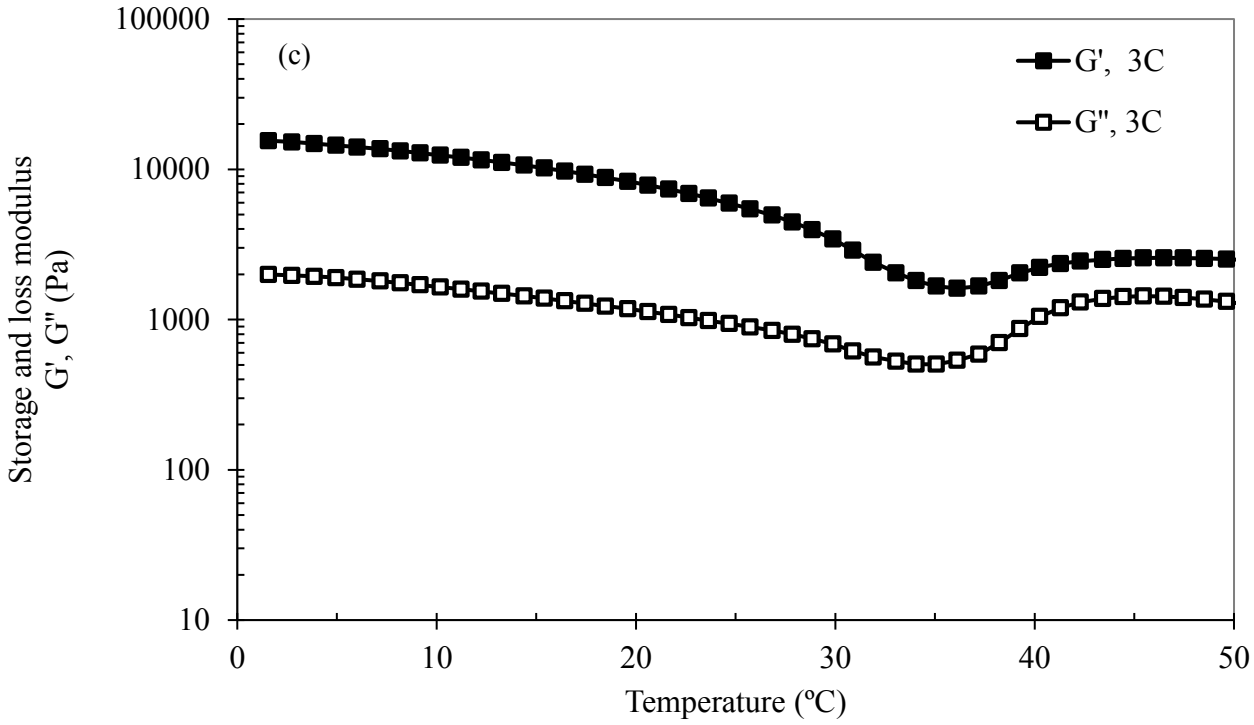
(c)
G', 3C
G", 3C
Storage and loss modulus
G', G" (Pa)
100000
10000
1000
100
10
0
10
20
30
40
50
Temperature (ºC)

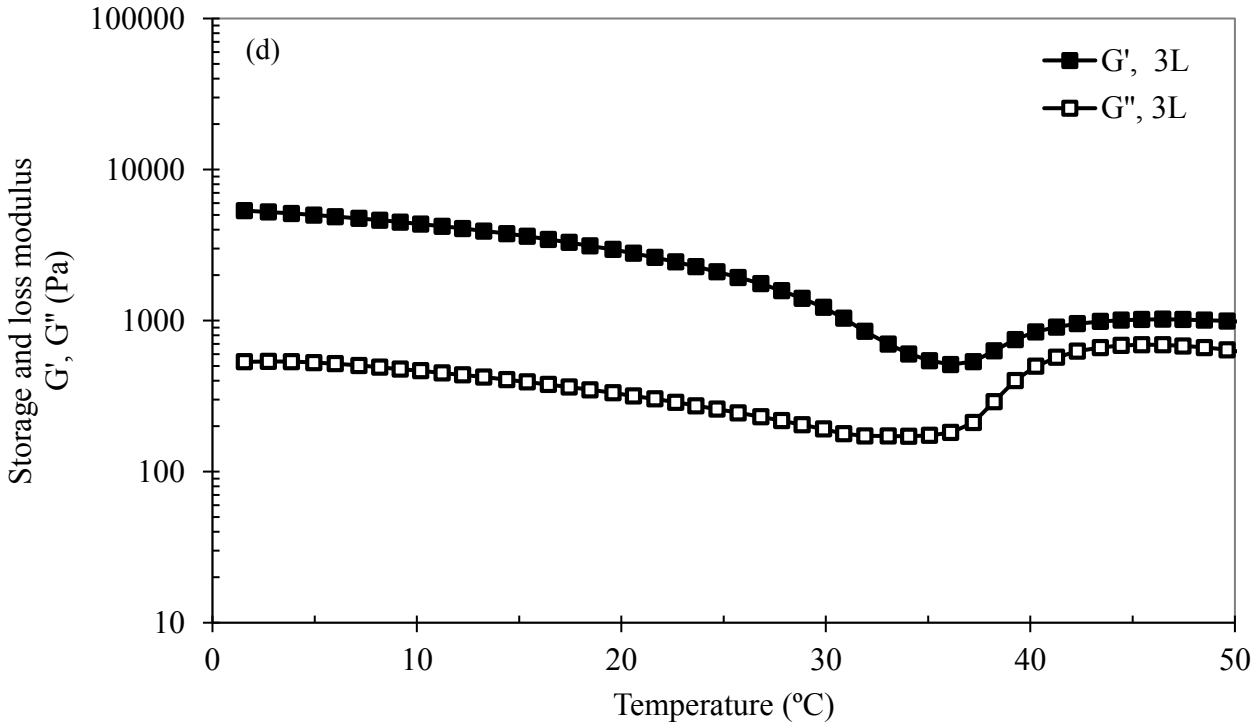
(d)
G', 3L
G", 3L
Storage and loss modulus
G', G" (Pa)
100000
10000
1000
100
10
0
10
20
30
40
50
Temperature (ºC)

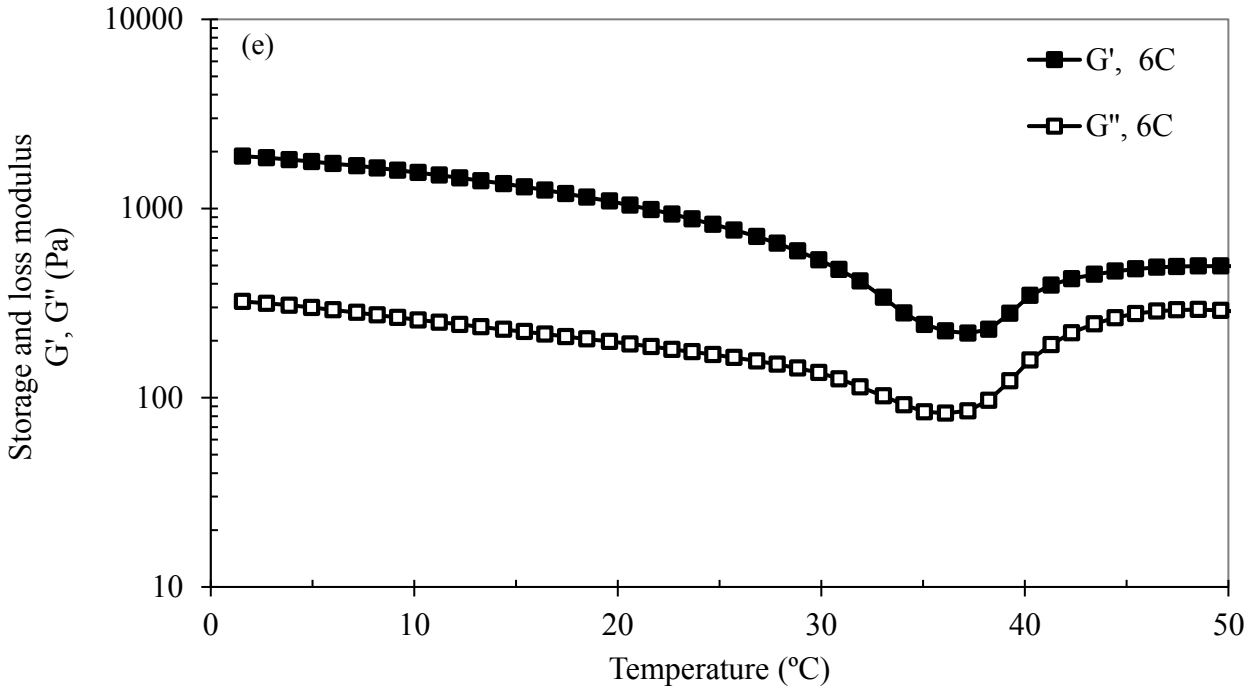
(e)
G', 6C
G", 6C
Storage and loss modulus
G', G" (Pa)
10000
1000
100
10
0
10
20
30
40
50
Temperature (ºC)

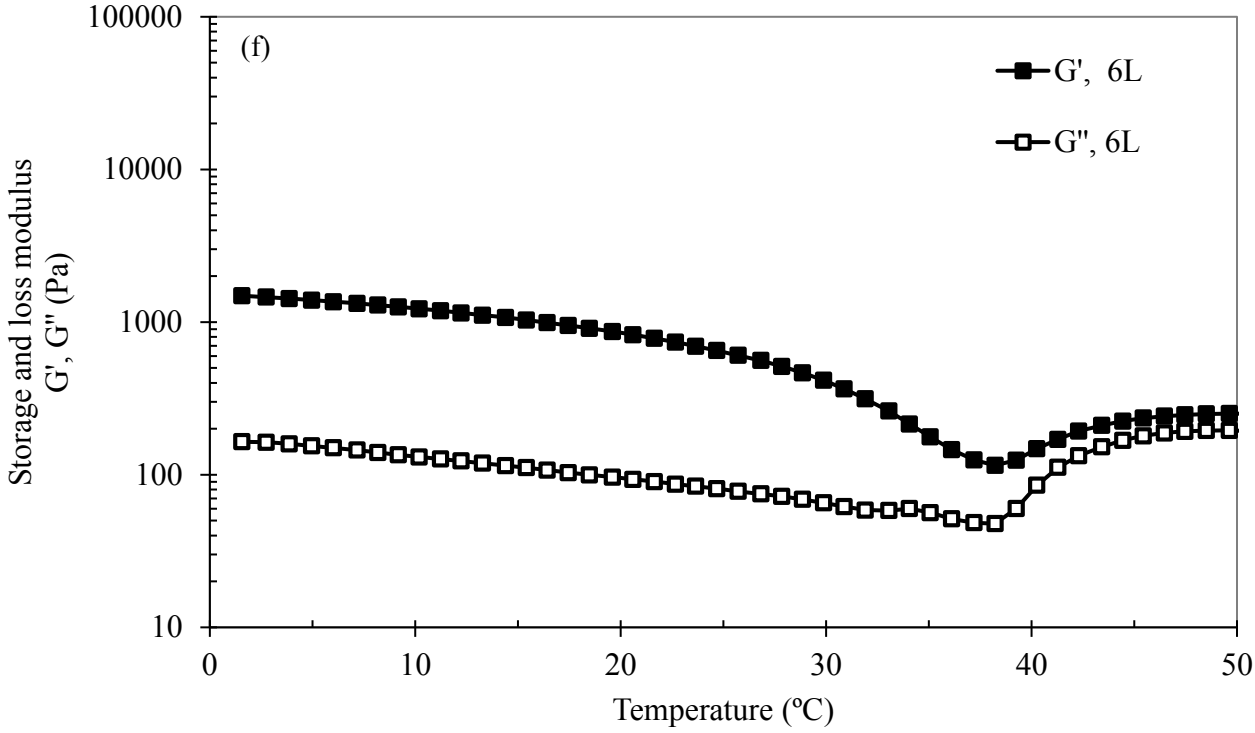
(f)
G', 6L
G", 6L
Storage and loss modulus
G', G" (Pa)
100000
10000
1000
100
10
0
10
20
30
40
50
Temperature (ºC)

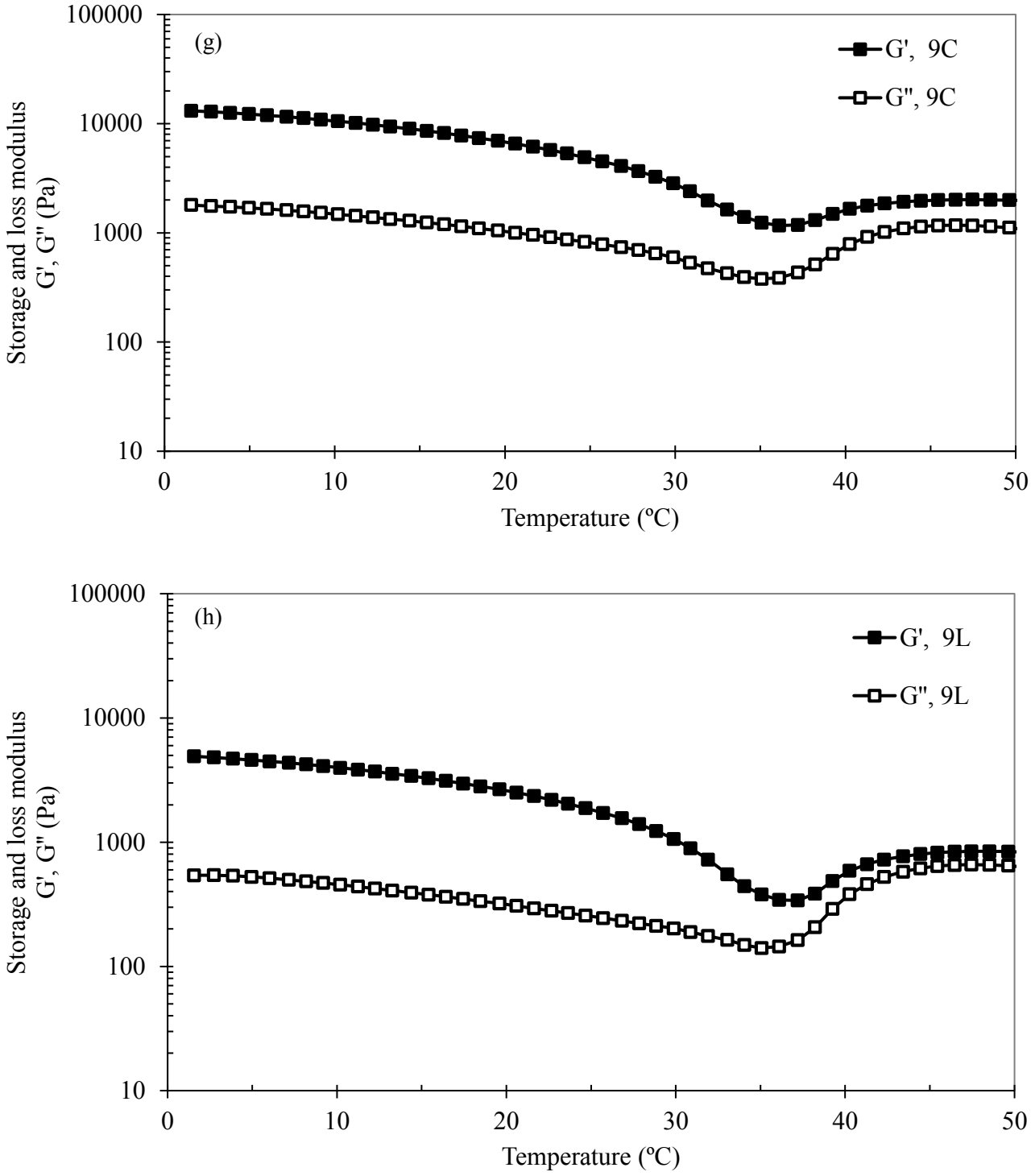

Figure 4.17. Temperature ramp of the control and lignin-based hydrogels: (a) 2C, (b) 2L, (c) 3C, (d) 3L, (e) 6C, (f) 6L, (g) 9C, (h) 9L

4.11.4 Structure recovery

The structure recovery of the control hydrogel samples was determined by inputting an oscillating strain and observing the samples' storage modulus output response. Figure 18 illustrates the step change exhibited by the hydrogel samples and demonstrates their recovery after undergoing over 100% strain rate. The storage modulus recovered was approximately 96.7%, 94.8%, 92.2%, and 87.2% for samples 3C, 6C, 9C, and 2C, respectively. This overall high structure recovery indicated a well-developed three-dimensional polymer network and allowed for further understanding the hydrogels' capabilities to withstand applied force during processing. In other words, the data suggests that the hydrogels are recoverable after applying stress, which makes them suitable for processing (Omidian et al., 2005). Furthermore, the recovery of the hydrogels was found to be directly related with swelling ratio, the recovery percentage increasing with hydrogels exhibiting increased swelling capacity.

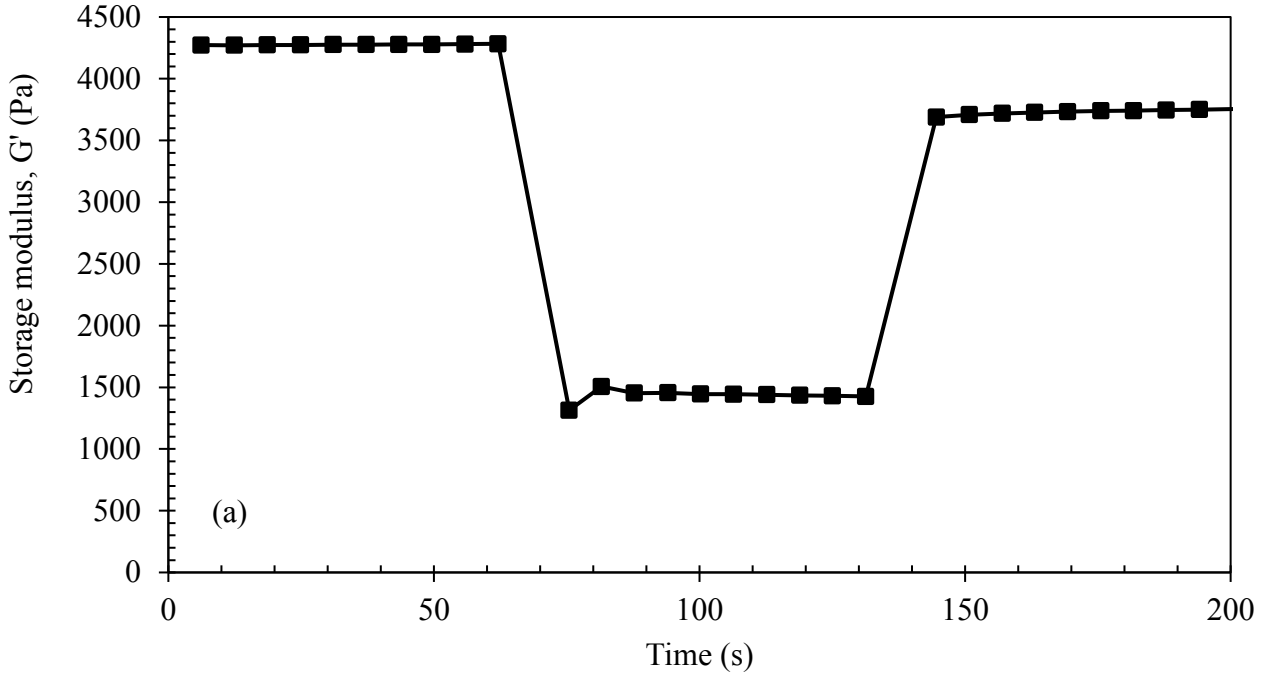
Storage modulus, G' (Pa)
4500
4000
3500
3000
2500
2000
1500
1000
500
0
(a)
0
50
100
150
200
Time (s)

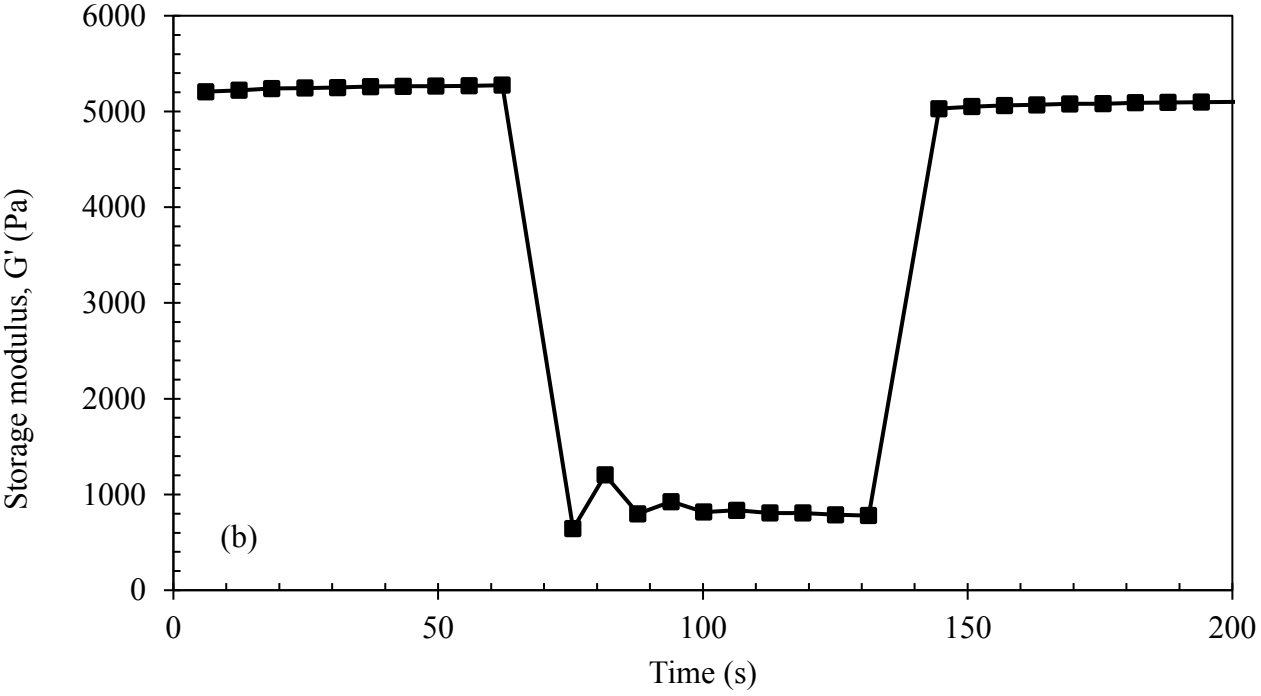
Storage modulus, G' (Pa)
6000
5000
4000
3000
2000
1000
0
(b)
0
50
100
150
200
Time (s)

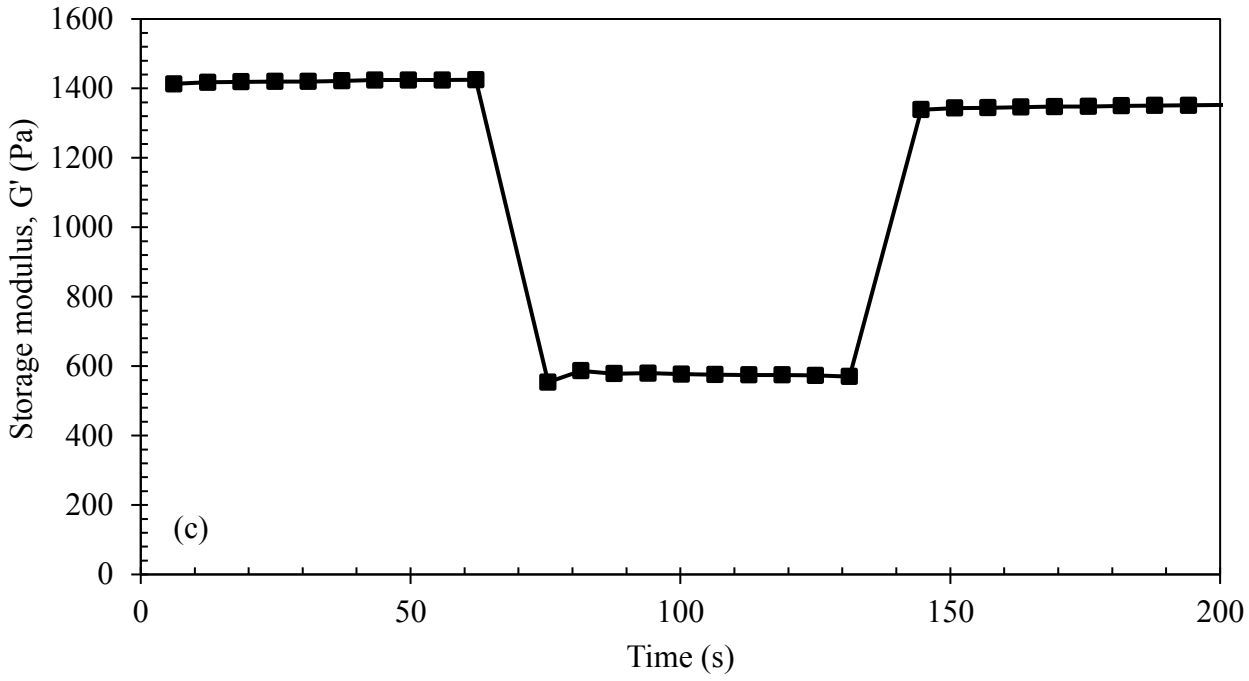

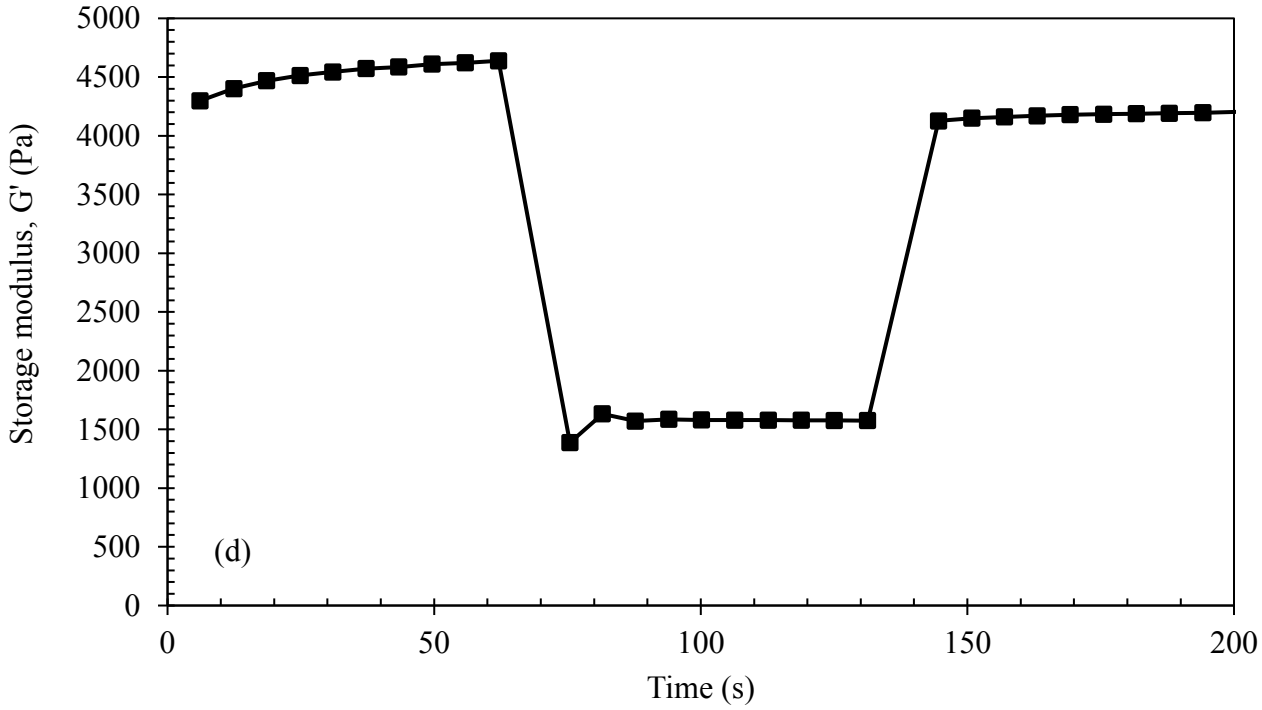

Figure 4.18. Structure recovery of the control hydrogels: (a) 2C, (b) 3C, (c) 6C, (d) 9C

4.12 References

Ahmaruzzaman, M. (2008). Adsorption of phenolic compounds on low-cost adsorbents: a review. Advances in colloid and interface science, 143(1), 48-67.

Alao, A.-R., Konneh, M. (2011). Application of Taguchi and Box-Behnken designs for surface roughness in precision grinding of silicon. International Journal of Precision Technology, 2(1), 21-38

Antony, J. (2006). Taguchi or classical design of experiments: a perspective from a practitioner. Sensor Review, 26, 227-230

Avşar, A., Gökbulut, Y., Ay, B., & Serin, S. (2017). A novel catalyst system for the synthesis of N, N′-Methylenebisacrylamide from acrylamide. Designed Monomers and Polymers, 20(1), 434-440

Brown, C.E. (1998). Applied Multivariate Statistics in Geohydrology and Related Sciences. Springer: Berlin

Carraher, C. E. Jr. (2013). Introduction to Polymer Chemistry, 3rd ed., CRC Press Taylor & Francis Group: London

Chen, H., Zhao, J., Wu, J., Dai, G. (2011). Isotherm, thermodynamic, kinetics and absorption mechanism studies of methyl orange by surfactant modified silkworm exuviae. Journal of hazardous materials, 192(1), 246-254.

Deen, G. R. (2012). Solution Properties of Water-Soluble "Smart" Poly (N-acryloyl-N′-ethyl piperazine-co-methyl methacrylate). Polymers, 4(1), 32-45

Demšar, J. (2006). Statistical comparisons of classifiers over multiple data sets. Journal of Machine learning research, 7, 1-30.

Erbil, C., Kazancıoğlu, E., Uyanık, N. (2004). Synthesis, characterization and thermoreversible behaviours of poly (dimethyl siloxane)/poly (N-isopropyl acrylamide) semi-interpenetrating networks. European polymer journal, 40(6), 1145-1154

Feng, Q., Chen, F., Wu, H. (2011). Preparation and characterization of a temperature-sensitive lignin-based hydrogel. BioResources, 6(4), 4942-4952

Fernandes, E.M., Pires, R.A., Mano, J.F., Reis, R.L. (2013). Bionanocomposites from lignocellulosic ressources: Properties, applications and future trends for their use in the biomedical field. Progress in Polymer Science, 38, 1415-1441

Freundlich, H.M.F. (1906). Over the absorption in solution. Journal of Physical Chemistry, 57, 385-470

Fu, Y., Kao, W. J. (2009). Drug release kinetics and transport mechanisms from semi-interpenetrating networks of gelatin and poly (ethylene glycol) diacrylate. Pharmaceutical research, 26(9), 2115-2124.

Geever, L. M., Devine, D. M., Nugent, M. J., Kennedy, J. E., Lyons, J. G., Higginbotham, C. L. (2006). The synthesis, characterisation, phase behaviour and swelling of temperature sensitive physically crosslinked poly (1-vinyl-2-pyrrolidinone)/poly (N-isopropylacrylamide) hydrogels. European polymer journal, 42(1), 69-80

Han, J., Lei, T., Wu, Q. (2014). High-water-content mouldable polyvinyl alcohol-borax hydrogels reinforced by well-dispersed cellulose nanoparticles: Dynamic rheological properties and hydrogel formation mechanism. Carbohydrate polymers, 102, 306-316

Hodkingson, J.M. (2000). Mechanical Testing of Advanced Fibre Composites. Woodhead Publishing Ltd.: Boston.

Iler, H. D., Rutt, E., Althoff, S. (2006). An Introduction to Polymer Processing, Morphology, and Property Relationships through Thermal Analysis of Plastic PET Bottles. Exercises Designed to Introduce Students to Polymer Physical Properties. Journal of Chemical Education, 83(3), 439

Jadhav, N., Gaikwad, V., Nair, K., Kadam, H. (2009). Glass transition temperature: Basics and application in pharmaceutical sector. Asian Journal of Pharmaceutics, 3(2), 82

Kadla, J. F., Kubo, S. (2004). Lignin-based polymer blends: analysis of intermolecular interactions in lignin–synthetic polymer blends. Composites Part A: Applied Science and Manufacturing, 35(3), 395-400

Kadla, J. F., Kubo, S., Venditti, R. A., Gilbert, R. D., Compere, A. L., Griffith, W. (2002). Lignin-based carbon fibers for composite fiber applications. Carbon, 40(15), 2913-2920

Khare, A. R., Peppas, N. A. (1995). Swelling/deswelling of anionic copolymer gels. Biomaterials, 16(7), 559-567.

Kim, Y.S., Kadla, J.F. (2010). Preparation of a Thermoresponsive Lignin-Based Biomaterial through Atom Transfer Radical Polymerization. Biomacromolecules, 11, 981-988

Konduri, M., Fatehi, P. (2016). Synthesis and characterization of carboxymethylated xylan and its application as a dispersant. Carbohydrate Polymers, 146, 26-35

Konduri, M., Kong, F., Fatehi, P. (2015). Production of carboxymethylated lignin and its application as a dispersant. European Polymer Journal, 70, 371-383

Koo, T. K., Li, M. Y. (2016). A guideline of selecting and reporting intraclass correlation coefficients for reliability research. Journal of chiropractic medicine, 15(2), 155-163

Langmuir, I. (1918). The absorption of gases on plane surfaces of glass, mica and platinum. Journal of the American Chemical Society, 40(9), 1361-1403

Liang, X., Huang, Z., Zhang, Y., Hu, H., Liu, Z. (2013). Synthesis and properties of novel superabsorbent hydrogels with mechanically activated sugarcane bagasse and acrylic acid. Polymer bulletin, 70(6), 1781-1794.

Ling, Y., Lu, M. (2009). Thermo and pH dual responsive Poly (N-isopropylacrylamide-co-itaconic acid) hydrogels prepared in aqueous NaCl solutions and their characterization. Journal of Polymer Research, 16(1), 29-37

Montgomery, D. (2013). Design and Analysis of Experiments, 8th ed., John Wiley & Sons: Danvers

Niang, P. M., Huang, Z., Dulong, V., Souguir, Z., Le Cerf, D., Picton, L. (2016). Thermo-controlled rheology of electro-assembled polyanionic polysaccharide (alginate) and polycationic thermo-sensitive polymers. Carbohydrate polymers, 139, 67-74.

Odian, G. (2004) Principles of Polymerization, 4th ed., John Wiley & Sons: New Jersey

Okay, O., Oppermann, W. (2007). Polyacrylamide-Clay Nanocomposite Hydrogels: Rheological and Light Scattering Characterization. Macromolecules, 40, 3378-3387

Omidian, H., Rocca, J.G., Park, K. (2005). Advances in superporous hydrogels. Journal of Controlled Release, 102, 3-12

Passauer, L., Fischer, K., Liebner, F. (2011). Preparation and physical characterization of strongly swellable oligo(oxyethylene) lignin hydrogels. Holzforschung, 65, 309-317

Peng, Z., Chen, F. (2011). Synthesis and Properties of Lignin-Based Polyurethane Hydrogels. International Journal of Polymeric Materials, 60, 674-683

Ramazani-Harandi, M. J., Zohuriaan-Mehr, M. J., Yousefi, A. A., Ershad-Langroudi, A., Kabiri, K. (2006). Rheological determination of the swollen gel strength of superabsorbent polymer hydrogels. Polymer testing, 25(4), 470-474

Raschip, I.E., Hitruc, G.E., Vasile, C., Popescu, M.-C. (2013). Effect of the lignin type on the morphology and thermal properties of the xanthan/lignin hydrogels. International Journal of Biological Macromolecules, 54, 230-237

Ricciardi, R., Gaillet, C., Ducouret, G., Lafuma, F., Lauprêtre, F. (2003). Investigation of the relationships between the chain organization and rheological properties of atactic poly (vinyl alcohol) hydrogels. Polymer, 44(11), 3375-3380

Rodríguez, R., Alvarez-Lorenzo, C., & Concheiro, A. (2003). Cationic cellulose hydrogels: kinetics of the cross-linking process and characterization as pH-/ion-sensitive drug delivery systems. Journal of Controlled Release, 86(2), 253-265

Schawe, J. E. (2002). About the changes of heat capacity, glass transition temperature and relaxation time during the polymerization reaction of thermosetting systems. Thermochimica acta, 391(1), 279-295.

Seddiki, N., Aliouche, D. (2013). Synthesis, rheological behavior and swelling properties of copolymer hydrogels based on poly (N-isopropylacrylamide) with hydrophilic monomers. Bulletin of the Chemical Society of Ethiopia, 27(3), 447-457

Stile, R. A., Burghardt, W. R., Healy, K. E. (1999). Synthesis and characterization of injectable poly (N-isopropylacrylamide)-based hydrogels that support tissue formation in vitro. Macromolecules, 32(22), 7370-7379

Su, E., Okay, O. (2017). Polyampholyte hydrogels formed via electrostatic and hydrophobic interactions. European Polymer Journal, 88, 191-204.

Su, W.-F. (2013). Principles of Polymer Design and Synthesis, vol. 82, Springer: New York

Thakur V.K., Thakur M.K. (2015). Recent advances in green hydrogels from lignin: a review. International Journal of Biological Macromolecules, 72, 834-847

Thomas, N. L., & Windle, A. H. (1982). A theory of case II diffusion. Polymer, 23(4), 529-54

Tukey, J. W. (1949). Comparing individual means in the analysis of variance. Biometrics, 99-114.

Uraki, T., Imura, T., Kishimoto, T., Ubukta, M. (2004) Body temperature-responsive gels derived from hydroxypropylcellulose bearing. Carbohydrate Polymers, 123-130

Van Den Bulcke, A.I., Bogdanov, B. De Rooze, N., Schacht, E.H., Cronelissen, M., Berghmans, M. (2000). Structural and Rheological Properties of Methacrylamide Modified Gelatin Hydrogels. Biomacromolecules, 1, 31-38

Varfolomeev, M. A., Grachev, A. N., Makarov, A. A., Zabelkin, S. A., Emel'yanenko, V. N., Musin, T. R., Gerasimov, A. V., Nurgaliev, D. K. (2015). Thermal analysis and calorimetric study of the combustion of hydrolytic wood lignin and products of its pyrolysis. Chemistry and Technology of Fuels and Oils, 51(1), 140-145

Vijayaraghavan, K., Padmesh, T. V. N., Palanivelu, K., Velan, M. (2006). Biosorption of nickel (II) ions onto Sargassum wightii: application of two-parameter and three-parameter isotherm models. Journal of hazardous materials, 133(1), 304-308.

Wu, H., Chen, F., Feng, Q., Yue, X. (2012). Oxidation and sulfomethylation of alkali-extracted lignin from corn stalk. BioResources, 7(3), 2742-2751

Xie, J., & Hsieh, Y. L. (2003). Thermosensitive poly (n-isopropylacrylamide) hydrogels bonded on cellulose supports. Journal of applied polymer science, 89(4), 999-1006

Yang, J. Y., Zhou, X. S., Fang, J. (2011). Synthesis and characterization of temperature sensitive hemicellulose-based hydrogels. Carbohydrate Polymers, 86(3), 1113-1117

Zarzyka, I., Pyda, M., Di Lorenzo, M. L. (2014). Influence of crosslinker and ionic comonomer concentration on glass transition and demixing/mixing transition of copolymers poly (N-isopropylacrylamide) and poly (sodium acrylate) hydrogels. Colloid and polymer science, 292(2), 485-492

Zhang, J., Xu, X. D., Wu, D. Q., Zhang, X. Z., Zhuo, R. X. (2009). Synthesis of thermosensitive P (NIPAAm-co-HEMA)/cellulose hydrogels via “click” chemistry. Carbohydrate polymers, 77(3), 583-589

5 CONCLUSIONS AND RECOMMENDATIONS

5.1 Conclusions

The MANOVA and Tukey Post Hoc analyses determined that reaction temperature, time, N-isopropylacrylamide content, and pH exhibited significant effects on both yield and swelling capacity. The signal-to-noise (SN) ratio was applied using Taguchi L9 models for both the control (C) and lignin-based (L) samples to determine the most optimal reaction parameters and reduce the sample size for subsequent tests. The SN ratio was found to be the highest for 3C and 6C, as well as 2L and 9L for the control and lignin-based hydrogels, respectively.

The chemical structure of the control and lignin-based hydrogels were found to be relatively similar according to the FTIR analysis. The most intense peaks were found at 1535 cm^{-1} and 1639 cm^{-1}, indicating the large presence of amide groups from N-isorpropylacrylamide (NIPAAm) and N,N'-methylenebisacrylamide (MBAAm). In addition, a large broad peak was visible between 3400 cm^{-1} to 3200 cm^{-1}, indicating the stretching of the N-H bond of NIPAAm. The high presence of NIPAAm was also reported in the ^{1}H NMR with large peaks present at 1.15 ppm and 4.1 ppm relative to the DMSO-d_6. The elemental analysis (CHNS) revealed that the control and lignin-based hydrogels were composed of approximately 11.4 wt.% and 10.6 wt.% nitrogen, respectively. The slightly lower nitrogen content for the lignin-based was attributed to the grafting of kraft lignin to the other polymers in the polymer network.

Thermogravimetric analysis (TGA) on the hydrogels determined their thermal behavior followed a similar trend to N,N'-methylenebisacrylamide. The hydrogels exhibited two stages of decomposition; the initial weight loss (at 198^{o}C) was attributed to the decomposition of the aliphatic alkenes groups, and the second weight loss (at 320^{o}C), to the breakdown of the

remaining carboxylic and amine groups (Avşar et al., 2017). This improvement in thermal stability suggests that the monomer was readily consumed during the polymerization reaction, and is present within the polymer network. Sample 6L was found to be the most resistant to temperature, suggesting that lignin also increased the thermal stability of the gels. Furthermore, according to DSC analysis, the hydrogels were found to exhibit an increased glass transition temperature (T_g) compared to N-isopropylacrylamide, ranging between 141.45^{o}C and 148.60^{o}C. Samples 6C and 6L, which only incorporated 1.2 g of the monomer, resulted in a higher T_g, confirming that N,N'-methylenebisacrylamide largely affected the thermal behavior of gels. In addition, the incorporation of lignin was found to increase the heat capacity of the lignin-based samples when compared to the control samples. This suggests that lignin could also have influenced the thermostability of the hydrogels.

The swelling behavior of the lignin-based hydrogels were evaluated and found to obey second order kinetics, and to follow pseudo-Fickian diffusion in water. Sample 6L was shown to exhibit a higher swelling rate, followed by 9L, 3L, and 2L, respectively. The pseudo-second order rate constant was found to be an order of magnitude greater for sample 6L, indicating that this hydrogel exhibited a significantly rapid swelling rate. The proportionality constants modeled by the Ritger-Peppas equation were consistent with swelling rates. This was described by the Branuer-Emmett-Teller (BET), which demonstrated that the increased swelling rate was due to increased surface area. Furthermore, the pore volume and pore size for sample 2L was found to be the greatest, allowing for a higher capacity of water to be retained. For this reason, sample 2L had the highest swelling capacity. Moreover, the equilibrium absorption of the hydrogels in methylene blue dye was studied and found to correlate more closely with the Freundlich isotherm model. Thus, this suggests that the hydrogels have a heterogeneous surface.

Furthermore, oscillatory rheological measurements were conducted to determine the viscoeleastic properties of swollen hydrogels. According to the obtained moduli, the hydrogels were found to be predominately elastic. In general, the amount of energy dissipated was found to be slightly greater for the control samples than the lignin-based samples. This may be due to the incorporation of lignin resulting in a less crosslinked structure.

With applied stress, the swollen hydrogels were found to exhibit a crossover from primary elastic to primary viscous. This crossover over was found to occur at a higher applied stress for the lignin-based hydrogels, which is most likely due to lignin's increased mechanical properties. Samples 3C and 2L were found to have the highest storage (elastic) modulus, indicating that the hydrogel is highly crosslinked. This is consistent with the data obtained from the swelling experiments, the high swelling ratio indicating a well-developed crosslinked network structure.

In addition, the effect of temperature on the storage and loss modulus of the swollen hydrogels were investigated. Both moduli decreased with increasing temperature, but were found to stabilize near 45^{o}C. Furthermore, the hydrogels exhibited a lower critical solution temperature (LCST) between 34^{o}C to 37^{o}C, which is due to the presence of N-isopropylacrylamide.

Finally, the structure recovery of the control hydrogels determined that they recovered 87.2% to 96.7% of their elastic moduli following 100% deformation. The increased recovery was also found to correlate with swelling ratio; and higher crosslinked structures demonstrated higher structural stability.

5.2 Future work

Alternative experimental design models could be considered for the optimization of reaction conditions. Instead of the Taguchi model, traditional design of experiments (DOE) could be

applied using only one or two independent variables. This would allow to better identify each interaction, and allow for better understanding of their effects on dependent variables. Furthermore, the effect of lignin content and initiator concentration should be applied in the following DOE models in order to better understand their effects on hydrogel crosslinking and swelling performance.

Additional swelling studies can be conducted with various solvents containing different concentrations of solute. The effect of pH and temperature should also be studied, as this has an important effect on fertilizers and wound dressings; the hydrogel swelling performance should mimic soil and/or internal body conditions, respectively. Additional studies on the effects of rheological parameters may be conducted on the hydrogels by varying stress and frequency over a larger range. In other words, the current rheological data can be repeated over multiple tests to include a greater range of constant values.

Finally, the effect of lignin type on hydrogel properties may be studied by only varying the origin or extraction methods for lignin. Consequently, the additional methods of synthesizing on a single type of lignin-based hydrogels may be studied by examining the effect of different crosslinkers and initiators. Furthermore, biocompatibility studies on lignin-based hydrogels would be beneficial for both medical and environmental applications.